# Determining the Asymptotic Expansion of Prolate Spin-Weighted Spheroidal Eigenvalues

A paper presented to the faculty of the Department of Physics of Wake Forest University in partial fulfillment of the requirements for graduation with Honors in Physics.

Daniel J. Vickers

May 4, 2018

Approved by:

____________________

Gregory B. Cook

____________________

Eric D. Carlson

____________________

Paul R. Anderson

## 1. Introduction

Black holes have long been of great interest to the field of astrophysics. With the recent detection of gravitational waves, black holes have gained great popularity and are very relevant in the current study of space. One such aspect of black holes, and gravitational waves themselves, is the study of the ring-down structure of gravitational waves, when the wave is damping.

One method of studying these ring-downs has been to resolve the quasi-normal modes of Kerr black holes, and particularly the asymptotic behavior of these modes. While exploring this, it became evident that these modes could be described with spin-weighted spheroidal harmonics[1]. This task would be made easier if analytic approximations for the asymptotic behaviors of these harmonics were resolved to high accuracy. The goal of this paper is to find these asymptotic approximations using numerical methods.

## 2. Spin-Weighted Spheroidal Harmonics

Spin-weighted spheroidal harmonics (SWSHs) are complete sets of orthonormal functions for describing the behavior of a function on the surface of spheroids. However, it is important to first understand functions that work in spherical coordinates, and how these relate to the spheroidal case.

In order to describe functions on the surface of a 2-sphere, one can use spherical harmonics, $Y_{\ell m}(\theta, \phi)$, which are functions of $\theta$ and $\phi$ in spherical coordinates. Spherical harmonics are the functions which satisfy the angular equation:

(2.1)

$$\sin(\theta)\frac{\partial}{\partial\theta}\left(\sin(\theta)\frac{\partial Y}{\partial\theta}\right)+\frac{\partial^2 Y}{\partial\phi^2}=-\ell(\ell+1)\sin^2(\theta)Y,$$

for which the solution is:

(2.2)

$$Y_{\ell m}(\theta,\phi)=(-1)^m\sqrt{\frac{(2\ell+1)(\ell-|m|)!}{4\pi(\ell+|m|)!}}e^{im\phi}P_{\ell m}(\cos(\theta)),$$

where $P_{\ell m}$(x) are the associated Legendre polynomials. Because the $\phi$ dependence is $e^{im\phi}$, then after the change in coordinates of $x=\cos(\theta)$, Eq. (2.1) can be written:

(2.3)

$$\frac{\partial}{\partial x}\left[(1-x^2)\frac{\partial}{\partial x}Y_{\ell m}\right]-\left[\frac{m^2}{1-x^2}\right]Y_{\ell m}=-\ell(\ell+1)Y_{\ell m}.$$

This is an eigenvalues problem of the form we will consider below. $Y_{\ell m}$ are the eigenfunctions and the eigenvalues are $\ell(\ell+1)$. More commonly in the context of harmonics, we think of $\ell(\ell+1)$ as the separation constant. For all subsequent eigenfunctions, the $\phi$ dependence is also of the form $e^{im\phi}$, as for $Y_{\ell m}$. The spheroidal harmonics exhibit two useful properties. First, they obey the relation:

(2.4)

$$\langle Y_{\ell m}|Y_{\ell' m'}\rangle=\int_0^{\pi}\int_0^{2\pi}Y^*_{\ell m}Y_{\ell' m'}\sin(\theta)\,d\phi d\theta=\delta_{\ell\ell'}\delta_{mm'}.$$

This is the property of orthonormality where none of these functions can be described in terms of the others. Spherical harmonics also have the property of being complete, which means that any scalar function on the 2-sphere can be completely described as a linear combination of these basis functions:

(2.5)

$$f(\theta, \phi) = \sum_{\ell, m} C_{\ell m}\, Y_{\ell m}(\theta, \phi),$$

where the $C_{\ell m}$'s are complex coefficients.

Notice that the function $f(\theta, \phi)$ is scalar-valued, meaning that there is no information regarding the direction of values on the surface of the 2-sphere. In order to describe objects with higher-rank, one must use vector or tensor-spherical harmonics or, more generally, spin-weighted spherical harmonics, which satisfy the differential equation[2][3]:

(2.6)

$$\frac{\partial}{\partial x}\left[(1 - x^2)\frac{\partial}{\partial x}\, {}_sY_{\ell m}\right] + \left[s - \frac{(m + sx)^2}{1 - x^2}\right] {}_sY_{\ell m} = -\big(\ell(\ell + 1) - s(s + 1)\big)\, {}_sY_{\ell m}.$$

These spin-weighted spherical harmonics, ${}_sY_{\ell m}(\theta, \phi)$, take into account $s$, the spin-weight of the harmonic. The separation constant is $\big(\ell(\ell + 1) - s(s + 1)\big)$. In the case $s = 0$, ${}_0Y_{\ell m}(\theta, \phi) = Y_{\ell m}(\theta, \phi)$, which are the spherical harmonics. When $s = \pm 1$, ${}_sY_{\ell m}(\theta, \phi)$ can be used to represent vector-valued functions. Values of $s = -2, 0, 2$, can be used to represent second-rank tensors. This can be continued to increase the rank of these spin-weighted spherical harmonics to any rank required. In general, any rank object can be represented in terms of spin-weighted spherical harmonics.

The spin-weighted spherical harmonics are naturally associated with a spherical coordinate system/geometry; however, it is sometimes necessary to work in non-spherical coordinates. In the case of scalar valued functions, scalar spheroidal harmonics $S_{\ell m}(c;\theta,\phi)$ are well known**.** These spheroidal harmonics satisfy the equation[4][5]:

$$\frac{\partial}{\partial x}\left[(1-x^2)\frac{\partial}{\partial x}S_{\ell m}\right]+\left[(cx)^2-\frac{m^2}{1-x^2}\right]S_{\ell m}=-A_{\ell m}S_{\ell m}. \tag{2.7}$$

The subscript $\ell$, the multipole moment, can be a positive integer, odd half-integer value, or zero. However, for this paper, we will not consider the odd half-integer cases. In other words, $\ell \in \mathbb{N} \cup \{0\}$. The second subscript $m=-\ell,-\ell+1,\ldots,\ell-1,\ell$, is the azimuthal index. The variable $c \in \mathbb{C}$ is the oblateness parameter, which describes the shape of the spheroid. For values of $c \in \mathbb{R}$, the spheroid is oblate. If $c$ is purely imaginary, the spheroid is prolate, and when $c=0$, the coordinates become spherical. Finally, $A_{\ell m}$, the angular separation constant, is the eigenvalue of this differential equation. Notice that if $c=0$, then $A_{\ell m}=\ell(\ell+1)$.

These scalar spheroidal harmonics are useful, but again are scalar valued. In order to describe higher rank objects, one again needs to take into account an additional spin-weight parameter, $s$. The needed functions are called spin-weighted spheroidal harmonics, and they satisfy the modified version of Eq. (2.7) known as the angular Teukolsky equation[1][2][6]:

$$\frac{\partial}{\partial x}\left[(1-x^2)\frac{\partial}{\partial x}\,{}_sS_{\ell m}\right]+\left[(cx)^2-2csx+s-\frac{(m+sx)^2}{1-x^2}\right]\,{}_sS_{\ell m}=-\,{}_sS_{\ell m}\,{}_sA_{\ell m}. \tag{2.8}$$

So, Eq. (2.8), and therefore ${}_sA_{lm}$ and ${}_sS_{lm}$, now depends upon the spin weight $s$. It is then clear that at $s=0$, Eq.(2.8) becomes Eq.(2.7) to describe scalar spheroidal harmonics.

Spin-weighted spheroidal harmonics were first defined by Teukolsky in the context of perturbations on Kerr geometries[1]. This type of behavior is particularly important in understanding objects like black holes. They have application in problems involving perturbations in Kerr, such as extreme mass-ratio black hole binaries, quasi-normal modes, etc.

## 3. Particular Cases for Spin-Weighted Spheroidal Harmonics

In general, there are no closed-form analytic solutions for the SWSHs. Numerous approximation methods are available to find the separation constant ${}_sA_{lm}$ and its associated eigenfunction ${}_sS_{lm}$[2][6]. These solutions to the eigenvalue problem have been solved for various cases of $c$. Most of these methods are numerical, but expansions for small $|c|$ are known as are certain asymptotic expansions[6].

In the oblate case of large values of $|c|$, analytic solutions for $s=0$ have been known for the power-series expansion in $c$. This was later expanded to include behavior for varying values of $s$[6].

When working in the prolate case, for large values of $|c|$ for scalar spheroidal harmonics, there is an approximation for calculating the eigenvalues[6]:

$$
{}_0A_{lm} = |c|(2L+1) - \left(\frac{1}{2}L^2 + \frac{1}{2}L + \frac{3}{4} - m^2\right) - \frac{1}{|c|}(2L+1)\left(\frac{1}{16}L^2 + \frac{1}{16}L + \frac{3}{16} - \frac{1}{2}m^2\right) - \frac{1}{|c|^2}\left[\frac{5}{64}(L^4 + 2L^3 + 7L + 3) - \frac{3}{4}m^2(2L^2 + 2L + 1)\right] + \vartheta\left(\frac{1}{|c|^3}\right), \tag{3.1}
$$

where $L = \ell - \max(|m|, |s|)$. However, there has yet to be any successful extension to $s \neq 0$.

## 4. Methods

We want to expand Eq. (3.1) to include the cases of $s \neq 0$. In order to find the full asymptotic behavior of ${}_sA_{lm}$, it was important to generate data to which fits could be made. So, this project began by numerically approximating the eigenvalues and eigenvectors of the spin-weighted spheroidal harmonic solutions to Eq.(2.8). This was done by converting the equation into a matrix eigenvalue problem. The SWSH eigenvectors were defined as a linear combination of the spin-weighted spherical harmonic eigenvectors:

$$
{}_sS_{\ell m}(c;\theta,\phi) = \sum_{\ell'} C_{\ell' \ell m}(c)\, {}_sY_{\ell' m}(\theta,\phi). \tag{4.1}
$$

Inserting Eq. (4.1) into Eq. (2.8), and using recurrence relations for the ${}_sY_{\ell m}(\theta,\phi)$, this was converted to a matrix eigenvalue problem[2]. For fixed values of $m$, $s$, and $c$ we obtain an infinite-dimensional matrix eigenvalue problem. The set of solutions are indexed by the multipole moment, $\ell$. This eigenvalue problem can be solved numerically by truncating the matrix to dimension *N*. The eigenvalues will be the ${}_sA_{lm}(c)$, and the eigenvectors give the $C_{\ell'\ell m}(c)$ in Eq. (4.1).

Because of the truncation, the numerical solutions come with some amount of error. In order to check the accuracy of the approximate values, the contribution of each spin-weighted spherical harmonic $C_{\ell'\ell m}$ was checked for the eigenvector associated with the largest multipole moment, $\ell = n$, of interest. In the convergent regime, the magnitude of the $C_{\ell'\ell m}$ will decrease exponentially with increasing $\ell'$. So, after calculating the eigenvectors, the values for the two highest values of $\ell'$ were pulled out, which are $C_{(N-1)nm}(c)$ and $C_{Nnm}(c)$. If either of the normalized coefficients made a contribution to the eigenvector greater that $10^{-15}$, the error was deemed to be too high. In this case, the matrix size was increased, and the eigenvectors were then recalculated. The process was repeated until a sufficiently large matrix was used to give solutions to the desired accuracy. Then solutions were generated as $c$ varies along the sequence of solutions.

This was done for values of $m = -5, -4, \dots ,5$ and $s = -3, \dots ,3,$. Then the eigenvalues ${}_sA_{lm}$ for the terms $L = \ell - \max(|m|, |s|) = 0, \dots ,6$ were saved. Equation (3.1) is an approximation for ${}_sA_{lm}$ for $s = 0$ and large values of $|c|$. The $s = 0$ data were used to confirm the validity of this method, and the remaining $s$ values were used to fit for this function's dependence upon the spin-weight of the SWSHs.

## 5. Results

Figures 1 and 2 shows the behavior of the real and imaginary contributions to the separation constant ${}_sA_{lm}(c)$ for the representative case of $m = 5$, $s = 2$, vs. values of $c = 0$ to $c = -20i$.

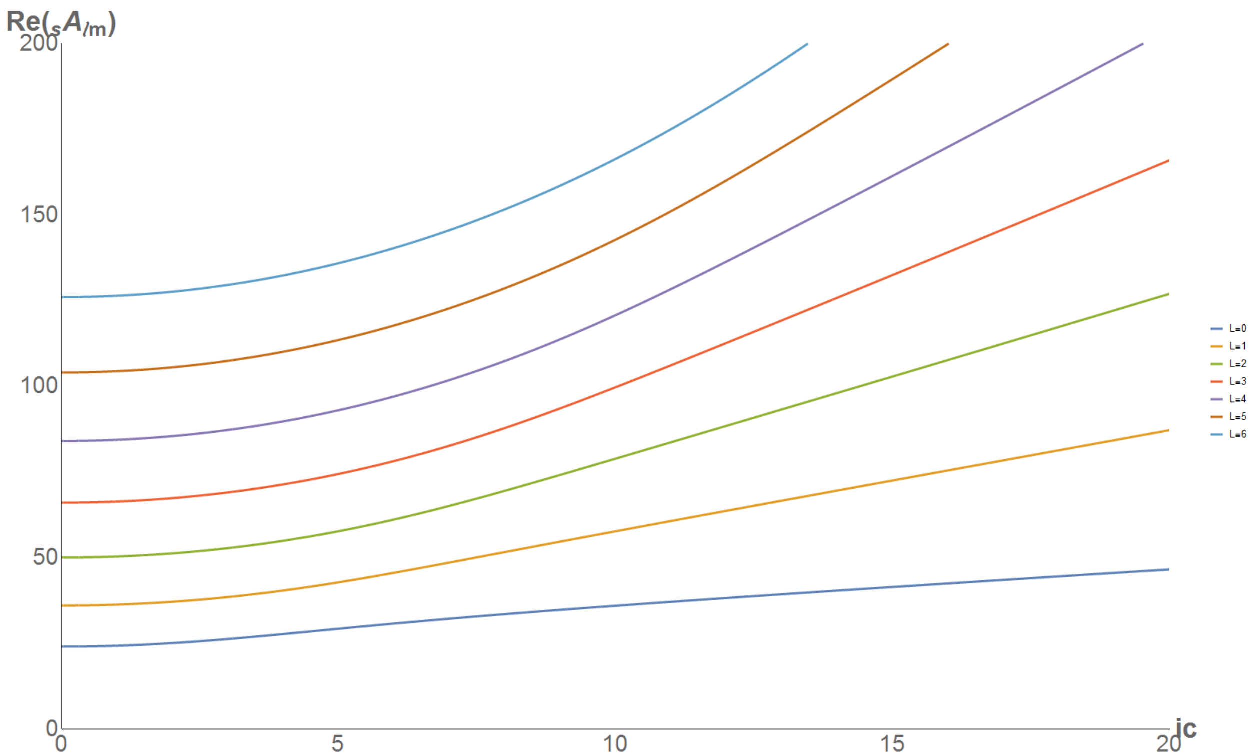


*Figure 1: Plot of Re(${}_sA_{lm}$) for SWSHs with m=5, s=2 from ic=0 to 20, and for L=0,...,6.*

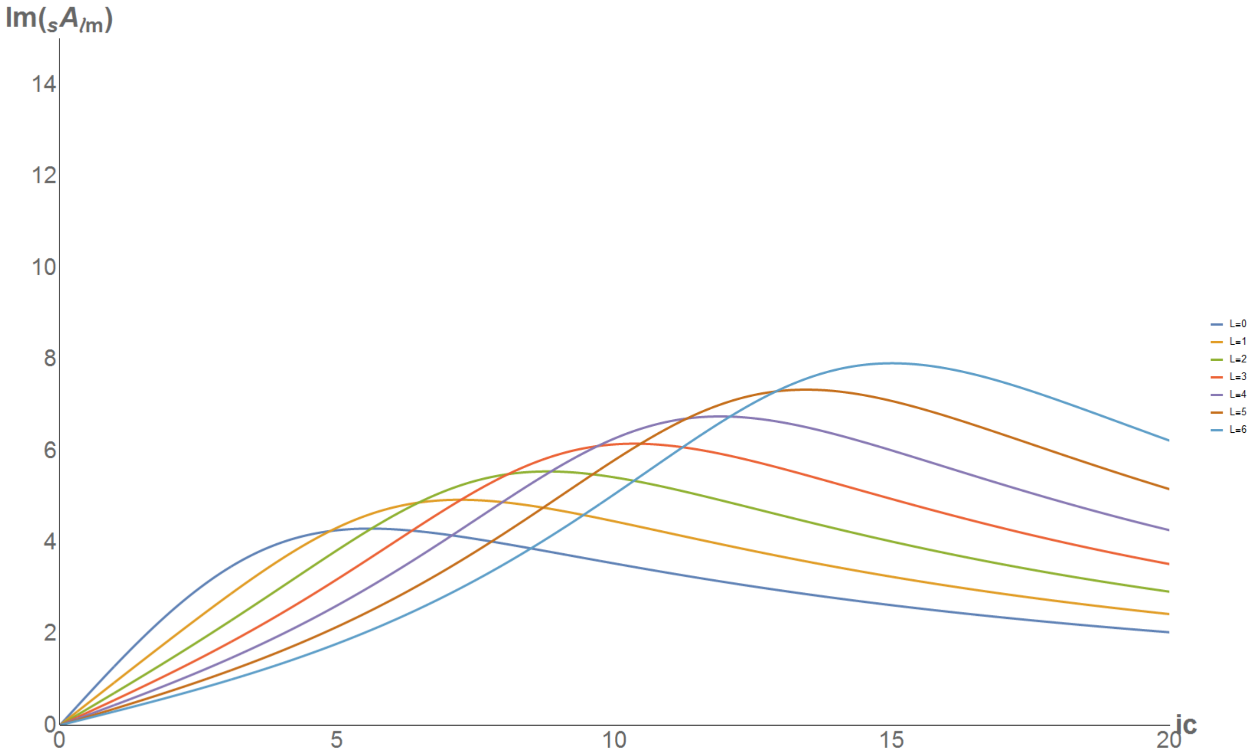


*Figure 2: Plot of Im($_sA_{lm}$) for SWSHs with m=5, s=2 from ic=0 to 20, and for L=0,...,6.*

All of the other sets of sequences for different values of $m$ and $s$ are similar, except in the 12 cases of $m = \pm 2$, $s = \pm 2, \pm 3$, and $m = \pm 3$, $s = \pm 3$. These will be discussed later. Also, for several of the imaginary plots, the imaginary contribution is simply zero. Figures 1 and 2 do not show the asymptotic behavior of the ${}_sA_{lm}(c)$. For this, we need to consider large values of $|c|$. Figures 3 and 4 show the log-log plot of the same data as in Figures 1 and 2, but to much larger values of $|c|$.

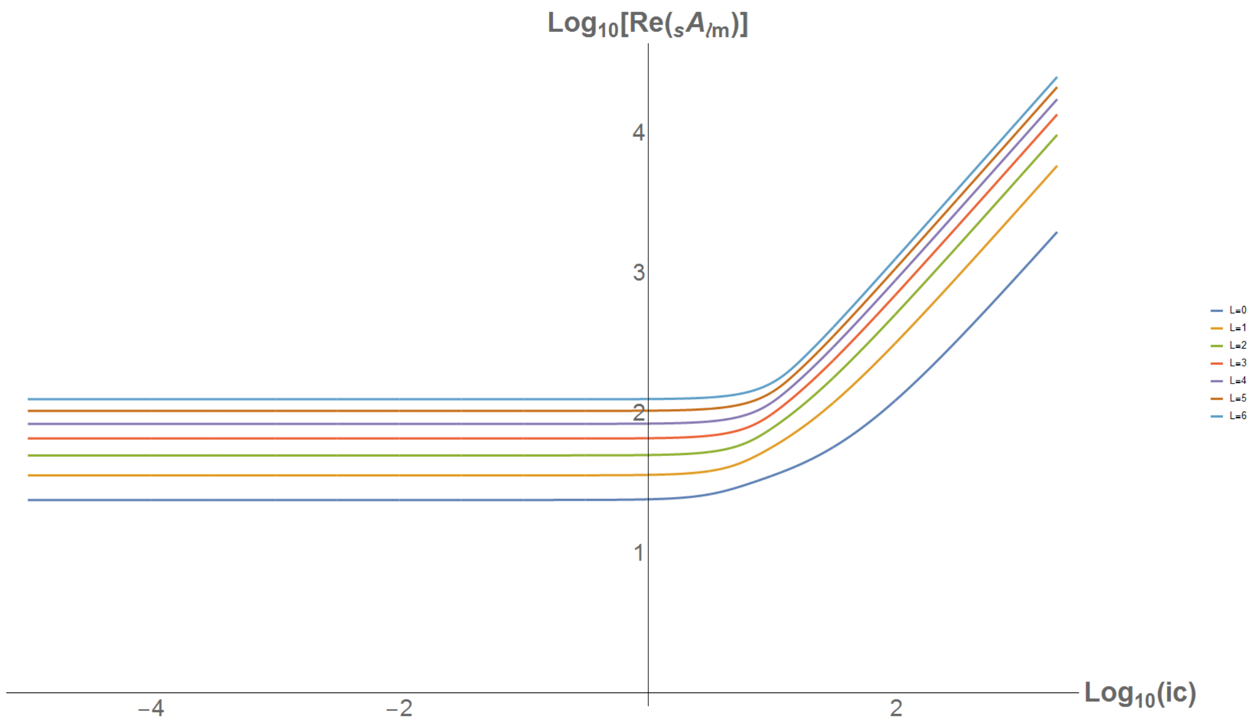


*Figure 3: Log-log Plot of $Re({}_sA_{lm})$ for SWSHs with m=5, s=2. The domain where Eq.(3.1) becomes applicable is $|c| \gtrsim 100$.*

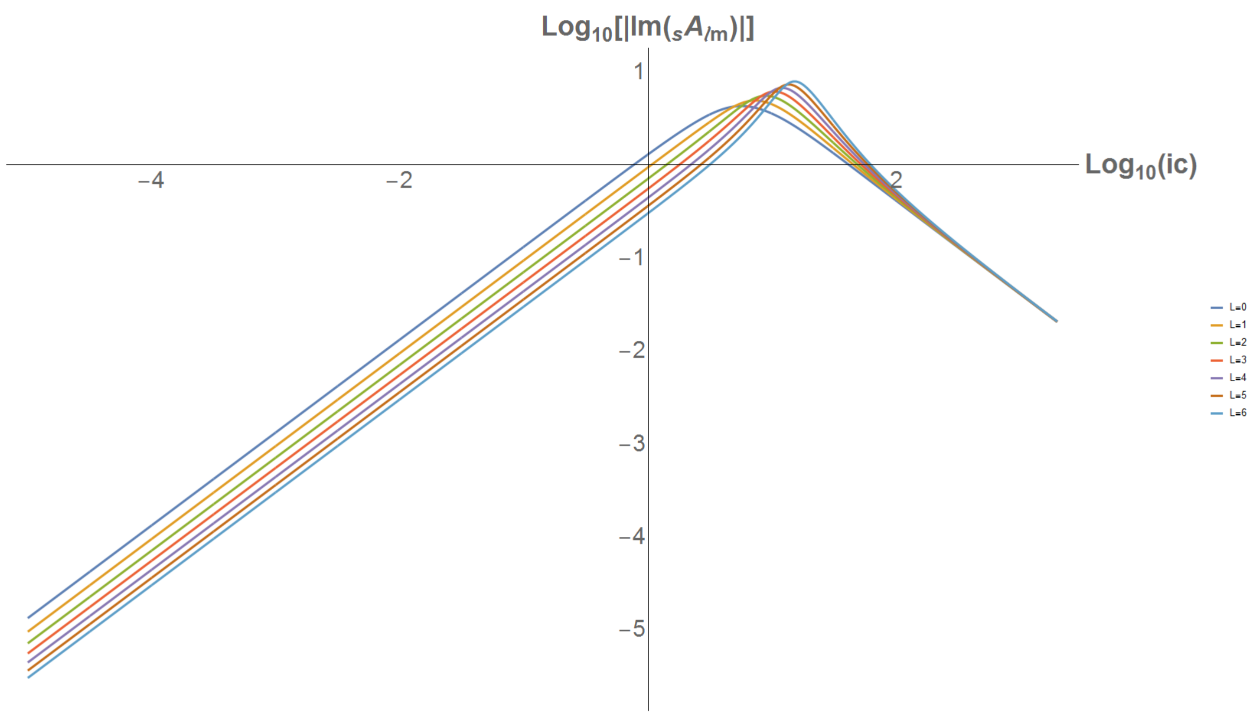


*Figure 4: : Log-log Plot of $Im({}_sA_{lm})$ for SWSHs with m=5, s=2. The domain where Eq.(3.1) becomes applicable is $|c| \gtrsim 100$.*

The real and imaginary contributions were fit separately. As can be seen in Figure 3, for the case of $m = 5$, $s = 2$ the behavior of the eigenvalues change around $|c| \gtrsim 10^2$. It is in this domain where Eq. (3.1) becomes applicable.

In order to fit for this data, we used a function of the form

$$ {}_sA_{lm} = B_1|c| + B_2 + B_3\frac{1}{|c|} + B_4\frac{1}{|c|^2} + B_5\frac{1}{|c|^3}, \tag{5.1} $$

where the $B_i$ are the fitting coefficients. The data was then used to perform a non-linear least-square fit for each term. When fitting for any particular term, the relevant fits for $B_i$ were calculated for each value of m, $s$, and $L$. The first term fitted was the leading order term, $B_1$. From equation (3.1), it is known that for the $s = 0$ case, the expected coefficient is $B_1 = 2L + 1$. Working under the assumption that this fit should be similar to the $s = 0$ case, the real part of the $B_1$ terms were then fit with the equation:

$$ B_1 = A_1L + A_2. \tag{5.2} $$

In order to confirm agreement between the generated data and the analytic approximation, this fit was checked for all $s = 0$ cases. For all cases, it was found that $A_1 = 2$ and $A_2 = 1$, which agrees with Eq.(3.1). These coefficients were then also checked for varying values of $s$.

For example, looking at the $m = 5$ case, the leading order coefficient, $B_1$, was pulled out for each value of $L$ and $s$. Next, all coefficients were grouped by their value of $s$. These coefficients were then again fitted for the terms $A_1$, and $A_2$ as they depend upon $L$ for each $s$ trajectory. If there is no $s$ dependence in the function, then one would expect to obtain the same linear $L$ dependence seen in Eq. (2.1). The linear term in $L$, $A_1$, is shown in Table 1.

| s | Fitted Term | Remainder | Fit Error |
|---|---|---|---|
| **-3** | 2.00 | 6.18E-10 | 3.13E-10 |
| **-2** | 2.00 | -5.77E-11 | 4.57E-11 |
| **-1** | 2.00 | -1.35E-10 | 3.69E-11 |
| **0** | 2.00 | -8.82E-12 | 1.80E-12 |
| **1** | 2.00 | -1.35E-10 | 3.70E-11 |
| **2** | 2.00 | -6.62E-11 | 5.27E-11 |
| **3** | 2.00 | 7.02E-10 | 3.52E-11 |

*Table 1: Table of Re($A_1$) for m=5.*

Here, the remainder term is what is left when we take the difference of the fitted term with the putative value; two in this case. So, as can be seen, each value of $s$ produced a fit for the $L$ term as predicted in equation (2.1), out to an error that can be effectively called zero. Similarly, this was done for the constant term, $A_2$ in Table 2.

| s | Fitted Term | Remainder | Fit Error |
|---|---|---|---|
| **-3** | 1.00 | 2.24E-09 | 9.47E-10 |
| **-2** | 1.00 | 2.64E-10 | 1.38E-10 |
| **-1** | 1.00 | 1.71E-10 | 1.12E-10 |
| **0** | 1.00 | 7.68E-12 | 5.46E-12 |
| **1** | 1.00 | 1.72E-10 | 1.12E-10 |
| **2** | 1.00 | 3.04E-10 | 1.59E-10 |
| **3** | 1.00 | 2.52E-09 | 1.07E-09 |

*Table 2: Table of Re($A_2$) for m=5.*

Similarly, the imaginary part of $B_1$ was extracted and fit to a linear function in $L$. Looking at these coefficients, Table 3 and 4 shows the least-square fits for the imaginary components of $A_1$ and $A_2$ respectively.

| s | Fitted Term | Fit Error |
|---|---|---|
| **-3** | -2.91E-09 | 3.73E-10 |
| **-2** | -2.42E-10 | 3.03E-11 |
| **-1** | -5.95E-11 | 7.45E-12 |
| **0** | 0.00 | 0.00 |
| **1** | -5.95E-11 | 7.45E-12 |
| **2** | -2.78E-10 | 3.49E-11 |
| **3** | -3.28E-09 | 4.21E-10 |

*Table 3: Table of Im($A_1$) for m=5..*

| s | Fitted Term | Fit Error |
|---|---|---|
| **-3** | 3.47E-09 | 1.13E-09 |
| **-2** | 2.46E-10 | 9.19E-11 |
| **-1** | 5.48E-11 | 2.26E-11 |
| **0** | 0.00 | 0.00 |
| **1** | 5.48E-11 | 2.26E-11 |
| **2** | 2.83E-10 | 1.06E-10 |
| **3** | 3.92E-09 | 1.28E-09 |

*Table 4: Table of Im($A_2$) for m=5.*

Similar values were retrieved for all values of $m = -5, \dots, 5$, all of which were consistent with these values for the $m = 5$ case. The $s = 0$ term is zero, since the eigenvalues are purely real in the $s = 0$ case. Since it was observed that there was no $s$ dependence for any of these leading order terms, it is concluded from the data that there is no $s$ dependence in the leading order term, aside from the dependence of $L$ upon $s$. So, to a high degree of confidence, it can be concluded that this term remains the same as seen in Eq.(3.1).

Once the lack of $s$ dependence was confirmed for $B_1$, this term could be replaced in Eq (5.1) to get:

(5.3)

$$_sA_{lm} = (2L+1)|c| + B_2 + B_3\frac{1}{|c|} + B_4\frac{1}{|c|^2} + B_5\frac{1}{|c|^3}.$$

This new fitting function was then used to extract the behavior of $B_2$. For this term, we first verified that the $s = 0$ case was the same as that predicted for the scalar spheroidal harmonics, $B_2 = -\left(\frac{1}{2}L^2 + \frac{1}{2}L + \frac{3}{4} - m^2\right)$. This, as in the leading-order term case, was shown to hold true for all eleven values of $m$ generated.

Similarly to the process for the first term, the second order term was then fitted for all values of $s$ and $L$ for a particular value of $m$ using the fitting function:

$$B_2 = -(A_3L^2 + A_4L + A_5). \tag{5.4}$$

After the fits, the values of $A_3$, $A_4$, and $A_5$ were extracted and fitted for dependence upon $s$. It was observed that $A_3$ and $A_4$ both had no dependency on $s$; however, the constant term, given by $A_5 = \frac{3}{4} - m^2$ in the $s = 0$ case, varied as $s$ was changed. For example, looking at the $m = 1$ case, the $A_5$ dependence on $s$ is displayed in Table 5.

| s | Fitted Term | Remainder | Fit Error |
|---|---|---|---|
| **-3** | -12.25 | -6.99E-10 | 9.853E-10 |
| **-2** | -6.25 | -7.15E-11 | 1.705E-10 |
| **-1** | -2.25 | 2.78E-11 | 2.394E-10 |
| **0** | -0.25 | -3.02E-10 | 2.507E-10 |
| **1** | -0.25 | 2.84E-11 | 2.394E-10 |
| **2** | -2.25 | -6.93E-11 | 1.402E-10 |
| **3** | -6.25 | -6.99E-10 | 9.846E-10 |

*Table 5: Table of Re($A_5$), showing the s dependence.*

This function demonstrated clear quadratic behavior, so when fitted with a quadratic function, we found that $A_5 = \frac{3}{4} - m^2 + s - s^2$. These fits come with an error of $2.459 \cdot 10^{-11}$ for the $s^2$ term, and $4.259 \cdot 10^{-11}$ for the $s$ term. Fits for all other values of $m$ returned coefficients with similar errors for this correction. In the imaginary case, similarly to the case of $B_1$, all imaginary terms were zero for constant order with low error. This means that the overall term is:

$$B_2 = -\left(\frac{1}{2}L^2 + \frac{1}{2}L + \frac{3}{4} - m^2 + s - s^2\right). \tag{5.5}$$

This term was then added to the fit model to give the equation:

$${}_sA_{lm} = (2L+1)|c| - \left(\frac{1}{2}L^2 + \frac{1}{2}L + \frac{3}{4} - m^2 + s - s^2\right) + B_3\frac{1}{|c|} + B_4\frac{1}{|c|^2} + B_5\frac{1}{|c|^3}, \tag{5.6}$$

and fits for the third order term, $B_3$, were generated. For this term, in the $s = 0$ case, the behavior is expected to go as $-(2L+1)\left(\frac{1}{16}L^2 + \frac{1}{16}L + \frac{3}{16} - \frac{1}{2}m^2\right) = -[2L^3 + 3L^2 + L(7 - 16m^2) + 3 - 8m^2]/16$, and this relation was confirmed to hold for the data generated.

Due to the length of the $s = \pm 3$ terms, which have not been calculated to as large values of $c$ as $s = -2, \ldots, 2$, they were not resolved to high enough accuracy to make significant contributions out to the $B_3$ term. So using values of $s = -2, \ldots, 2$ and in the case of $m = 0$, the coefficients $B_3$ are shown in Table 6.

| s | L | Fit Parameter | Fit Error |
|---|---|---|---|
| **-2** | 0 | -61.00 | 6.266E-07 |
| **-2** | 1 | -177.00 | 8.234E-06 |
| **-2** | 2 | -275.00 | 1.824E-05 |
| **-2** | 3 | -343.00 | 1.872E-05 |
| **-2** | 4 | -369.00 | 8.852E-06 |
| **-2** | 5 | -341.01 | 8.876E-05 |
| **-1** | 0 | -13.00 | 5.188E-08 |
| **-1** | 1 | -33.00 | 7.887E-08 |
| **-1** | 2 | -35.00 | 1.188E-06 |
| **-1** | 3 | -7.00 | 6.111E-06 |

| | | | |
|---|---|---|---|
| **-1** | 4 | 63.00 | 1.732E-05 |
| **-1** | 5 | 187.00 | 3.641E-05 |
| **0** | 0 | 3.00 | 1.280E-09 |
| **0** | 1 | 15.00 | 1.490E-08 |
| **0** | 2 | 45.00 | 9.023E-08 |
| **0** | 3 | 105.00 | 3.757E-07 |
| **0** | 4 | 207.00 | 1.225E-06 |
| **0** | 5 | 363.00 | 3.361E-06 |
| **1** | 0 | -13.00 | 5.723E-08 |
| **1** | 1 | -33.00 | 8.758E-08 |
| **1** | 2 | -35.00 | 1.308E-06 |
| **1** | 3 | -7.00 | 6.744E-06 |
| **1** | 4 | 63.00 | 1.914E-05 |
| **1** | 5 | 187.00 | 4.028E-05 |
| **2** | 0 | -61.00 | 6.481E-07 |
| **2** | 1 | -177.00 | 8.528E-06 |
| **2** | 2 | -275.00 | 1.891E-05 |
| **2** | 3 | -343.00 | 1.944E-05 |
| **2** | 4 | -369.00 | 9.058E-06 |
| **2** | 5 | -341.01 | 9.179E-05 |

*Table 6: Fits for $B_3$ for m=4 and various values of s and L.*

Since the $s = 0$ term went as a cubic in $L$, the extracted values for $B_3$ were fit for a third-degree polynomial. It was found that the $L^3$ and $L^2$ terms remained unchanged. For the linear term, the fits all revealed the presence of the term $-2Ls^2 = -\frac{32Ls^2}{16}$. This coefficient came with an error of $1.64 \cdot 10^{-7}$. This makes the equation for $B_3$:

$$B_3 = -\frac{[2L^3 + 3L^2 + L(7 - 16m^2 - 32s^2) + 3 - 8m^2 + f(s,m)]}{16}. \tag{5.7}$$

After adding in this behavior, the values of the function $f(s,m)$ were extracted. Table 7 shows the behavior for $m = 4$.

| s | L | Fit Parameter | Remainder | Fit Error |
|---|---|---|---|---|
| **-2** | 0 | -64.00 | -1.873E-05 | 9.055E-08 |
| **-2** | 1 | -64.00 | 2.292E-05 | 3.803E-07 |
| **-2** | 2 | -64.00 | 9.919E-05 | 5.593E-07 |
| **-2** | 3 | -64.00 | 1.946E-04 | 8.202E-07 |
| **-2** | 4 | -64.00 | 2.798E-04 | 8.758E-07 |
| **-2** | 5 | -64.00 | 3.269E-04 | 1.512E-06 |
| **-1** | 0 | -16.00 | -2.300E-06 | 9.421E-08 |
| **-1** | 1 | -16.00 | 1.057E-05 | 4.043E-07 |
| **-1** | 2 | -16.00 | 2.578E-05 | 5.452E-07 |
| **-1** | 3 | -16.00 | 3.446E-05 | 7.795E-07 |
| **-1** | 4 | -16.00 | 1.542E-05 | 8.601E-07 |
| **-1** | 5 | -16.00 | -6.047E-05 | 1.440E-06 |
| **0** | 0 | 1.147E-06 | 3.129E-06 | 3.650E-07 |
| **0** | 1 | 6.397E-06 | 9.963E-06 | 1.421E-06 |
| **0** | 2 | 6.570E-06 | 2.184E-05 | 2.105E-06 |
| **0** | 3 | 1.001E-05 | 2.412E-05 | 3.070E-06 |
| **0** | 4 | 1.109E-05 | 1.540E-05 | 3.247E-06 |
| **0** | 5 | 1.032E-05 | 2.476E-05 | 5.422E-06 |
| **1** | 0 | -16.00 | -1.786E-06 | 8.462E-08 |
| **1** | 1 | -16.00 | 9.387E-06 | 3.563E-07 |
| **1** | 2 | -16.00 | 2.538E-05 | 4.521E-07 |
| **1** | 3 | -16.00 | 3.308E-05 | 7.548E-07 |
| **1** | 4 | -16.00 | 1.548E-05 | 8.178E-07 |
| **1** | 5 | -16.00 | -5.872E-05 | 1.178E-06 |
| **2** | 0 | -64.00 | -1.718E-05 | 9.178E-08 |
| **2** | 1 | -64.00 | 2.083E-05 | 3.716E-07 |
| **2** | 2 | -64.00 | 9.078E-05 | 5.470E-07 |
| **2** | 3 | -64.00 | 1.767E-04 | 7.520E-07 |
| **2** | 4 | -64.00 | 2.549E-04 | 8.504E-07 |
| **2** | 5 | -64.00 | 2.977E-04 | 1.418E-06 |

*Table 7: Fits for $f(s,m)$ for m=4 and various values of s and L.*

This function clearly behaves as $f(s,m) = -16s^2$, which was confirmed for all values of $m$. This brings the real component of the equation to:

(5.8)

$$B_3 = -\frac{[2L^3 + 3L^2 + L(7 - 16m^2 - 32s^2) + 3 - 8m^2 - 16s^2]}{16}$$
$$= -\frac{(2L+1)[L(L+1) + 3 - 8m^2 - 16s^2]}{16}.$$

A similar fit for the imaginary term was done. $B_3$ for $m = 5$ is shown in Table 8.

| s | L | Fit Parameter | Remainder | Fit Error |
|---|---|---|---|---|
| **-2** | 0 | 640 | -2.03E-05 | 1.198E-07 |
| **-2** | 1 | 640 | -5.40E-05 | 3.216E-07 |
| **-2** | 2 | 640 | -6.50E-05 | 3.891E-07 |
| **-2** | 3 | 640 | -3.71E-05 | 2.267E-07 |
| **-2** | 4 | 640 | 4.58E-05 | 2.638E-07 |
| **-2** | 5 | 640 | 2.00E-04 | 1.180E-06 |
| **-1** | 0 | 160 | -4.06E-06 | 9.412E-08 |
| **-1** | 1 | 160 | -1.04E-05 | 1.195E-07 |
| **-1** | 2 | 160 | -1.10E-05 | 6.622E-08 |
| **-1** | 3 | 160 | -2.09E-06 | 1.400E-08 |
| **-1** | 4 | 160 | 2.05E-05 | 1.200E-07 |
| **-1** | 5 | 160 | 6.07E-05 | 3.621E-07 |
| **0** | 0 | 0.00 | 0.00 | 0.00 |
| **0** | 1 | 0.00 | 0.00 | 0.00 |
| **0** | 2 | 0.00 | 0.00 | 0.00 |
| **0** | 3 | 0.00 | 0.00 | 0.00 |
| **0** | 4 | 0.00 | 0.00 | 0.00 |
| **0** | 5 | 0.00 | 0.00 | 0.00 |
| **1** | 0 | 160 | -4.06E-06 | 9.412E-08 |
| **1** | 1 | 160 | -1.04E-05 | 1.195E-07 |
| **1** | 2 | 160 | -1.10E-05 | 6.622E-08 |
| **1** | 3 | 160 | -2.09E-06 | 1.400E-08 |
| **1** | 4 | 160 | 2.05E-05 | 1.120E-07 |
| **1** | 5 | 160 | 6.07E-05 | 3.621E-07 |
| **2** | 0 | 640 | -2.25E-05 | 1.329E-07 |
| **2** | 1 | 640 | -6.00E-05 | 3.569E-07 |
| **2** | 2 | 640 | -7.22E-05 | 4.322E-07 |
| **2** | 3 | 640 | -4.13E-05 | 2.529E-07 |
| **2** | 4 | 640 | 5.07E-05 | 2.916E-07 |
| **2** | 5 | 640 | 2.22E-04 | 1.306E-06 |

*Table 8: Fits for Im($B_3$).*

As can be seen in the data, there was no $L$ dependence in Im($B_3$), but clear $s$ dependence. This particular term goes as $160is^2$ with an error of $2.620 \cdot 10^{-5}$. When looking at all fits for varying values of $m$, it is seen that this coefficient goes as $32ims^2$.

Because the fits were done along the negative imaginary axis of $c$, this brings the total equation for the imaginary components of the eigenvalue this far to:

$$\mathrm{Im}({}_sA_{lm}) = \frac{32ims^2}{16|c|} = \frac{2ims^2}{|c|} = \frac{2ms^2}{c}. \tag{5.9}$$

In this form, the contribution to $B_3$ is consistent with the fundamental symmetry of the separation constant ${}_sA^*_{lm}(c) = {}_sA_{lm}(c^*)$.

## 6. Irregularities

While fitting these curves, large errors occurred for $m = \pm 2$. For example, in the case of the leading order term, we get errors in both values of $m$ for the values of $s = \pm 2$ and $\pm 3$. In the case of $m = 2$, Table 9 shows the behavior of the fits for $A_1$.

| s | Fitted Term | Fit Error |
|---|---|---|
| **-3** | 132.80 | 4.970E+02 |
| **-2** | -520.25 | 6.109E+02 |
| **-1** | 2.00 | 1.297E-11 |
| **0** | 2.00 | 3.127E-13 |
| **1** | 2.00 | 1.183E-11 |
| **2** | -524.27 | 6.156E+02 |
| **3** | 132.493 | 5.035E+02 |

*Table 9: Fits for Re($A_1$) of m=2.*

Table 9 is fitting the same terms as seen in Table 1, but for the anomalous case with $m = 2$. Notice that the fits remain unchanged for $s = -1, 0,$ and 1. This is seen again in the fits for $A_2$ as shown in Table 10.

| s | Fitted Term | Fit Error |
|---|---|---|
| **-3** | 437.99 | 1.505E+03 |
| **-2** | 2319.88 | 1.850E+03 |
| **-1** | 1.00 | 3.928E-11 |
| **0** | 1.00 | 9.468E-13 |
| **1** | 1.00 | 3.582E-11 |
| **2** | 2337.77 | 1.864E+03 |
| **3** | 443.64 | 1.524E+03 |

*Table 10: Fits for Re($A_2$) of m=2.*

This table should compare directly to Table 2. Again, we see very large error for $s = \pm 2, \pm 3$ in this term. It is then evident that there is no linear dependence agreement between various $L$ values for $m = 2$, $s = \pm 2, \pm 3$. Similar errors were found for the $m = \pm 3$, $s = \pm 3$ coefficients as well. Figure 5 shows the real contribution of the $m = 2$, $s = 2$ case.

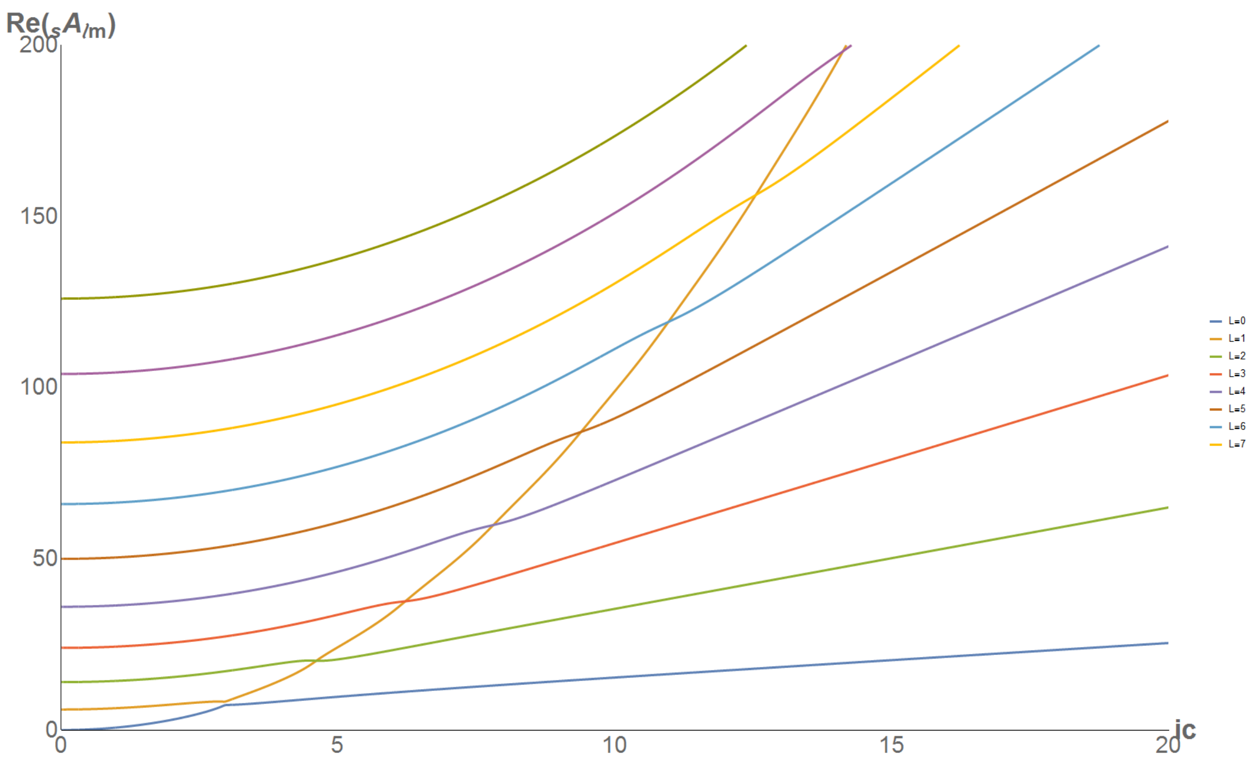


*Figure 5: Plot of different L trajectories for m=2, s=2 data.*

For reference, Figure 5 should compare directly with the $m = 5$, $s = 2$ case shown in Figure 1. As can be seen here, there is a deflection-like event going on around $c = -3i$ between the $L = 0$ and $L = 1$ lines. There is also an irregularity for the $L = 1$ line. In order to better understand the type of behavior happening here Figure 5 shows a magnified view near the deflection.

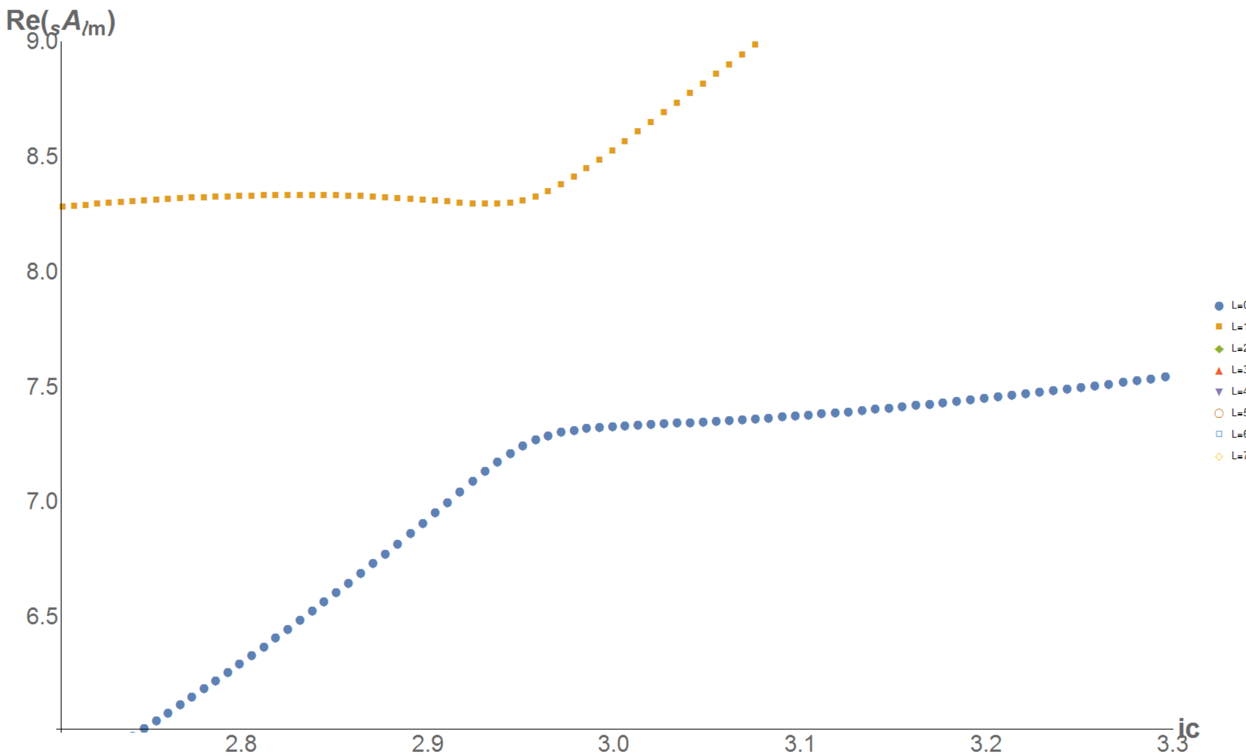


*Figure 6: Zoom in of Figure 5 at the deflection-like event occurring between L=0 and L=1.*

It can be seen here that there is no intersection of the $L = 0$ and $L = 1$ lines, and that there is no jump occurring between these two lines on the graph. Intersections with other lines can be observed as in the intersection between the $L = 1$ and $L = 2$ lines as seen in Figure 7.

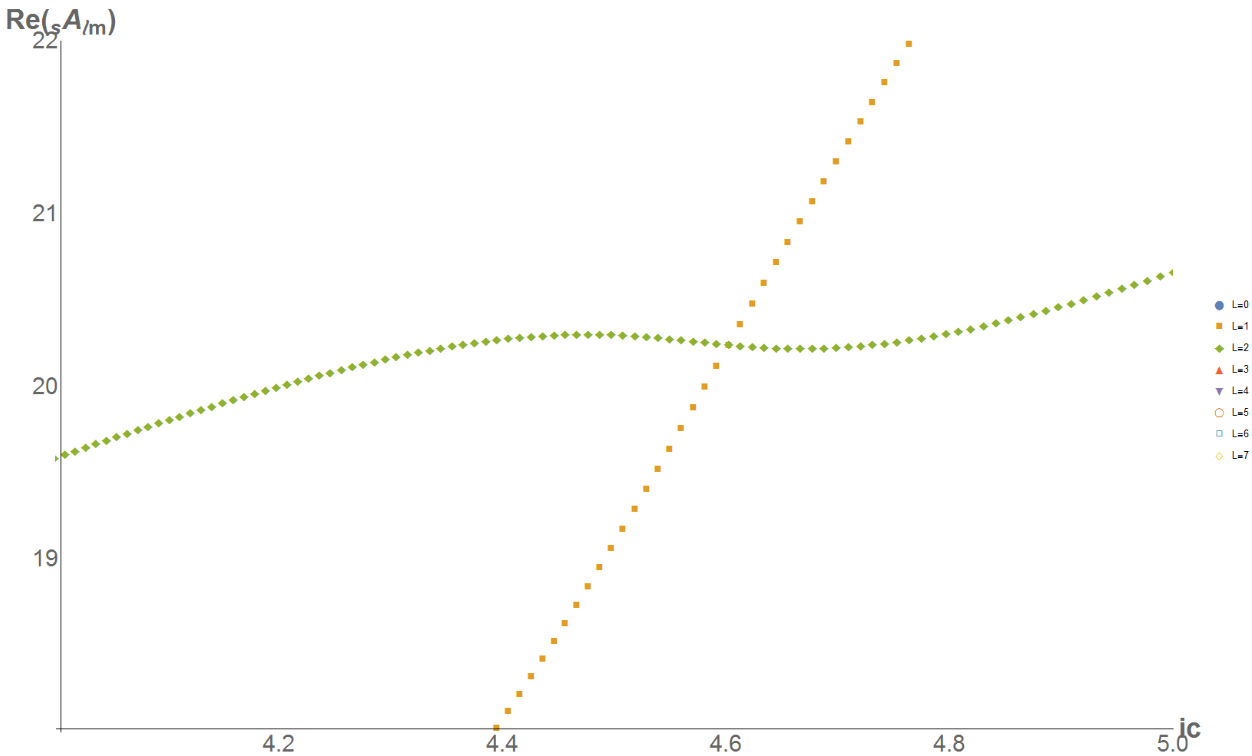


*Figure 7 Zoom in of Figure 5 at the intersecting occurring between L=1 and L=2.*

It can be seen that there is no deflection; rather, the $L = 1$ and $L = 2$ lines cross. Figure 7 is similar to all other intersections of the $L = 1$ line with lines $L = 3, \ldots, 6$ in this data set. Figures 5-7 also illustrate well the anomalous behavior that occurs for $m = \pm 2$, $s = \pm 2$, where large errors are being returned in the data set.

Exploring this behavior further, in the cases of $m = \pm 2$, $s = \pm 3$, we get similarly complicated plots. Particularly in the case of $m = 2$, $s = 3$, Figure 8 shows $\mathrm{Re}({}_sA_{lm})$.

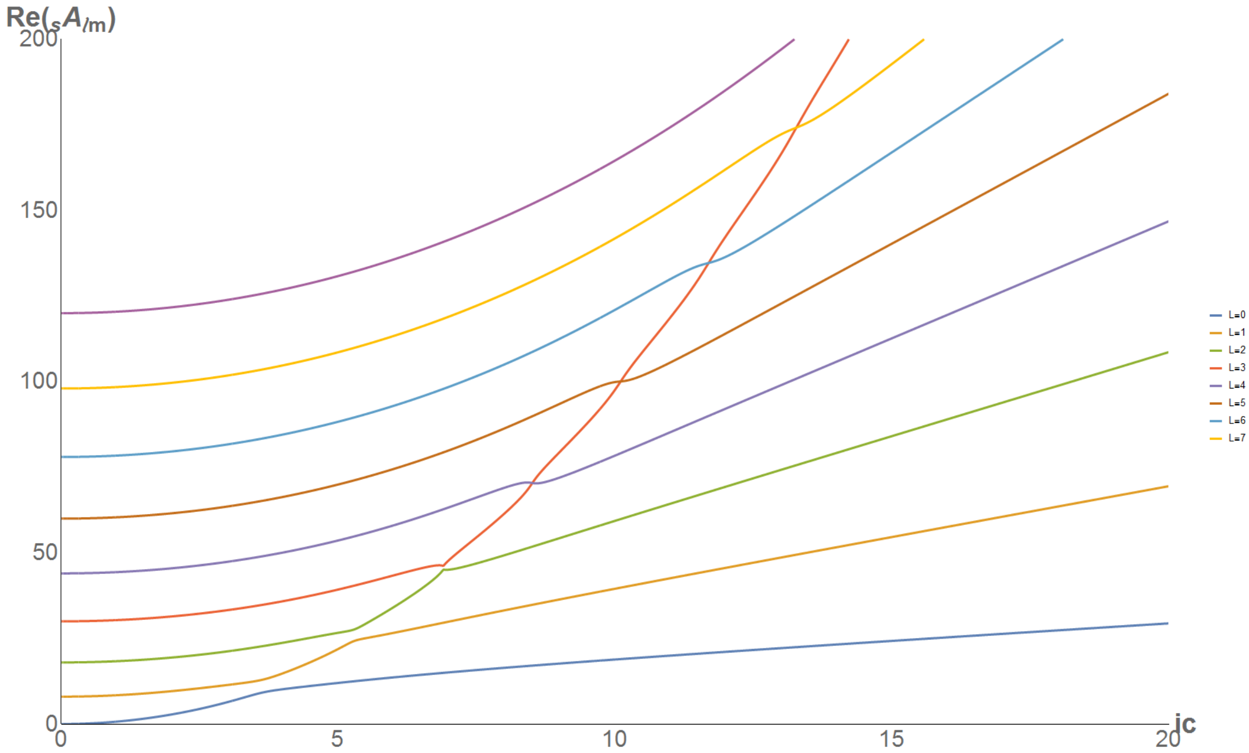


*Figure 8: Plot of different L trajectories for m=2, s=3 data.*

Figure 8 is characteristic of the behavior for the other values of m= $\pm2$,$s = \pm3$. Lastly, this anomalous behavior can be seen again for $m = \pm3$, $s = \pm3$. Figure 9 shows the case of $m = 3$, $s = 3$.

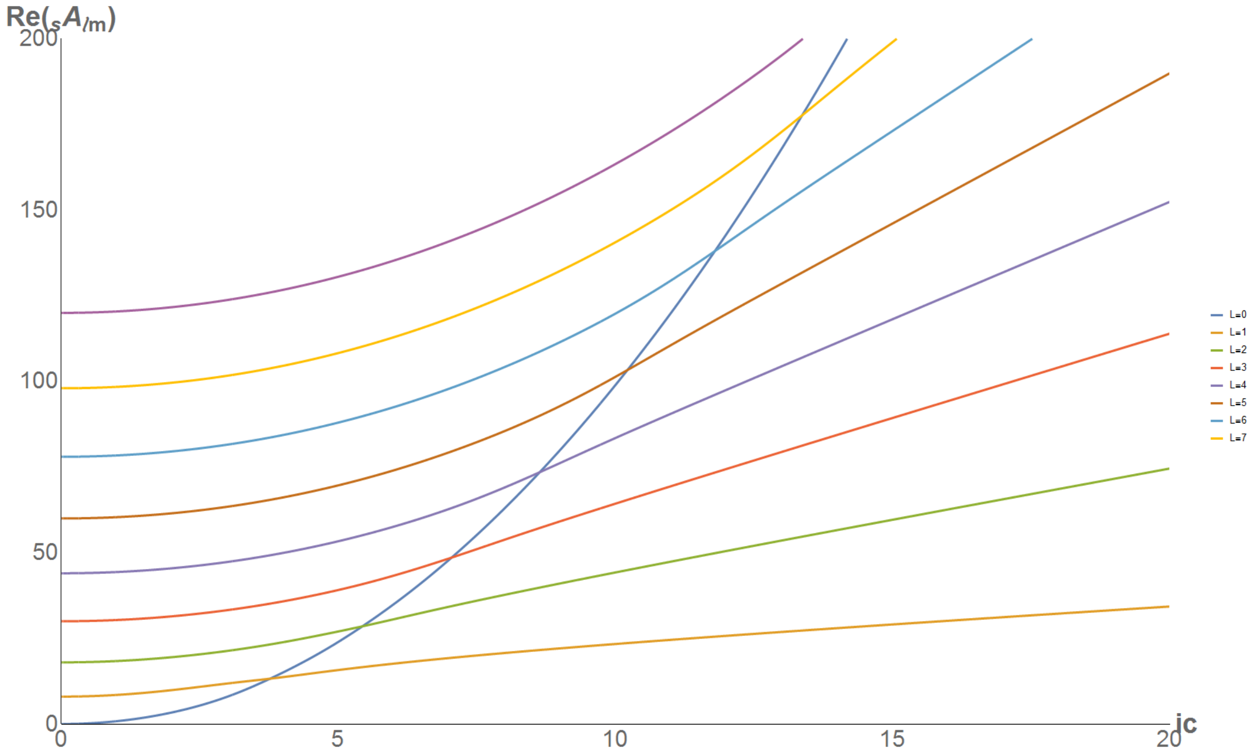


*Figure 9: Plot of different L trajectories for m=2, s=3 data.*

Again, this graph is representative of the other cases for $m = \pm 3$, $s = \pm 3$. We have not yet fully investigated the cause of this behavior.

## 7. Conclusion

The results of the fits yield a corrected form of equation (2.1):

(7.1)

$$
\begin{aligned}
{}_sA_{lm} = {} & |c|(2L+1) - \left(\frac{1}{2}L^2 + \frac{1}{2}L + \frac{3}{4} - m^2 + s - s^2\right) \\
& - \frac{(2L+1)[L(L+1) + 3 - 8m^2 - 16s^2]}{16|c|} - \frac{2ms^2}{c} + \vartheta\left(\frac{1}{|c|^2}\right),
\end{aligned}
$$

It was also shown that there is a clear anomalous, yet correct, behavior for the cases of $m = \pm 2$, $s = \pm 2, \pm 3$ and $m = \pm 3$, $s = \pm 3$. In these cases, a particular value of $L$ is the set of eigenvalues exhibits the behavior which makes these fits fail. This may be one of the reasons why no one has been able to approximate an analytic solution to resolving these eigenvalues. In the future, it will be necessary to separate out the anomalous sequences, and fit them separately. We will also want to check that the non-anomalous values of $L$ follow the fit for Eq. (6.1). We would also like to extend these fits to include the $B_4$ term and add it to Eq. (6.1).

[1] S. A. Teukolsky, Astrophys. J. **185**, 635 (1973)

[2] Gregory B. Cook* and Maxim Zalutskiy, Physical Review D **90**, 124021 (2014)

[3] Tevian Dray, J Math Phys. **26**, 1030 (1985)

[4] Flammer, C., Spheroidal Wave Functions, Stanford University Press, Stanford, USA (1957)

[5] Abramowitz, Milton, and Stegun, Irene A., Handbook of Mathematical Functions, Dover Publications, New York, USA (1964)

[6] Emanuele Bert, Vitor Cardoso, Marc Casals, Physical Review D **73**, 024013 (2006)

[7] Morse, P.M., and Feshbach, H., Methods of Theoretical Physics, Part II, pp.1502 ff., McGraw-Hill, New Yord, USA (1953)

## 8. Appendix

Here is a list of all real and imaginary Log-Log plots grouped by value of $m$ and $s$ for all zero and positive values of $m$. Since the eigenvalue is purely real when $s = 0$ and $m = 0$, imaginary $s = 0$ and $m = 0$ plots are excluded from this list.

$$m = 0$$

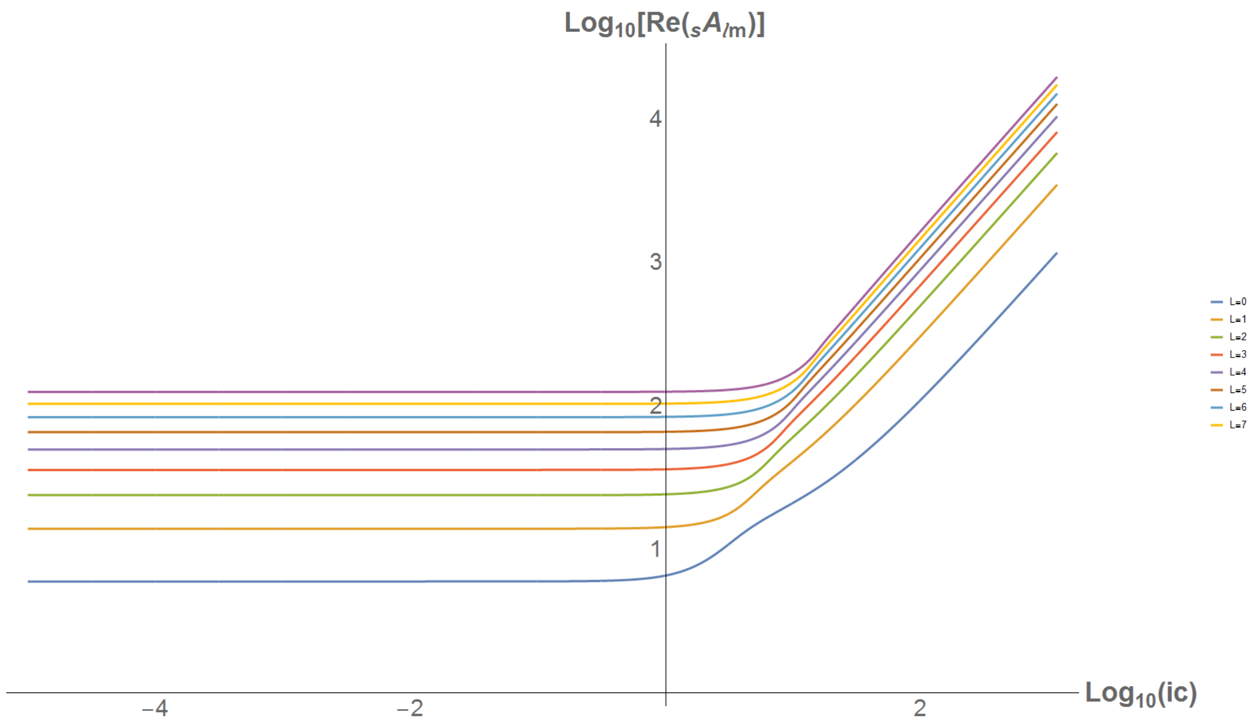


*Appendix 1: Log-log plot of $Re({}_sA_{lm})$ for SWSHs with m=0, s=-3 from ic=0 to 20, and for L=0,...,6.*

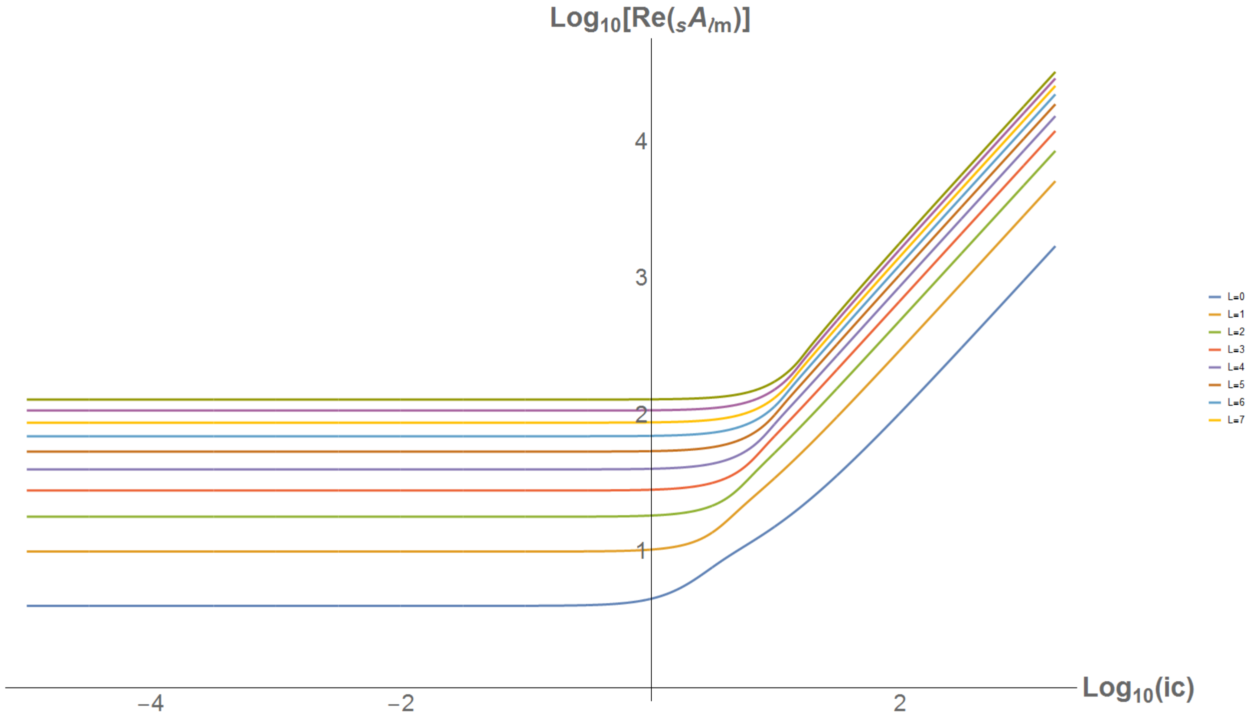


*Appendix 2: Log-log plot of Re($_sA_{lm}$) for SWSHs with m=0, s=-2 from ic=0 to 20, and for L=0,...,6*

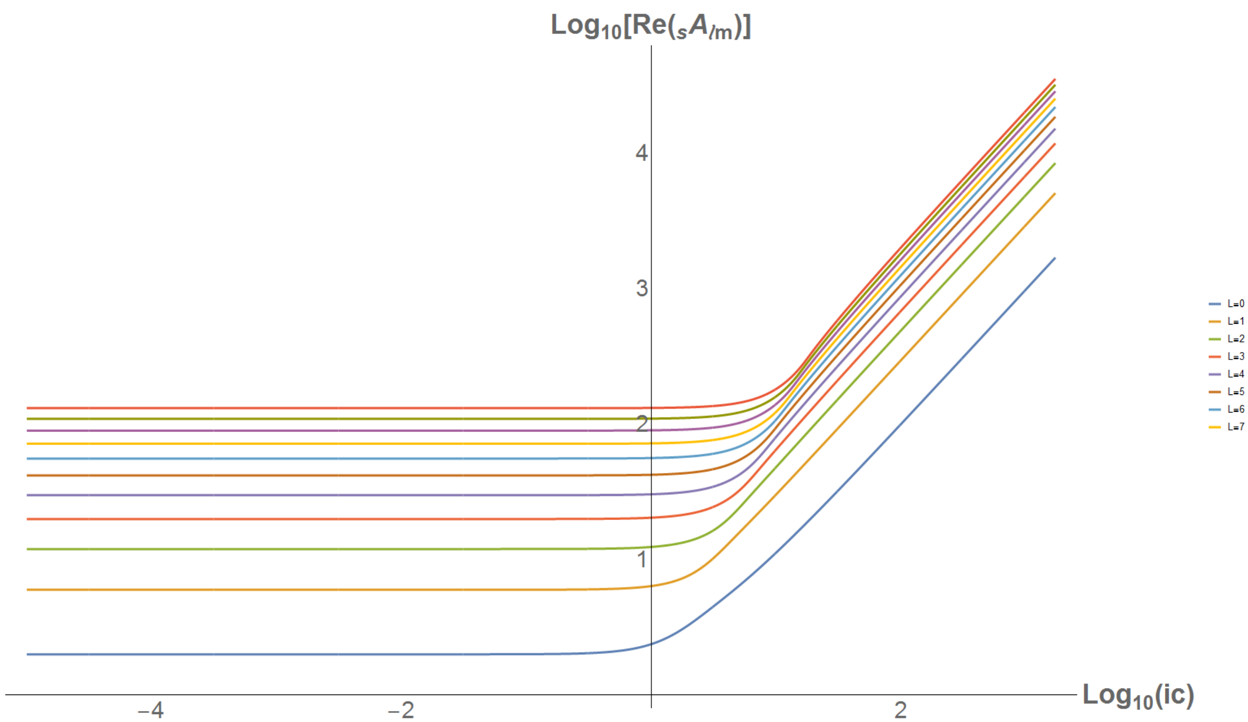


*Appendix 3: Log-log plot of Re($_sA_{lm}$) for SWSHs with m=0, s=-1 from ic=0 to 20, and for L=0,...,6.*

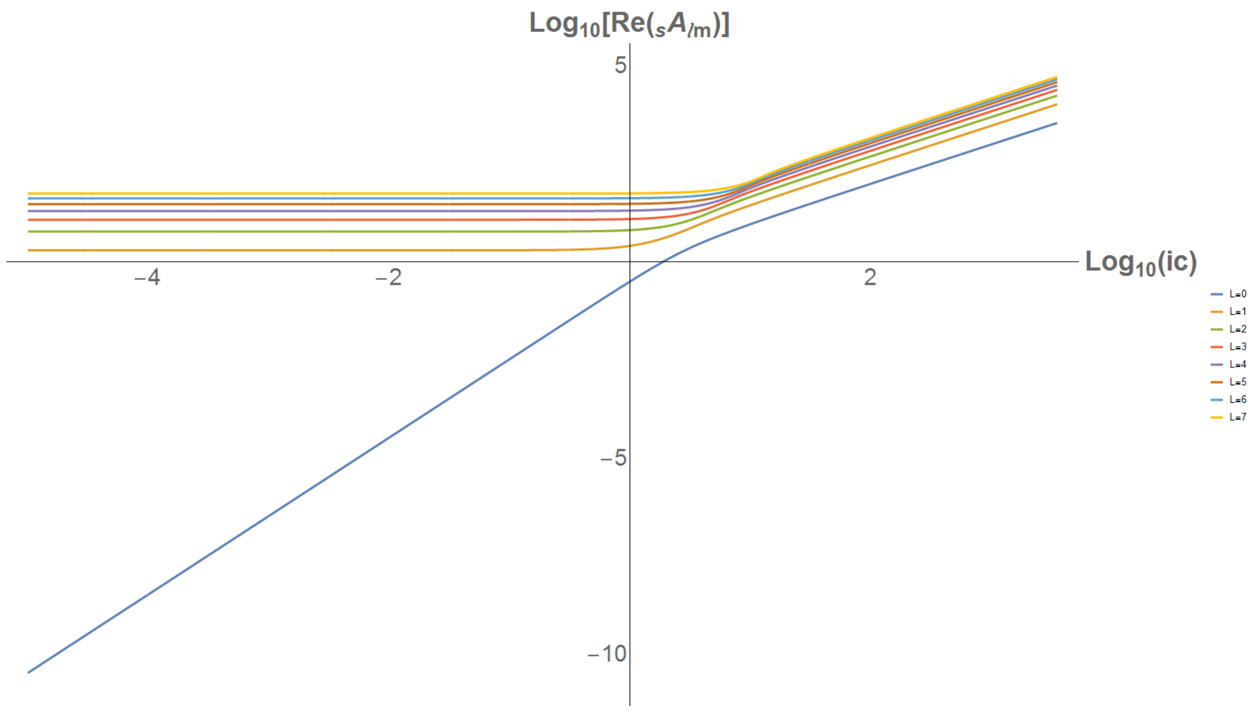


*Appendix 4: Log-log plot of Re($_sA_{lm}$) for SWSHs with m=0, s=0 from ic=0 to 20, and for L=0,...,6.*

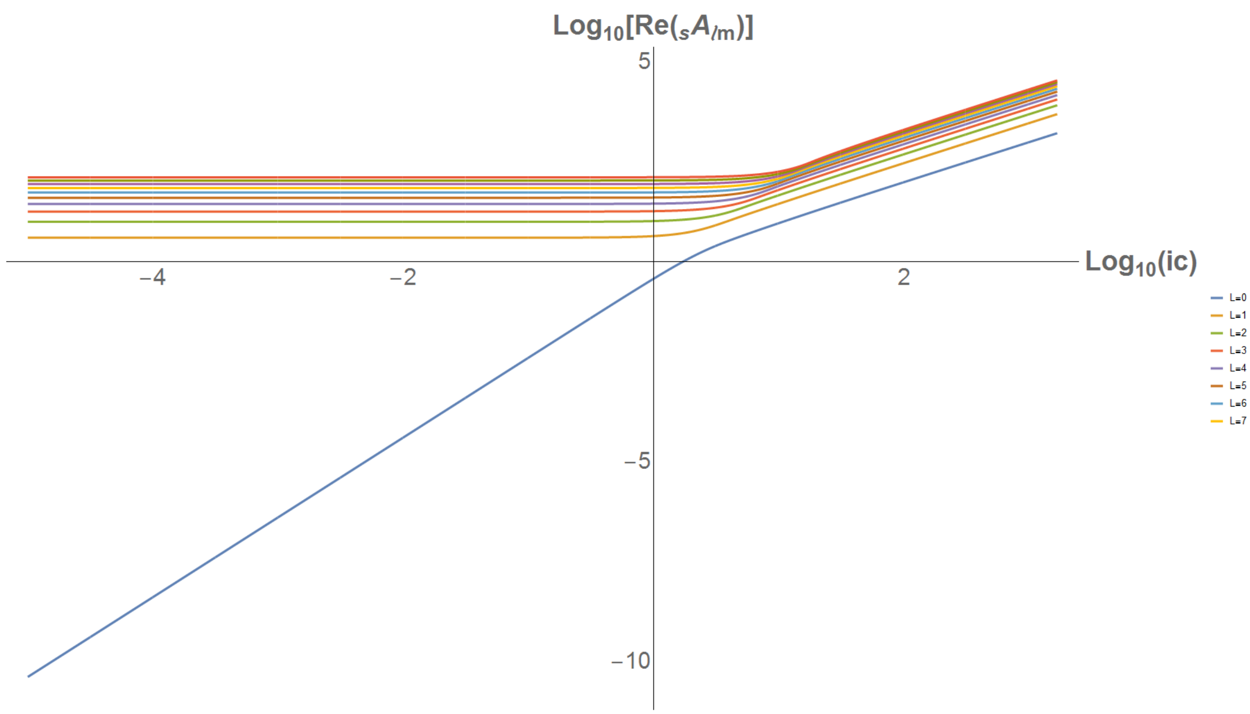


*Appendix 5: Log-log plot of Re($_sA_{lm}$) for SWSHs with m=0, s=1 from ic=0 to 20, and for L=0,...,6.*

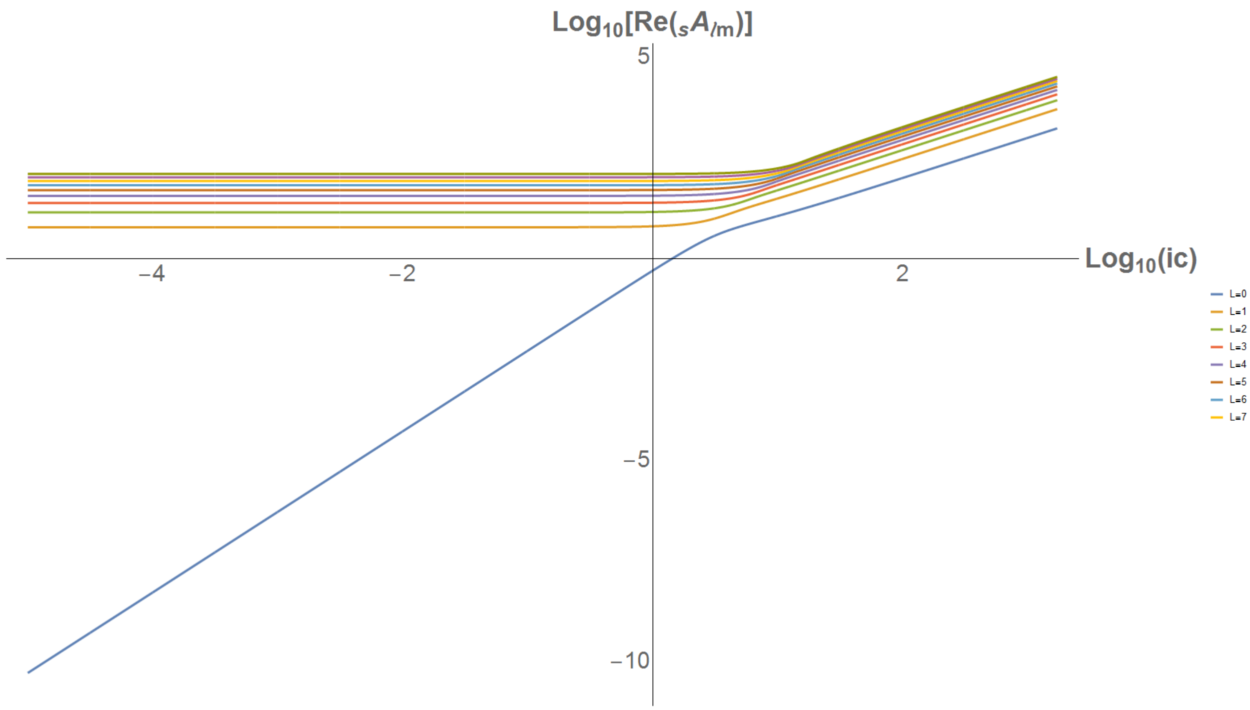


*Appendix 6: Log-log plot of $Re({}_sA_{lm})$ for SWSHs with m=0, s=2 from ic=0 to 20, and for L=0,...,6.*

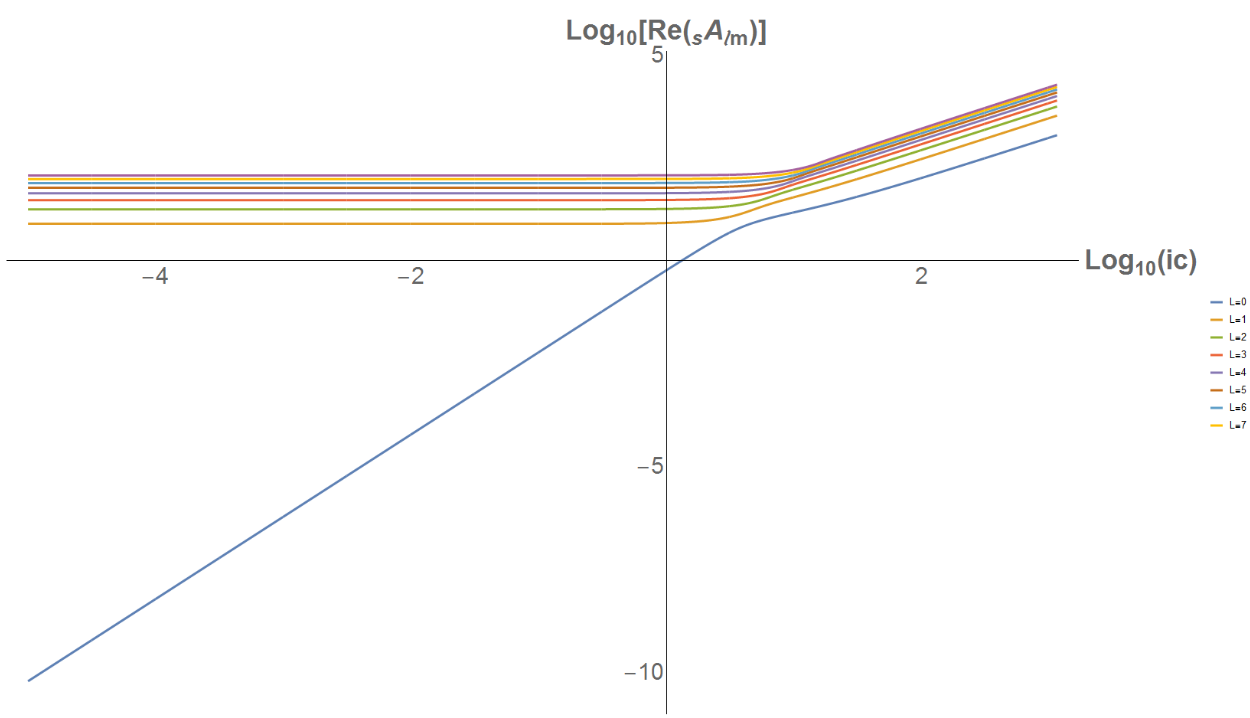


*Appendix 7: Log-log plot of $Re({}_sA_{lm})$ for SWSHs with m=0, s=3 from ic=0 to 20, and for L=0,...,6.*

m = 1

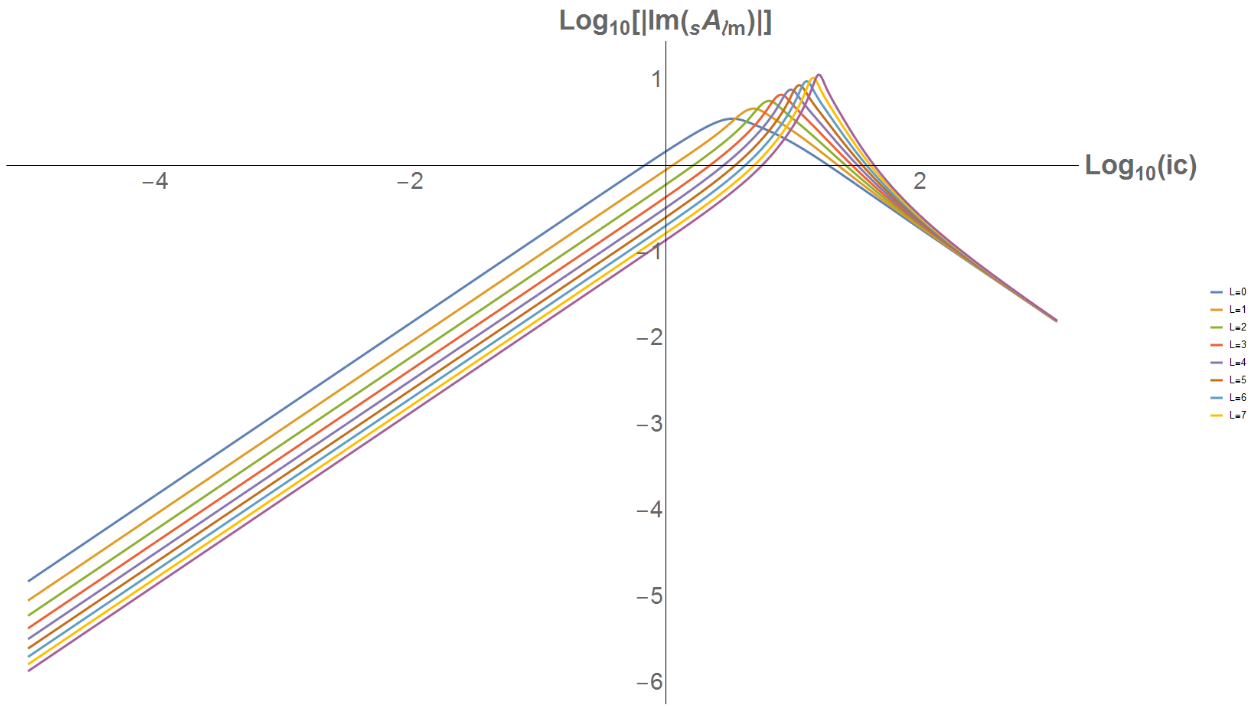


*Appendix 8: Log-log plot of Im($_sA_{lm}$) for SWSHs with m=1, s=-3 from ic=0 to 20, and for L=0,...,6.*

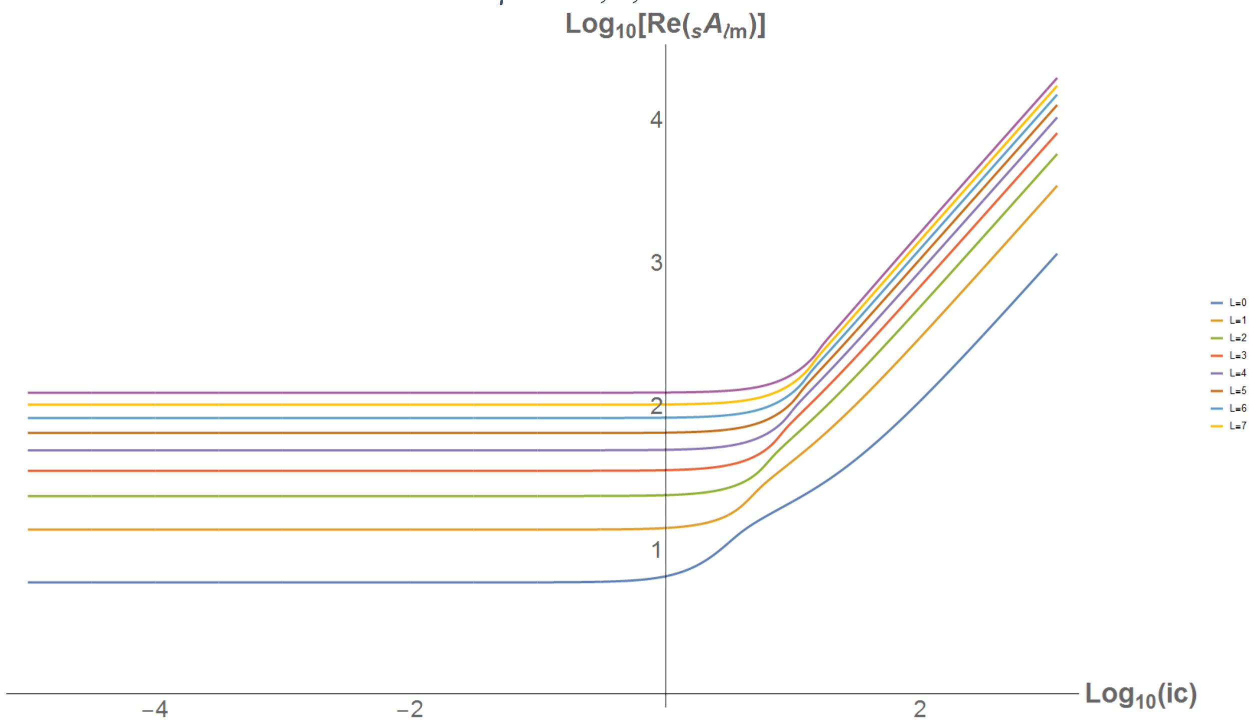


*Appendix 9: Log-log plot of Re($_sA_{lm}$) for SWSHs with m=1, s=-3 from ic=0 to 20, and for L=0,...,6.*

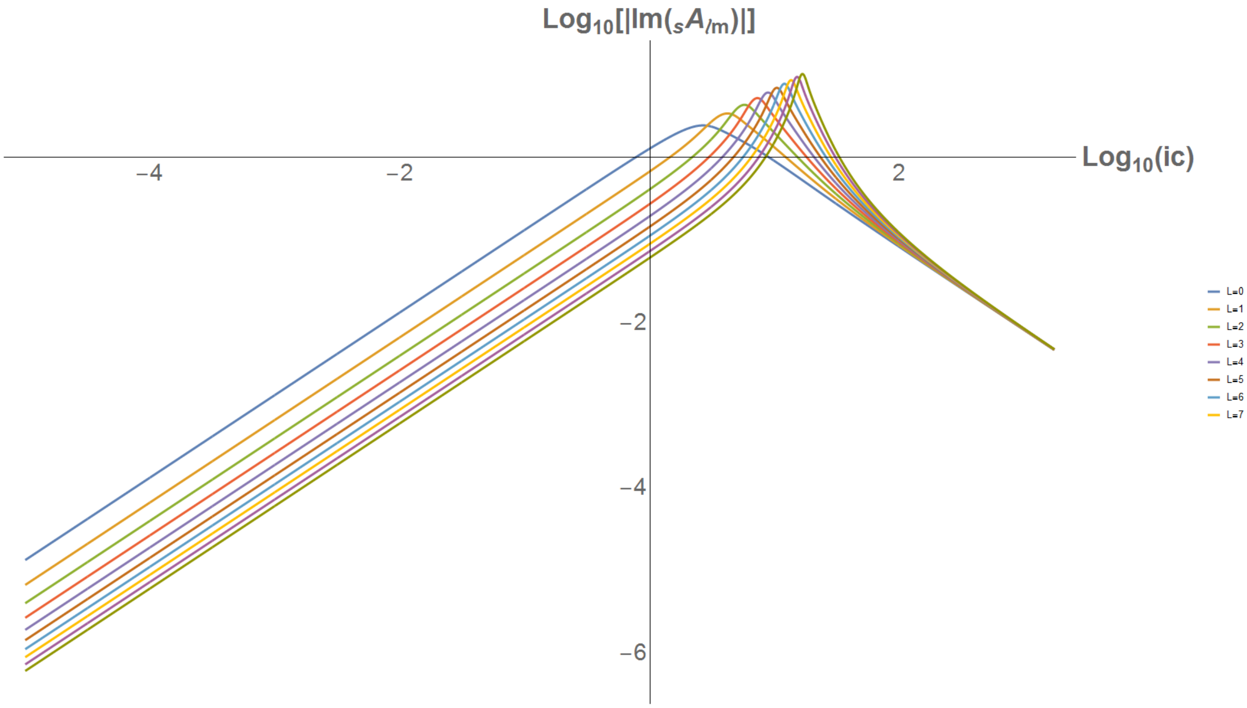


*Appendix 10: Log-log plot of $Im({}_sA_{lm})$ for SWSHs with m=1, s=-2 from ic=0 to 20, and for L=0,...,6.*

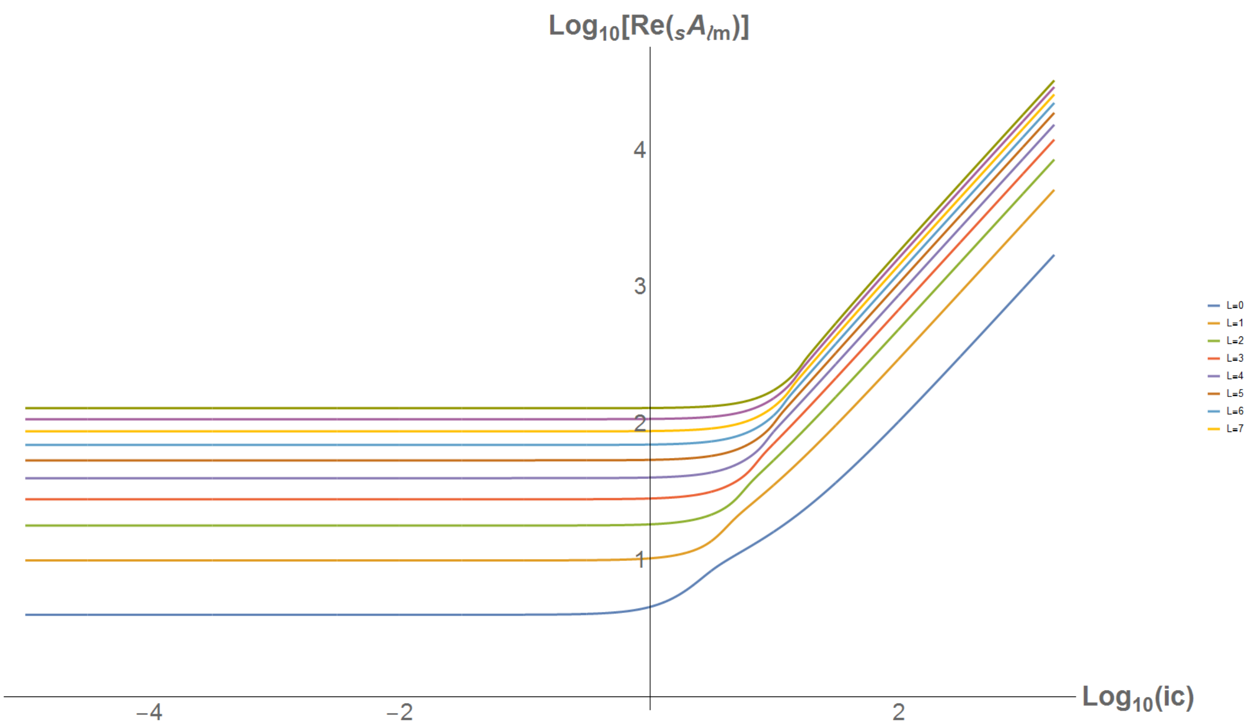


*Appendix 11: Log-log plot of $Re({}_sA_{lm})$ for SWSHs with m=1, s=-2 from ic=0 to 20, and for L=0,...,6.*

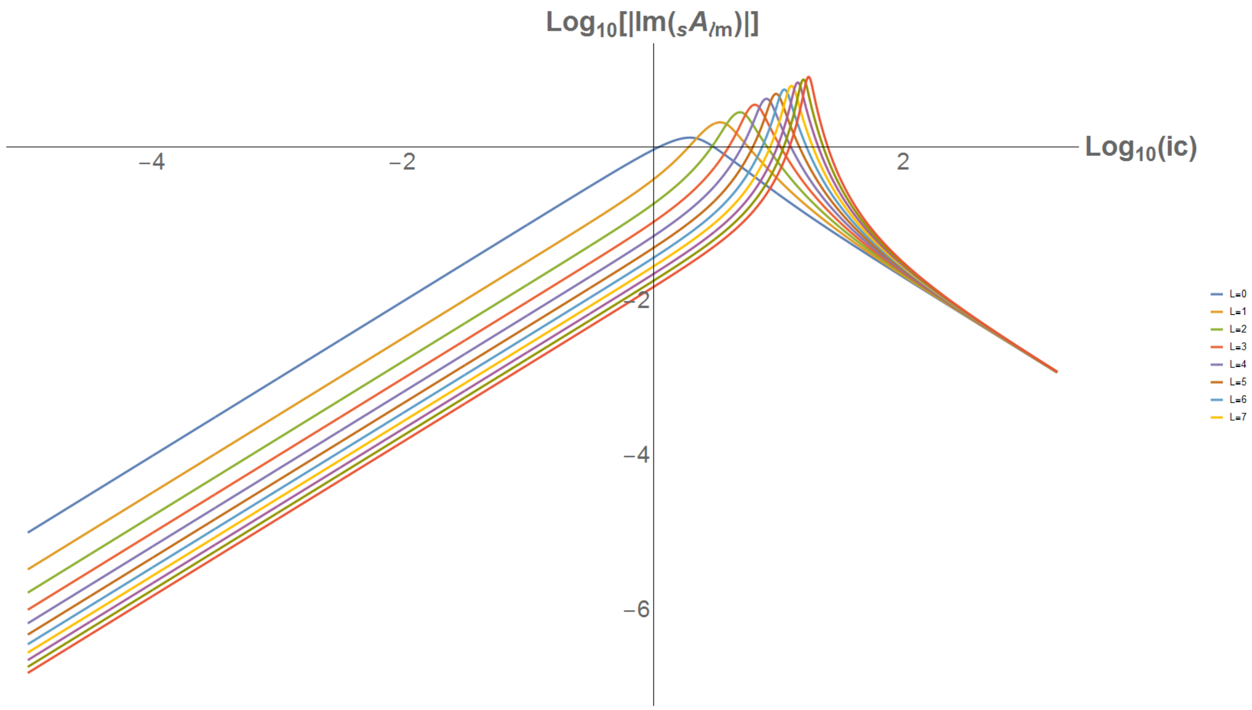


*Appendix 12: Log-log plot of $Im({}_sA_{lm})$ for SWSHs with m=1, s=-1 from ic=0 to 20, and for L=0,...,6.*

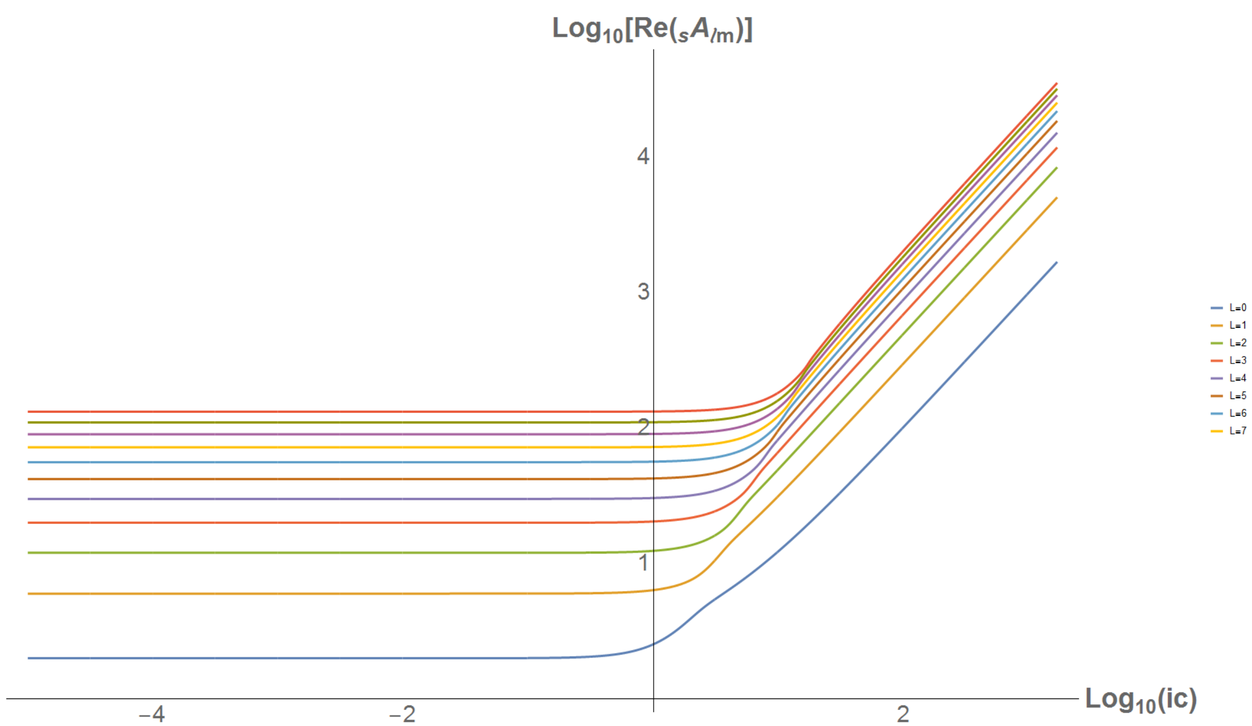


*Appendix 13: Log-log plot of $Re({}_sA_{lm})$ for SWSHs with m=1, s=-1 from ic=0 to 20, and for L=0,...,6.*

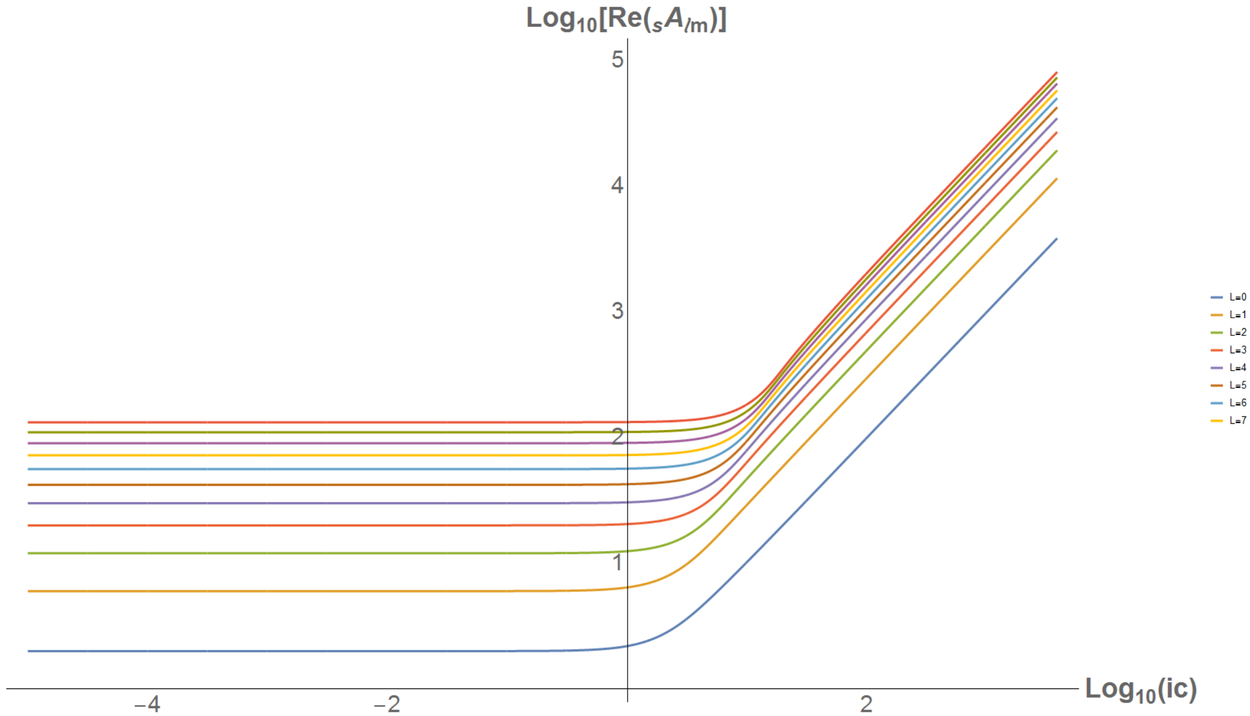


*Appendix 14: Log-log plot of $Re({}_sA_{lm})$ for SWSHs with m=1, s=0 from ic=0 to 20, and for L=0,...,6.*

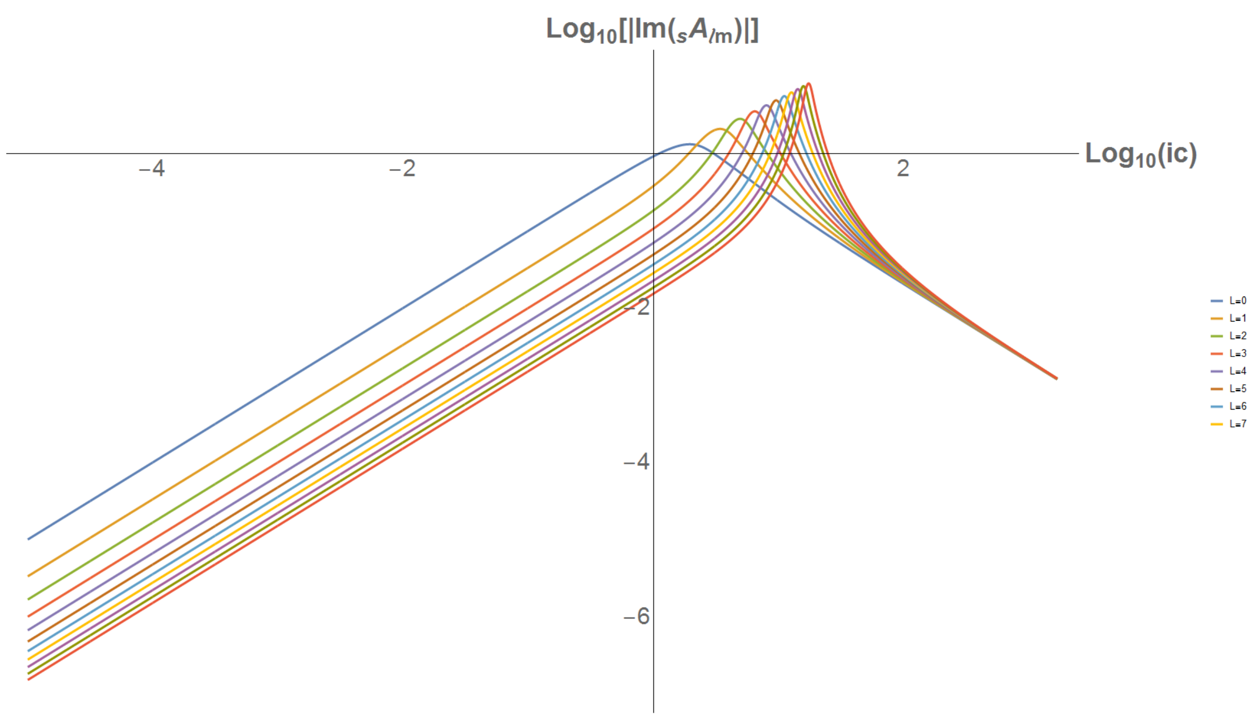


*Appendix 15: Log-log plot of $Im({}_sA_{lm})$ for SWSHs with m=1, s=1 from ic=0 to 20, and for L=0,...,6.*

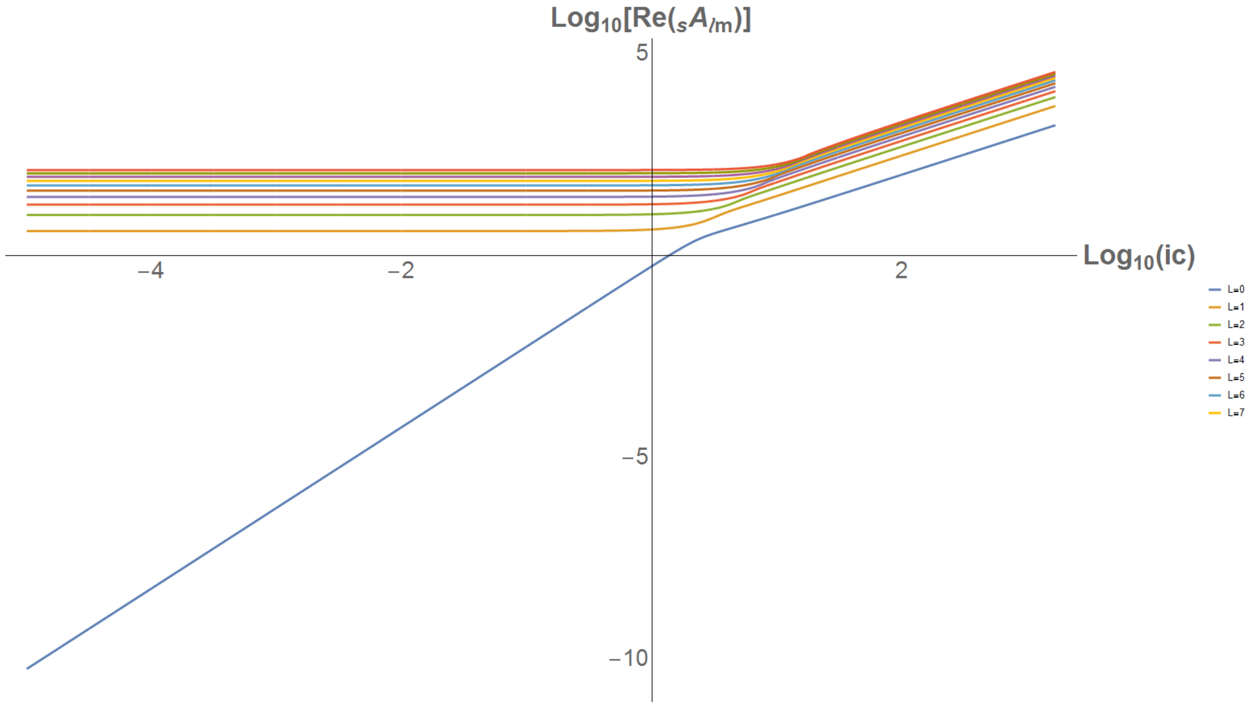


*Appendix 16: Log-log plot of Re($_sA_{lm}$) for SWSHs with m=1, s=1 from ic=0 to 20, and for L=0,...,6.*

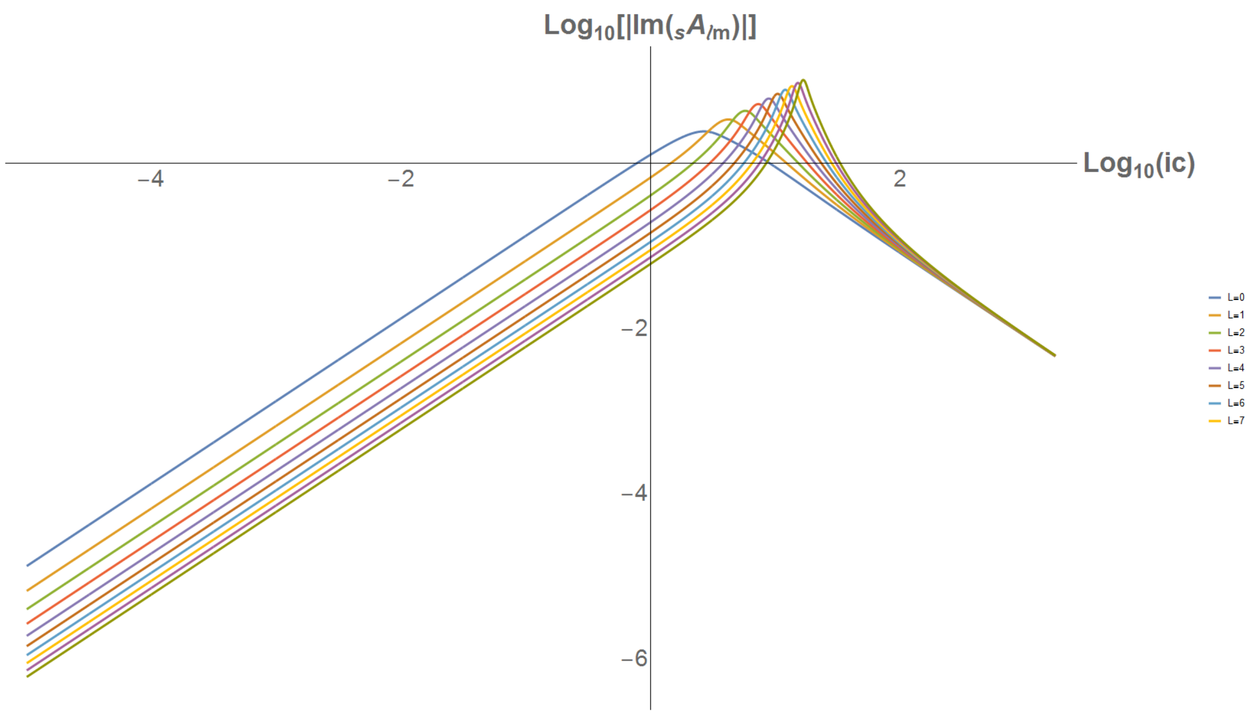


*Appendix 17: Log-log plot of Im($_sA_{lm}$) for SWSHs with m=1, s=2 from ic=0 to 20, and for L=0,...,6.*

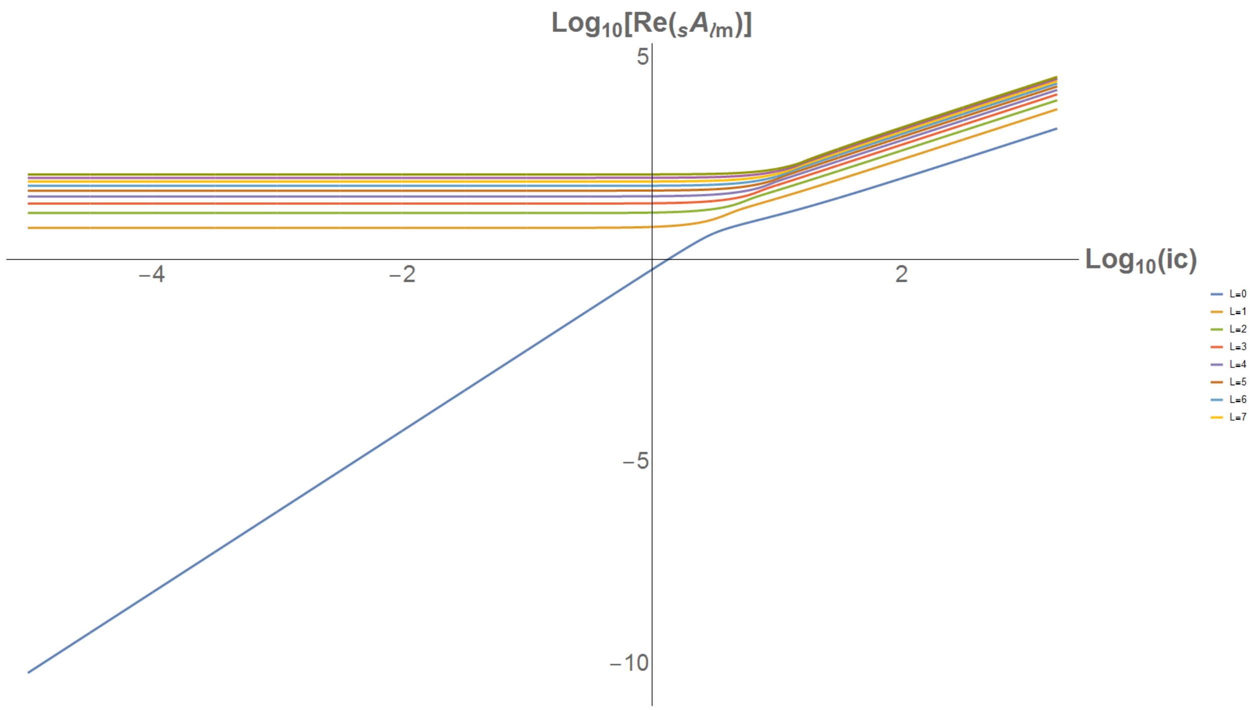


*Appendix 18: Log-log plot of Re($_sA_{lm}$) for SWSHs with m=1, s=2 from ic=0 to 20, and for L=0,...,6.*

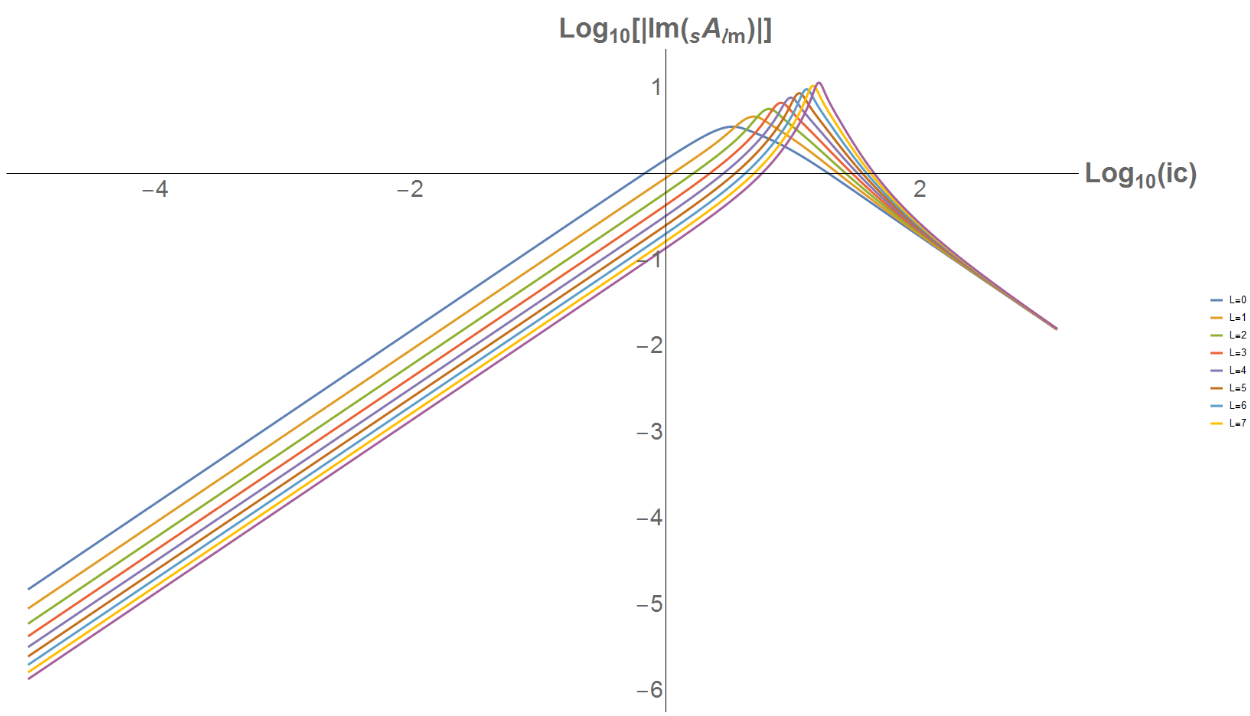


*Appendix 19: Log-log plot of Im($_sA_{lm}$) for SWSHs with m=1, s=3 from ic=0 to 20, and for L=0,...,6.*

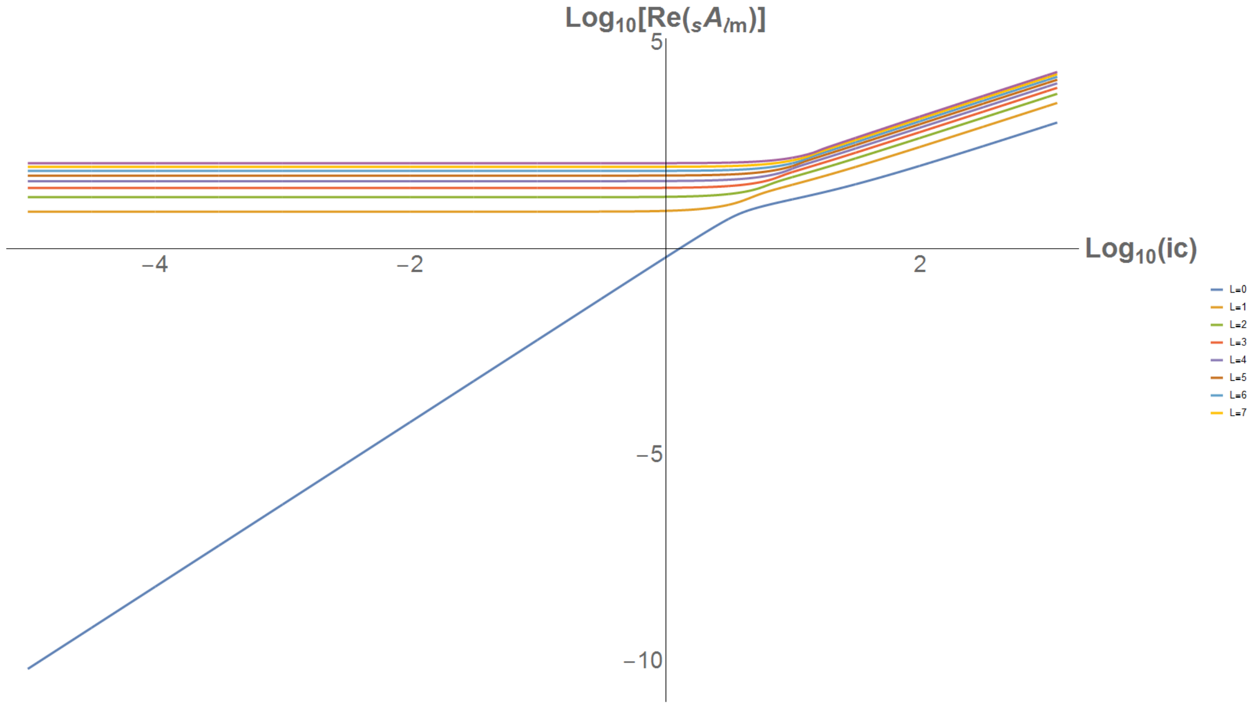


*Appendix 20: Log-log plot of Re($_sA_{lm}$) for SWSHs with m=1, s=3 from ic=0 to 20, and for L=0,...,6.*

$m = 2$

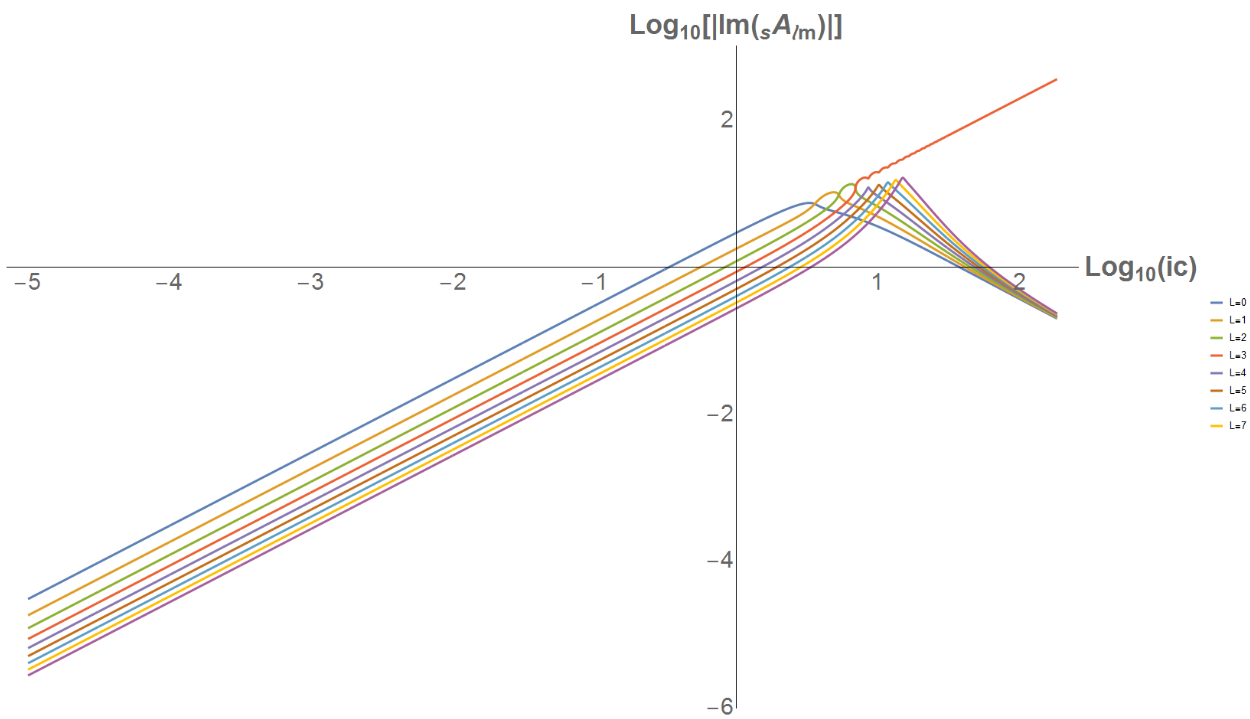


*Appendix 21: Log-log plot of Im($_sA_{lm}$) for SWSHs with m=2, s=-3 from ic=0 to 20, and for L=0,...,6.*

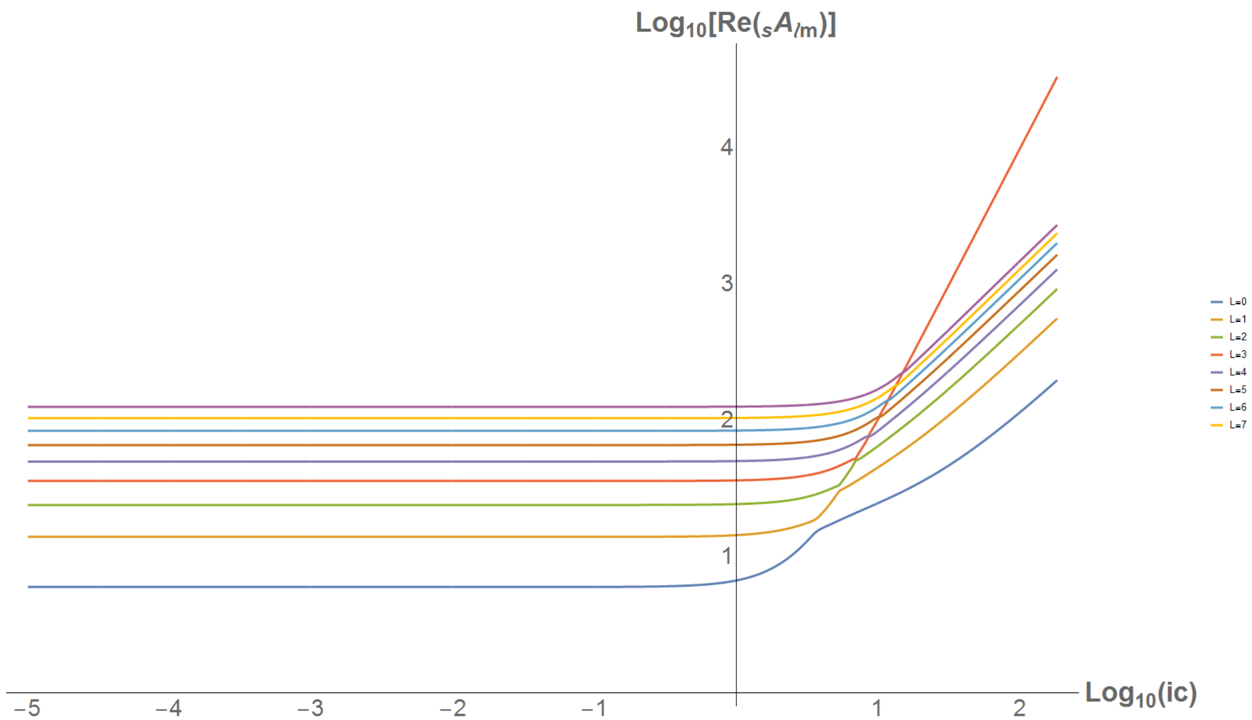


*Appendix 22: Log-log plot of $Re({}_sA_{lm})$ for SWSHs with m=2, s=-3 from ic=0 to 20, and for L=0,...,6.*

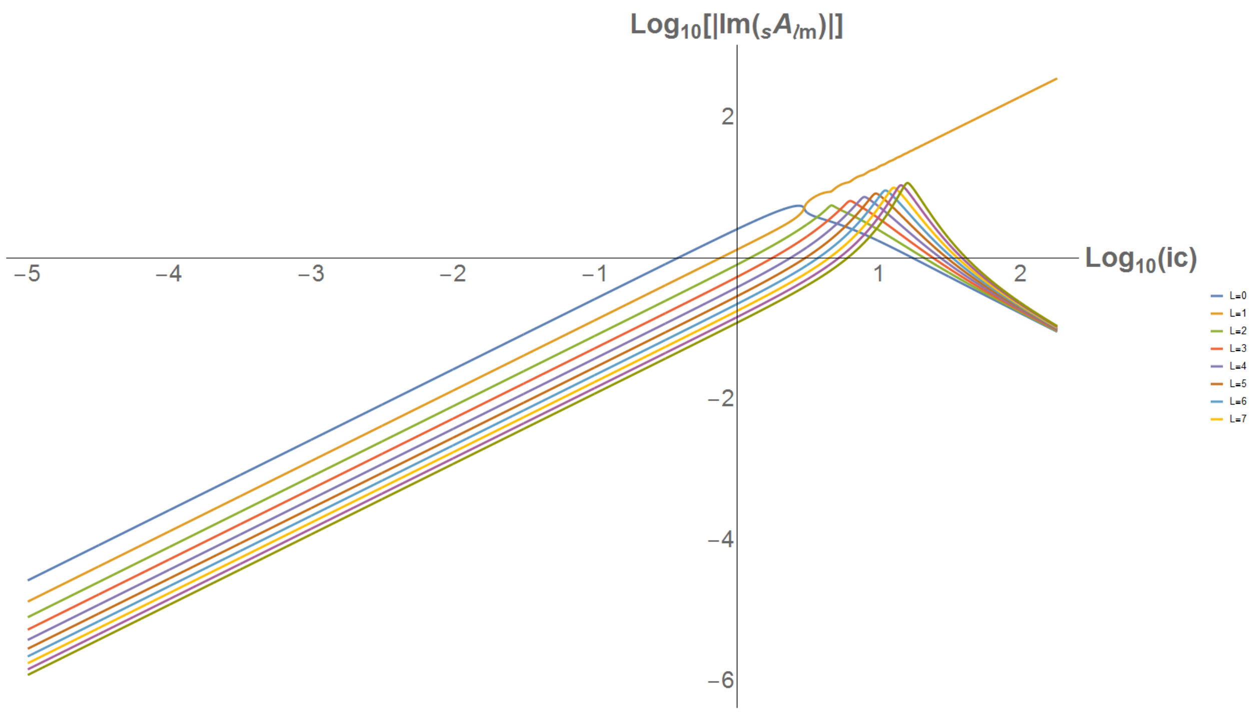


*Appendix 23: Log-log plot of $Im({}_sA_{lm})$ for SWSHs with m=2, s=-2 from ic=0 to 20, and for L=0,...,6.*

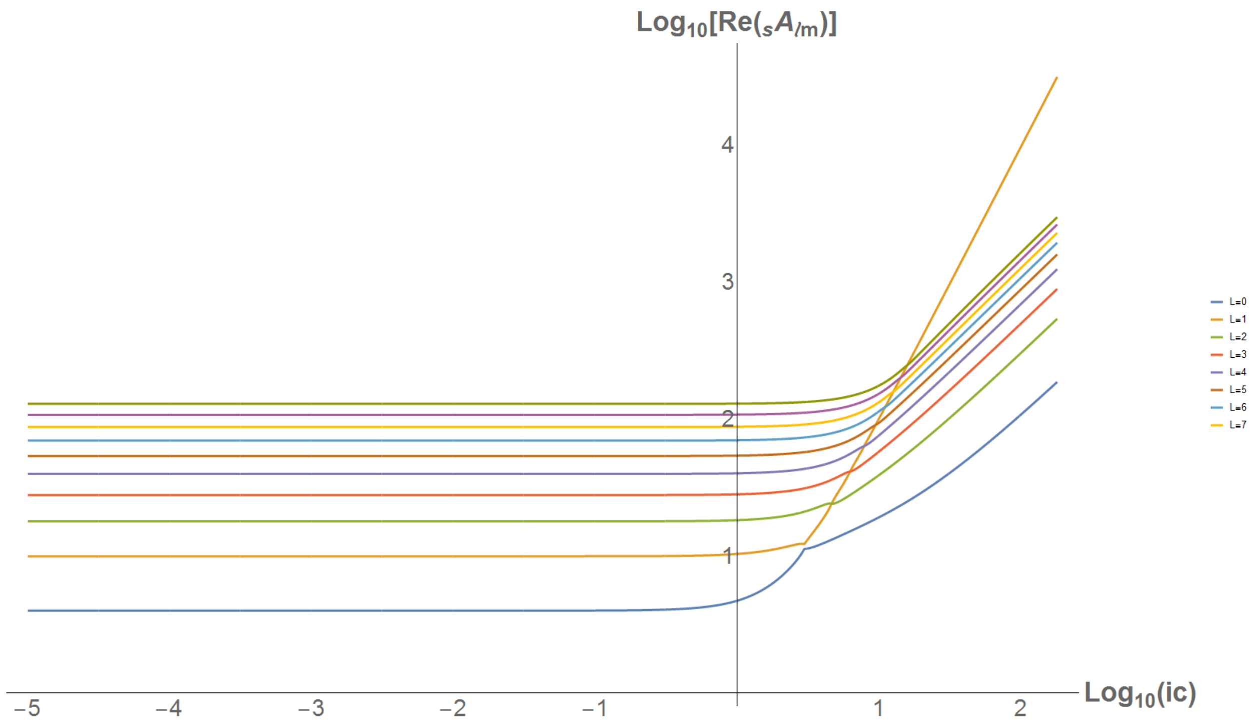


*Appendix 24: Log-log plot of $Re({}_sA_{lm})$ for SWSHs with m=2, s=-2 from ic=0 to 20, and for L=0,...,6.*

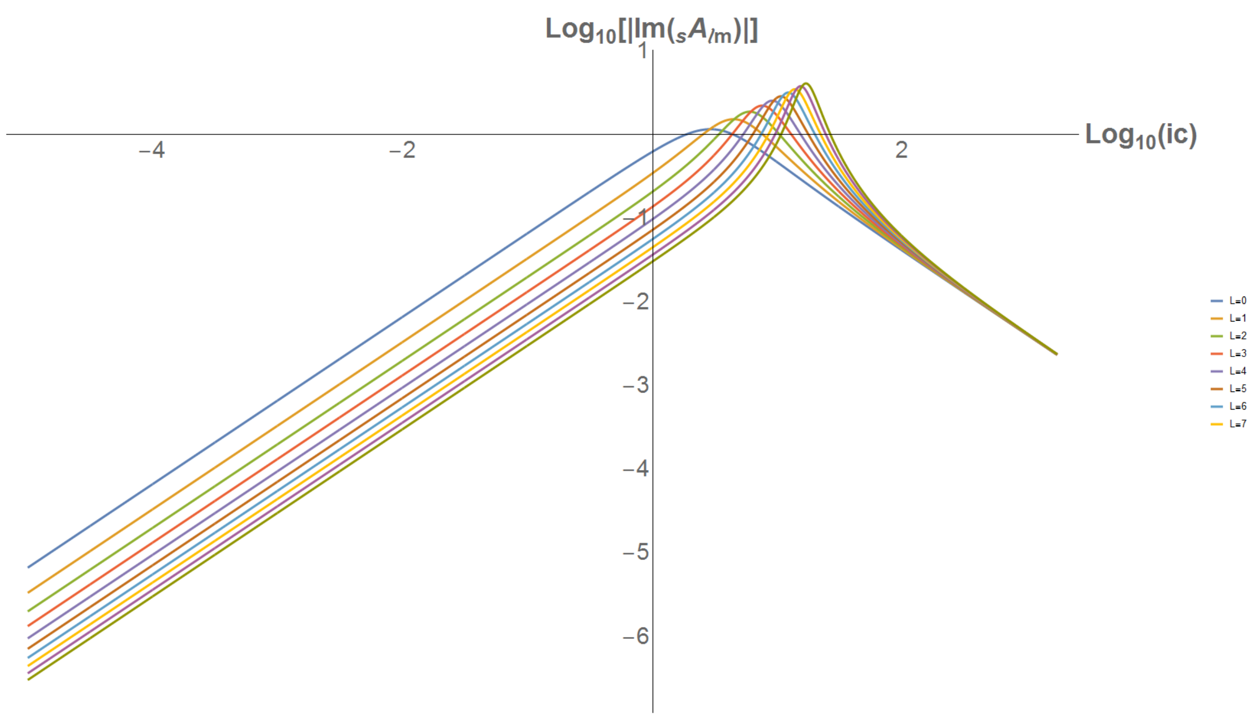


*Appendix 25: Log-log plot of $Im({}_sA_{lm})$ for SWSHs with m=2, s=-1 from ic=0 to 20, and for L=0,...,6.*

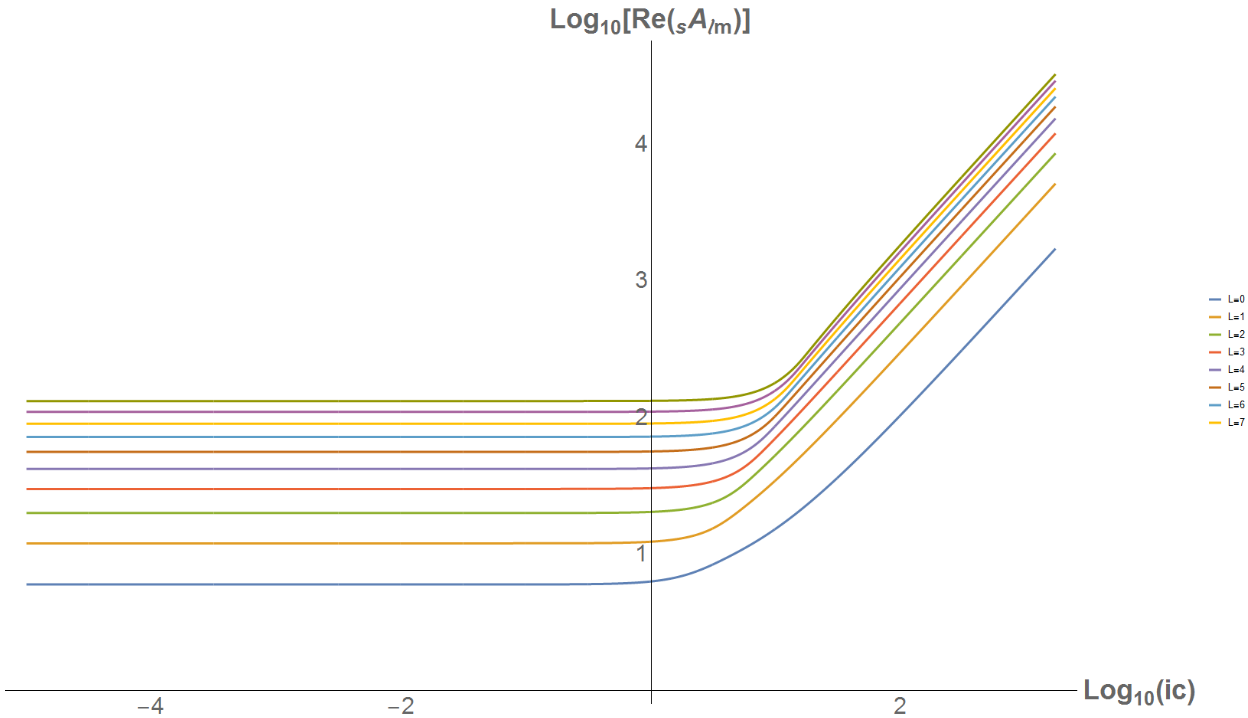


*Appendix 26: Log-log plot of Re($_sA_{lm}$) for SWSHs with m=2, s=-1 from ic=0 to 20, and for L=0,...,6.*

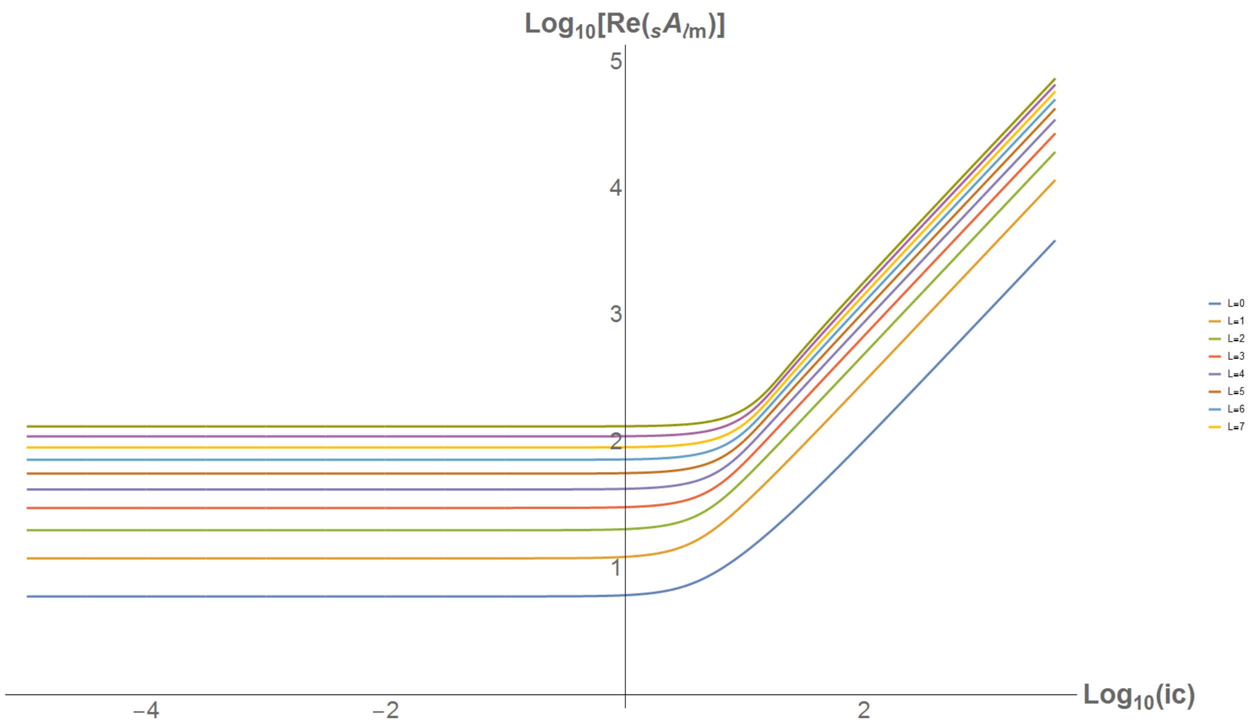


*Appendix 27: Log-log plot of Re($_sA_{lm}$) for SWSHs with m=2, s=0 from ic=0 to 20, and for L=0,...,6.*

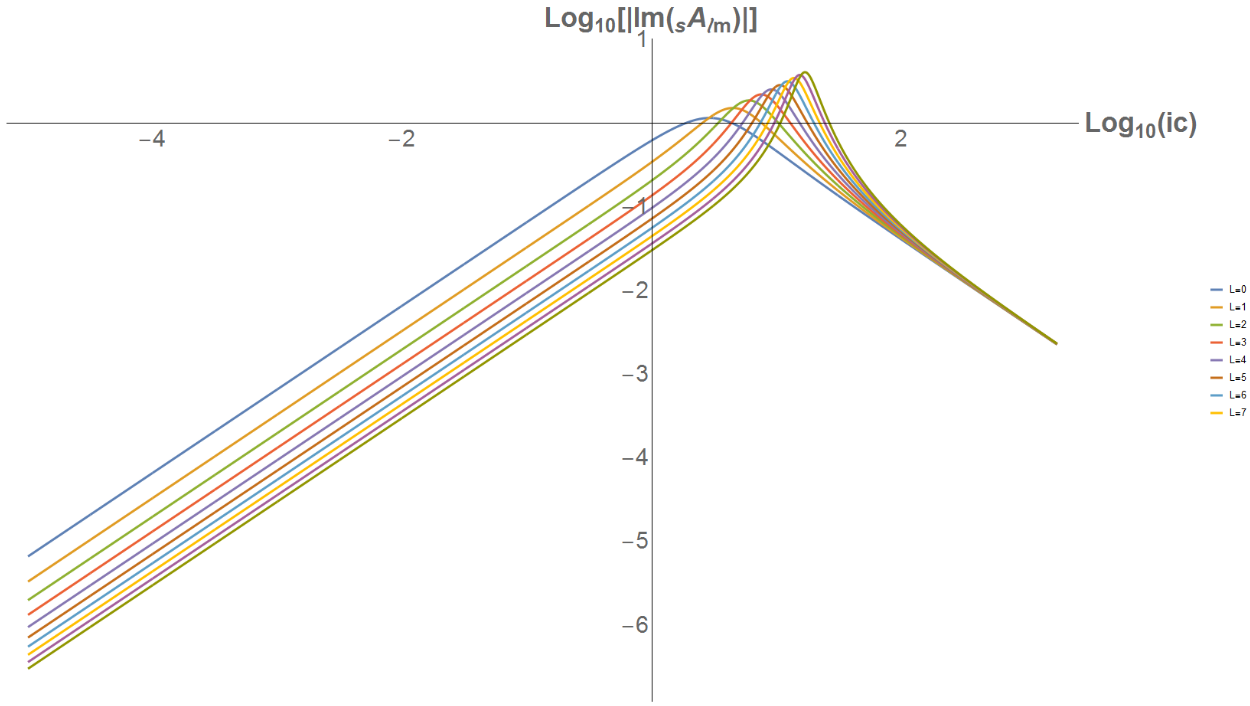


*Appendix 28: Log-log plot of $Im({}_sA_{lm})$ for SWSHs with m=2, s=1 from ic=0 to 20, and for L=0,...,6.*

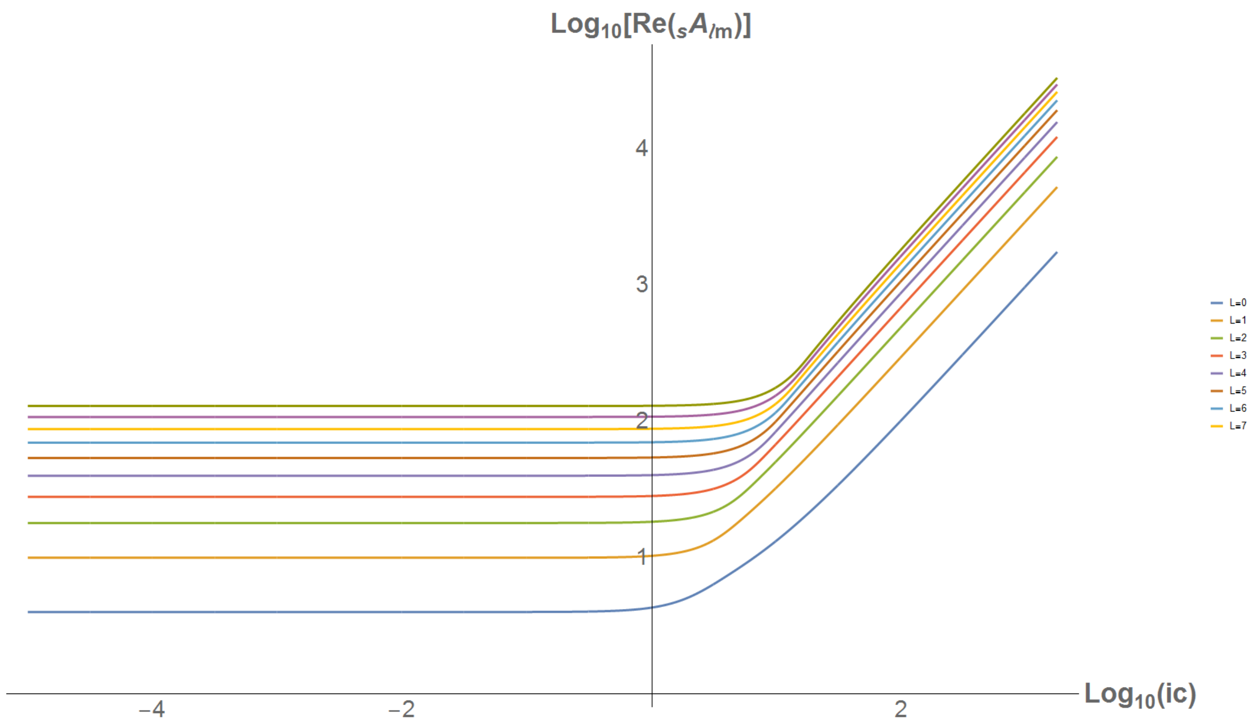


*Appendix 29: Log-log plot of $Re({}_sA_{lm})$ for SWSHs with m=2, s=1 from ic=0 to 20, and for L=0,...,6.*

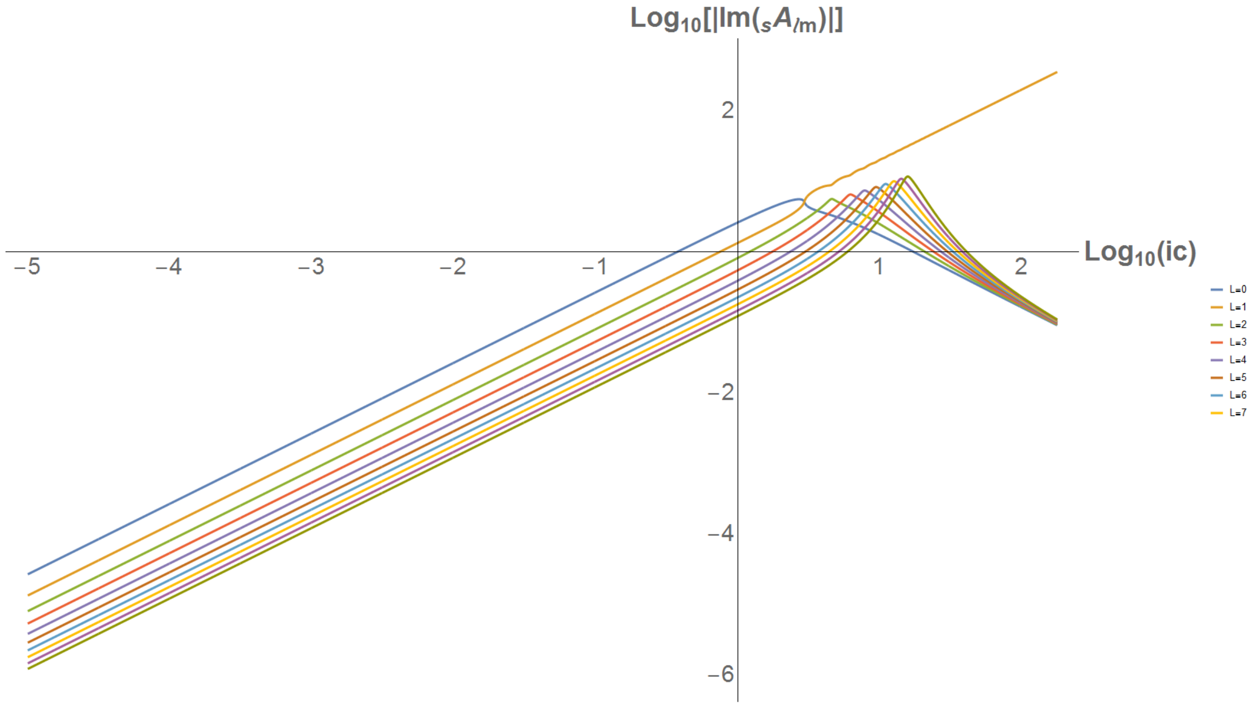


*Appendix 30: Log-log plot of $Im({}_sA_{lm})$ for SWSHs with m=2, s=2 from ic=0 to 20, and for L=0,...,6.*

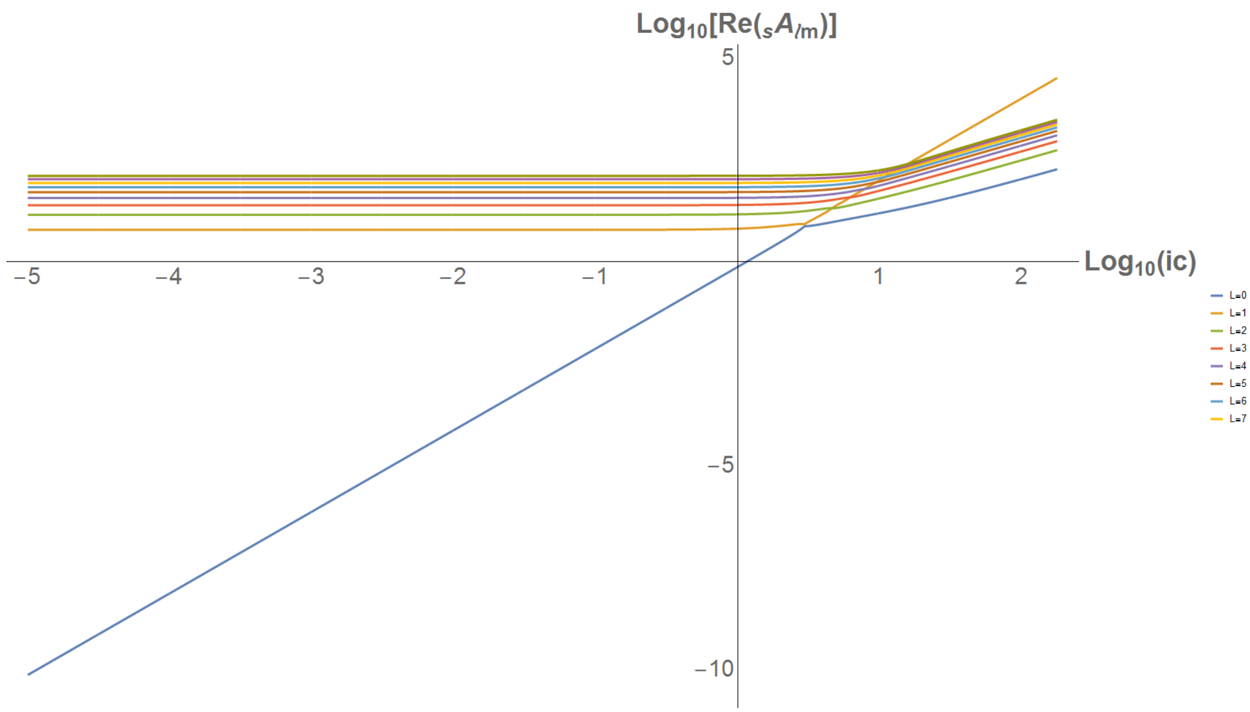


*Appendix 31: Log-log plot of $Re({}_sA_{lm})$ for SWSHs with m=2, s=2 from ic=0 to 20, and for L=0,...,6.*

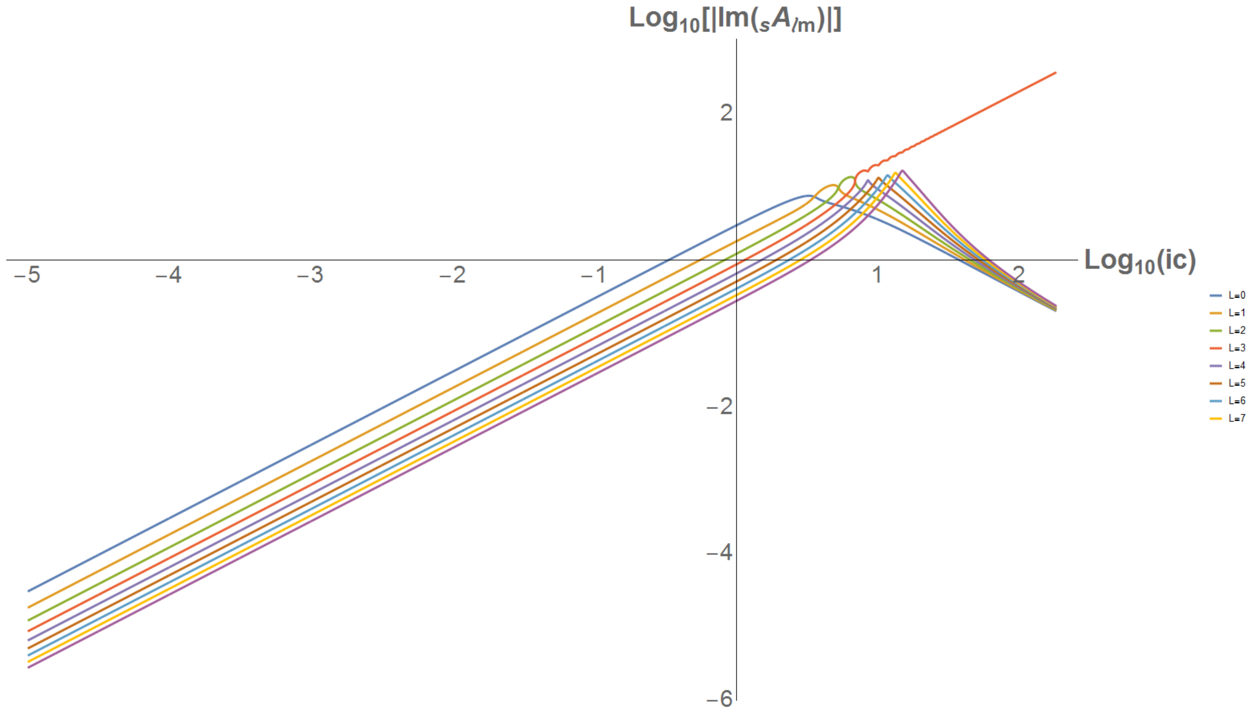


*Appendix 32: Log-log plot of Im($_sA_{lm}$) for SWSHs with m=2, s=3 from ic=0 to 20, and for L=0,...,6.*

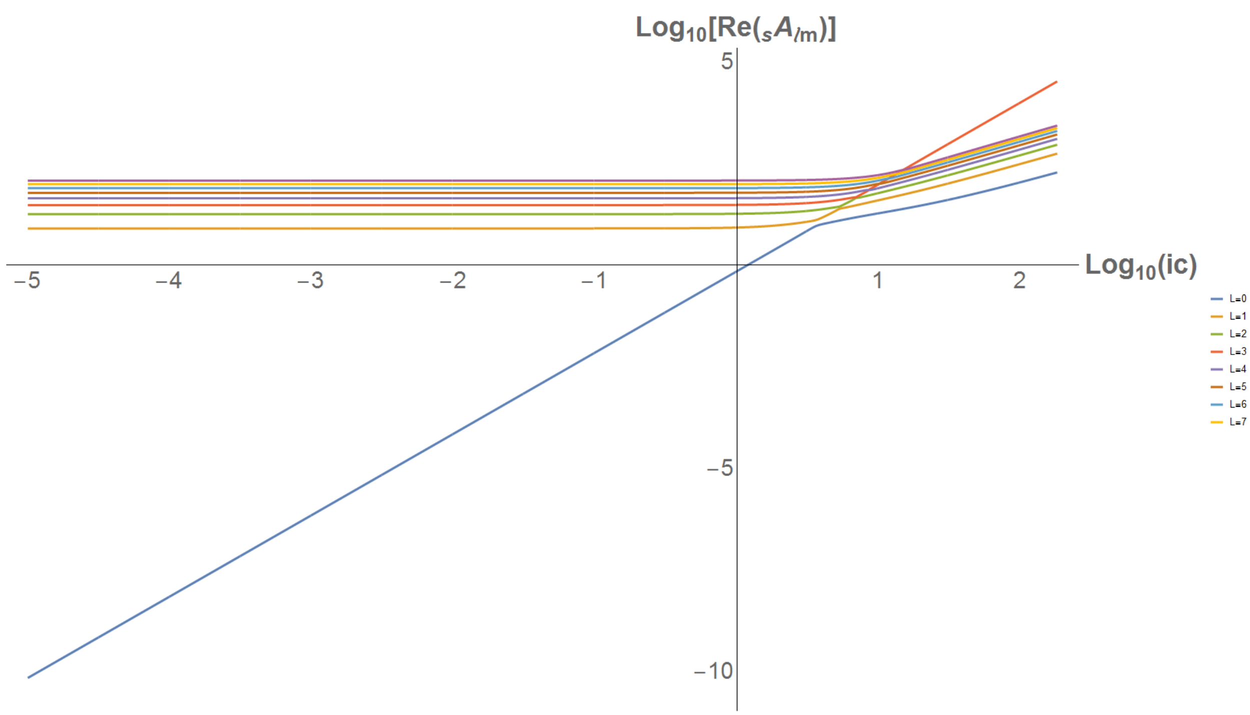


*Appendix 33: Log-log plot of Re($_sA_{lm}$) for SWSHs with m=2, s=3 from ic=0 to 20, and for L=0,...,6.*

$m = 3$

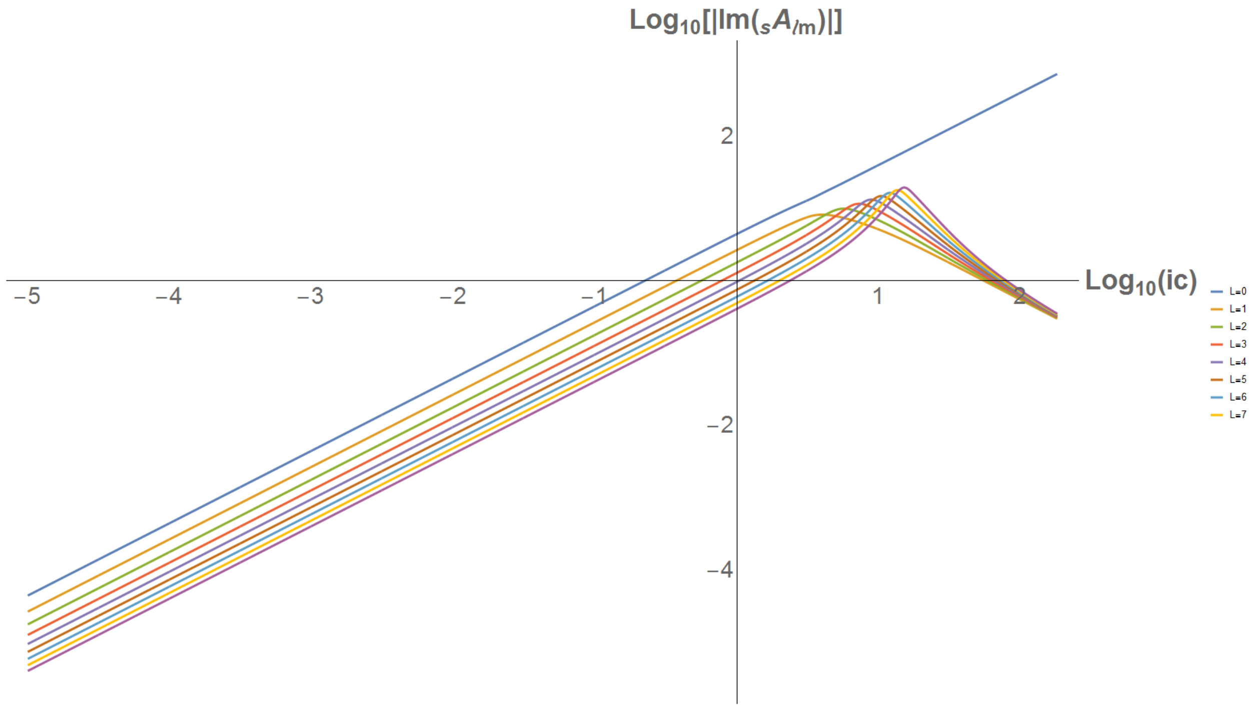


*Appendix 34: Log-log plot of Im($_sA_{lm}$) for SWSHs with m=3, s=-3 from ic=0 to 20, and for L=0,...,6.*

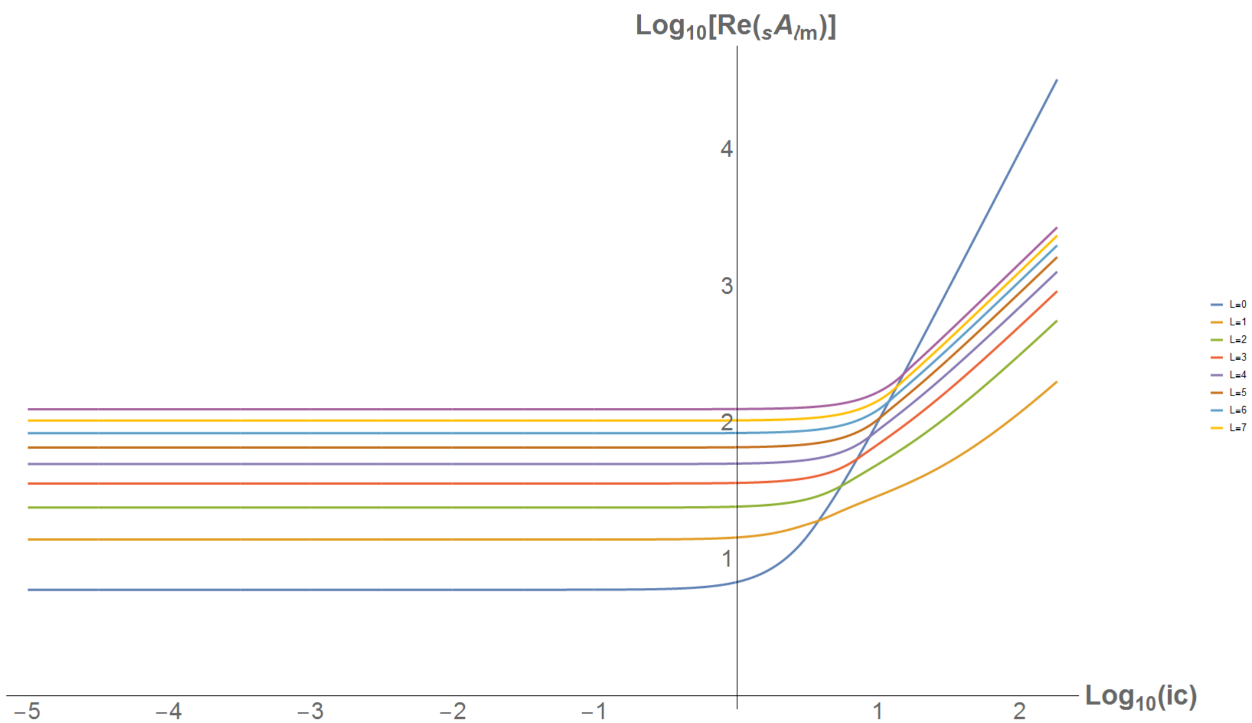


*Appendix 35: Log-log plot of Re($_sA_{lm}$) for SWSHs with m=3, s=-3 from ic=0 to 20, and for L=0,...,6.*

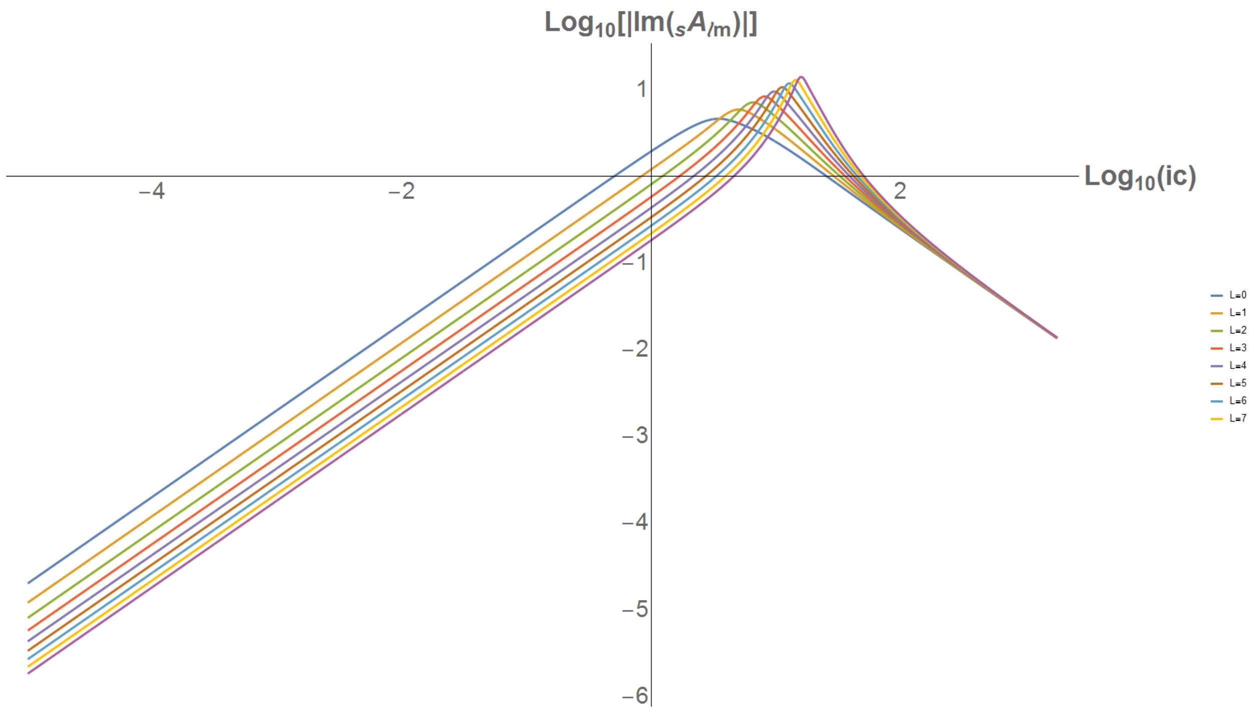


*Appendix 36: Log-log plot of $Im({}_sA_{lm})$ for SWSHs with m=3, s=-2 from ic=0 to 20, and for L=0,...,6.*

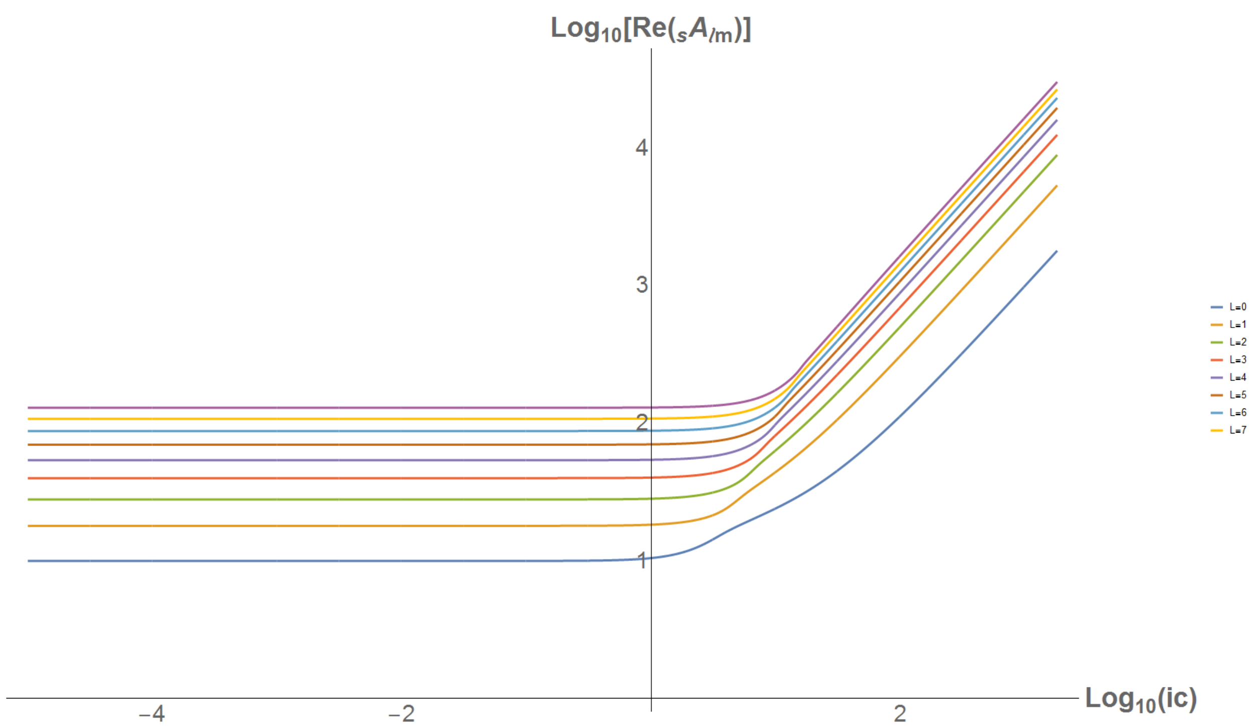


*Appendix 37: Log-log plot of $Re({}_sA_{lm})$ for SWSHs with m=3, s=-2 from ic=0 to 20, and for L=0,...,6.*

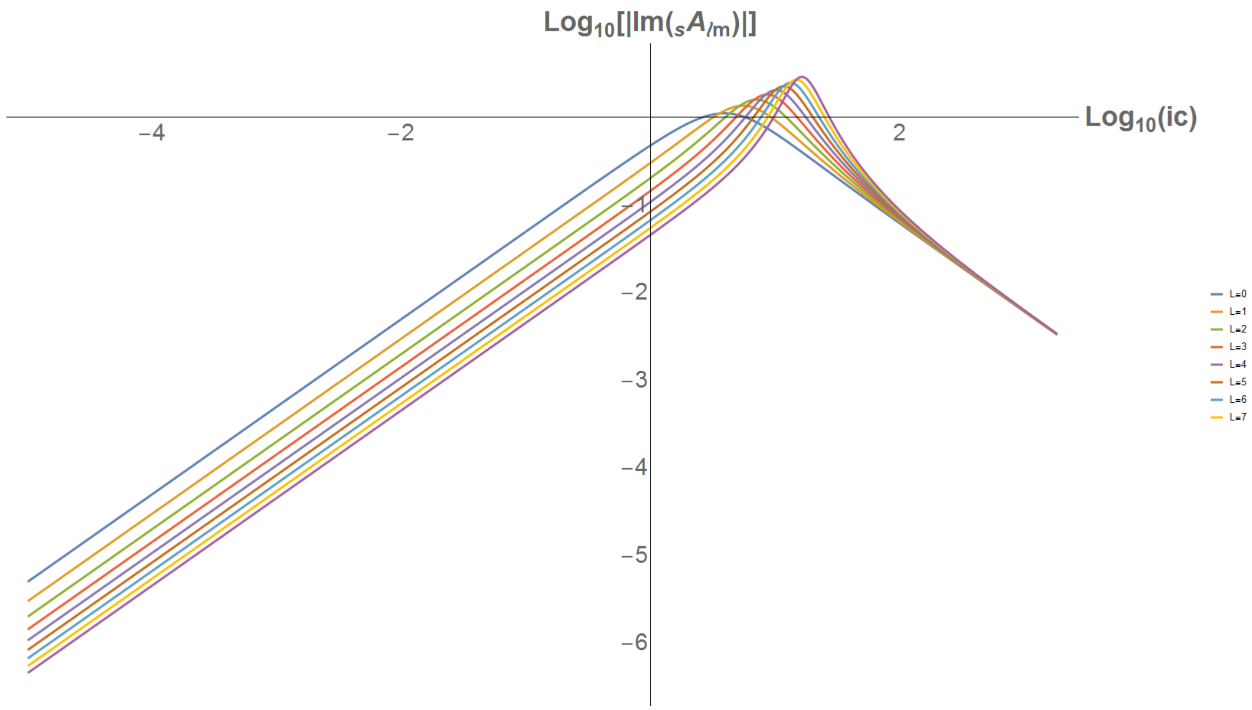


*Appendix 38: Log-log plot of Im($_sA_{lm}$) for SWSHs with m=3, s=-1 from ic=0 to 20, and for L=0,...,6.*

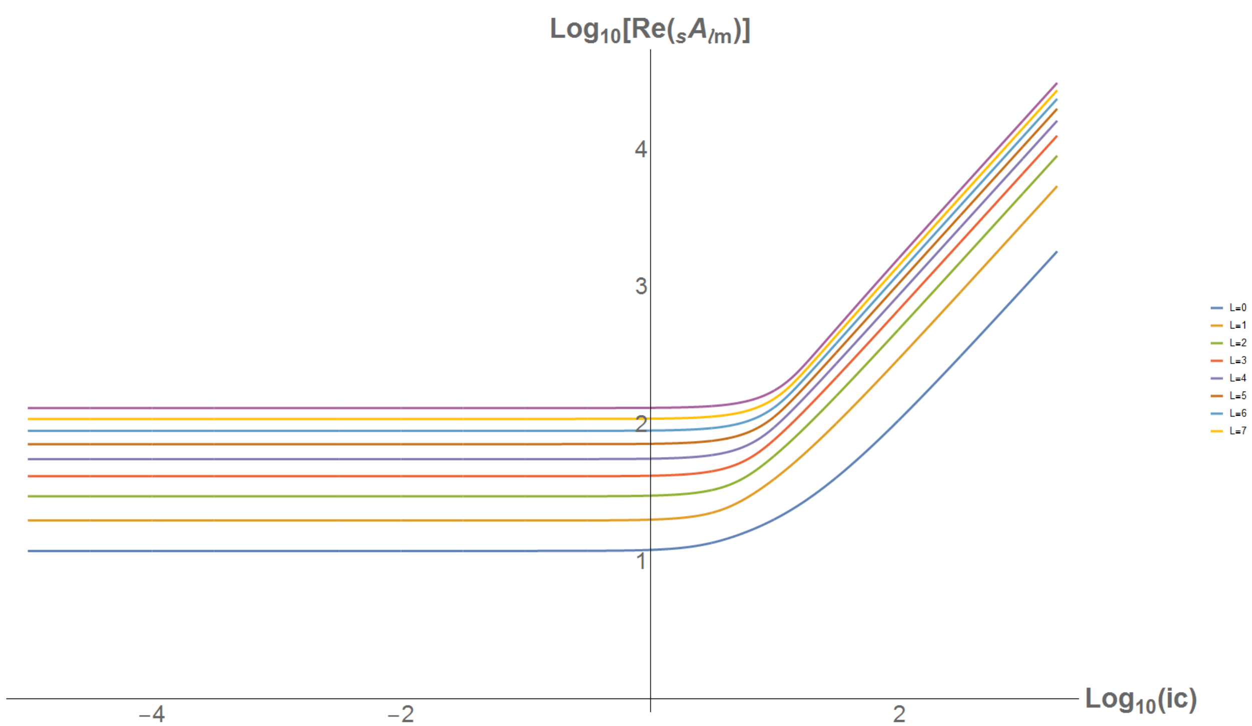


*Appendix 39: Log-log plot of Re($_sA_{lm}$) for SWSHs with m=3, s=-1 from ic=0 to 20, and for L=0,...,6.*

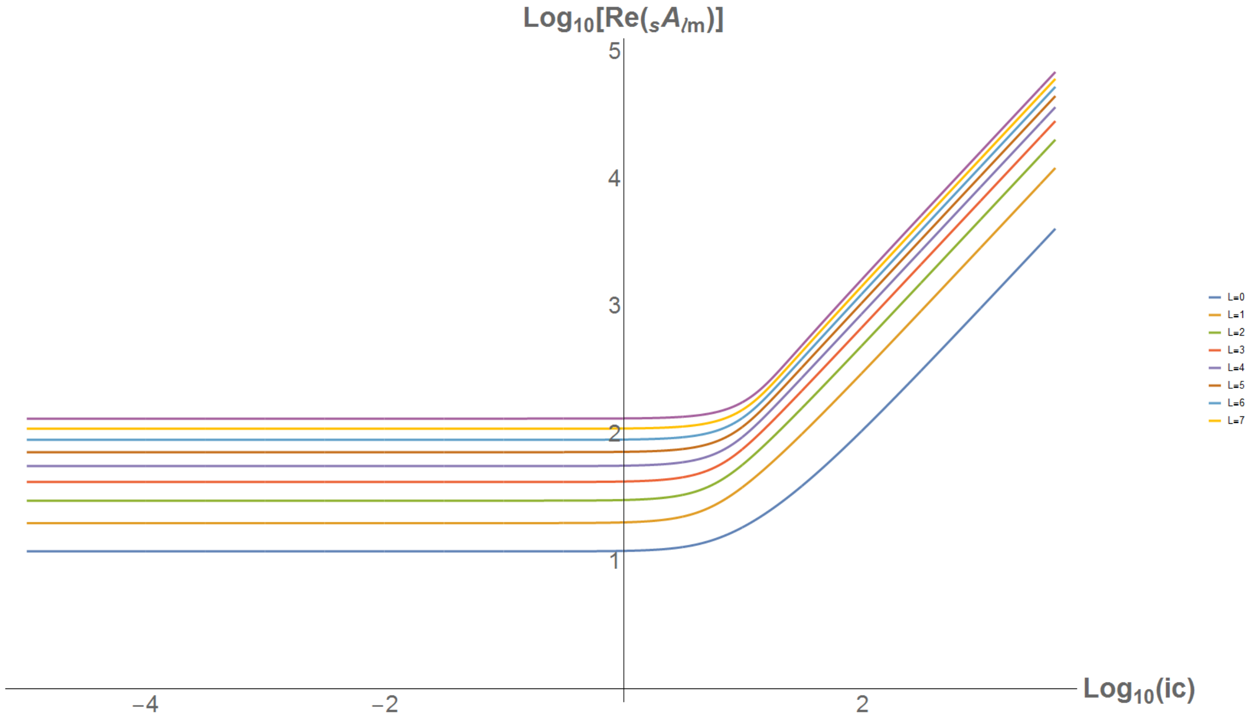


*Appendix 40: Log-log plot of Re($_sA_{lm}$) for SWSHs with m=3, s=0 from ic=0 to 20, and for L=0,...,6.*

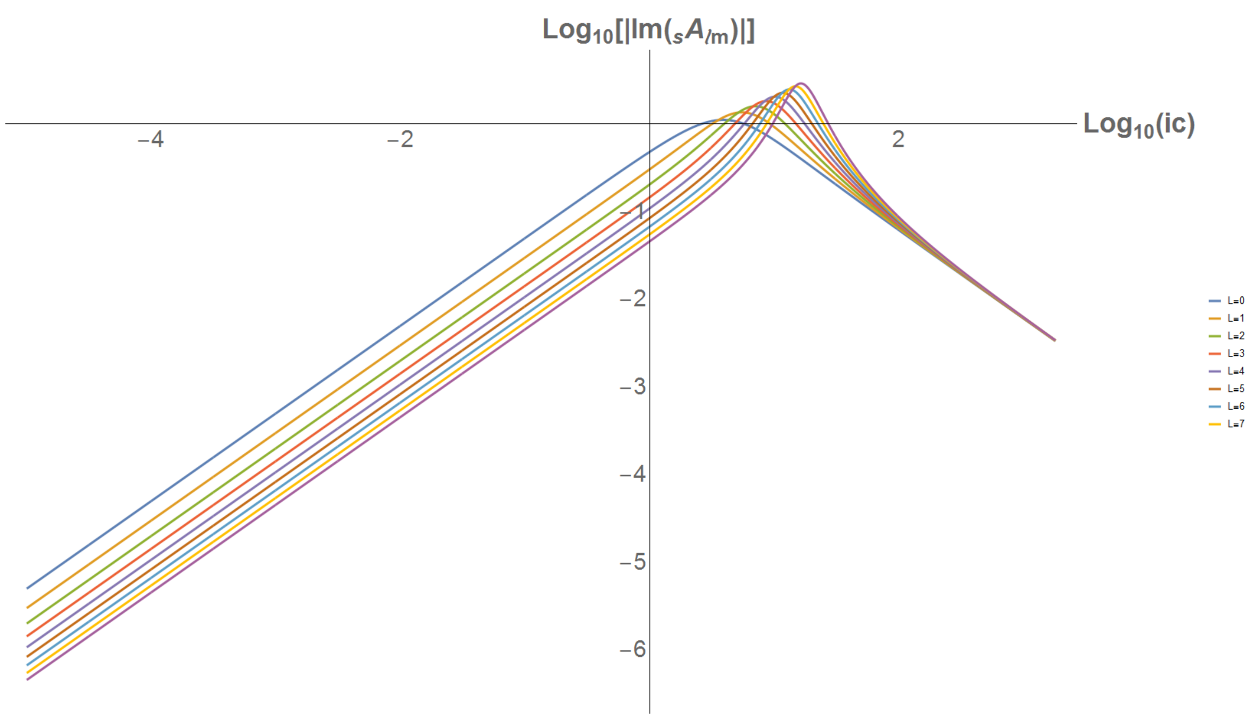


*Appendix 41: Log-log plot of Im($_sA_{lm}$) for SWSHs with m=3, s=1 from ic=0 to 20, and for L=0,...,6.*

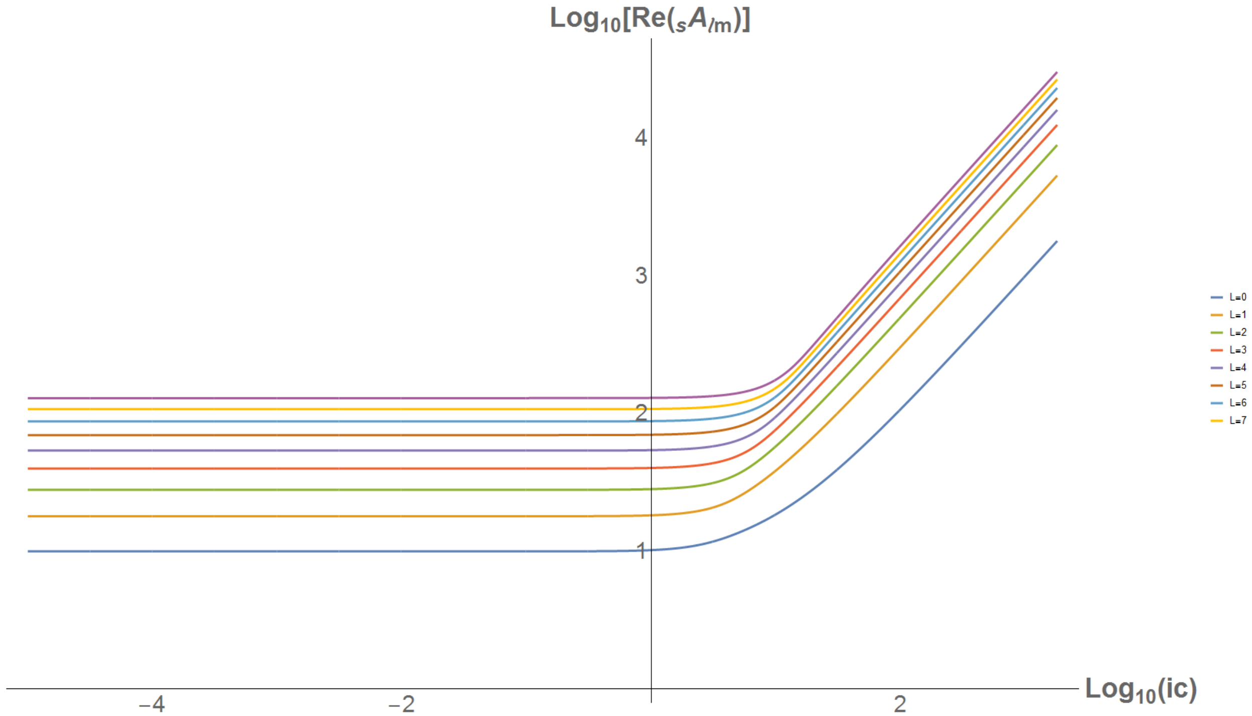


*Appendix 42: Log-log plot of $Re({}_sA_{lm})$ for SWSHs with m=3, s=1 from ic=0 to 20, and for L=0,...,6.*

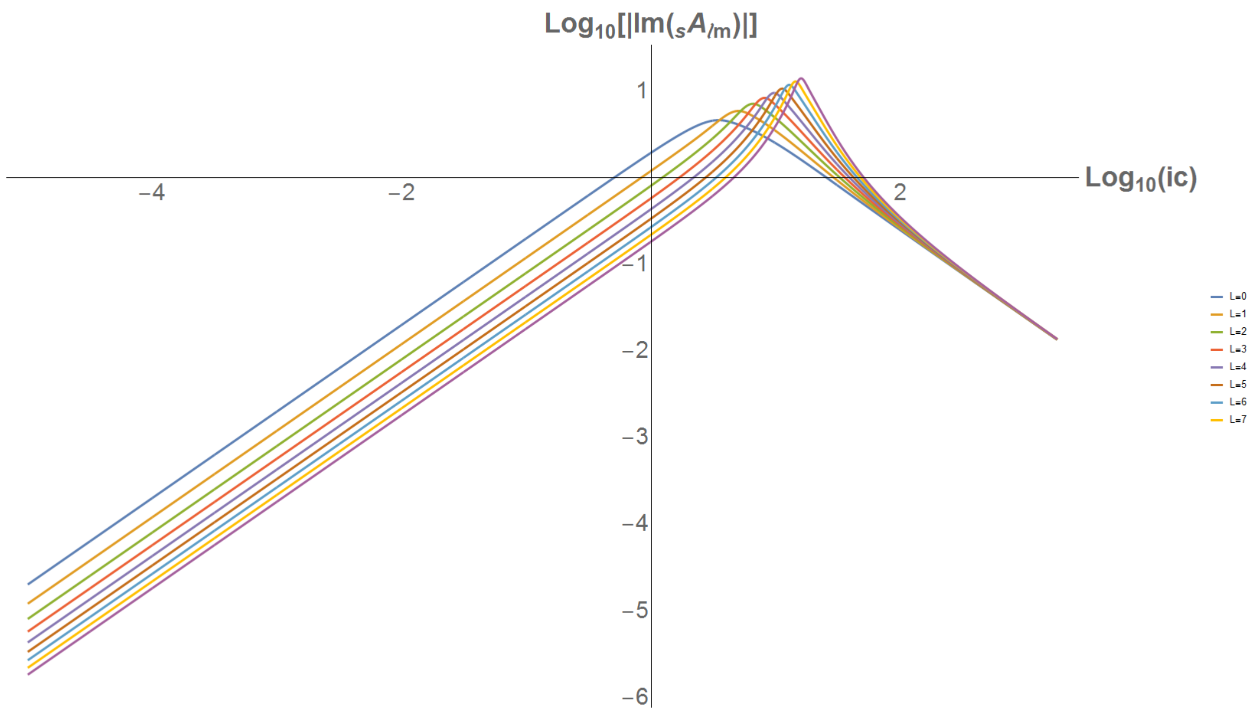


*Appendix 43: Log-log plot of $Im({}_sA_{lm})$ for SWSHs with m=3, s=2 from ic=0 to 20, and for L=0,...,6.*

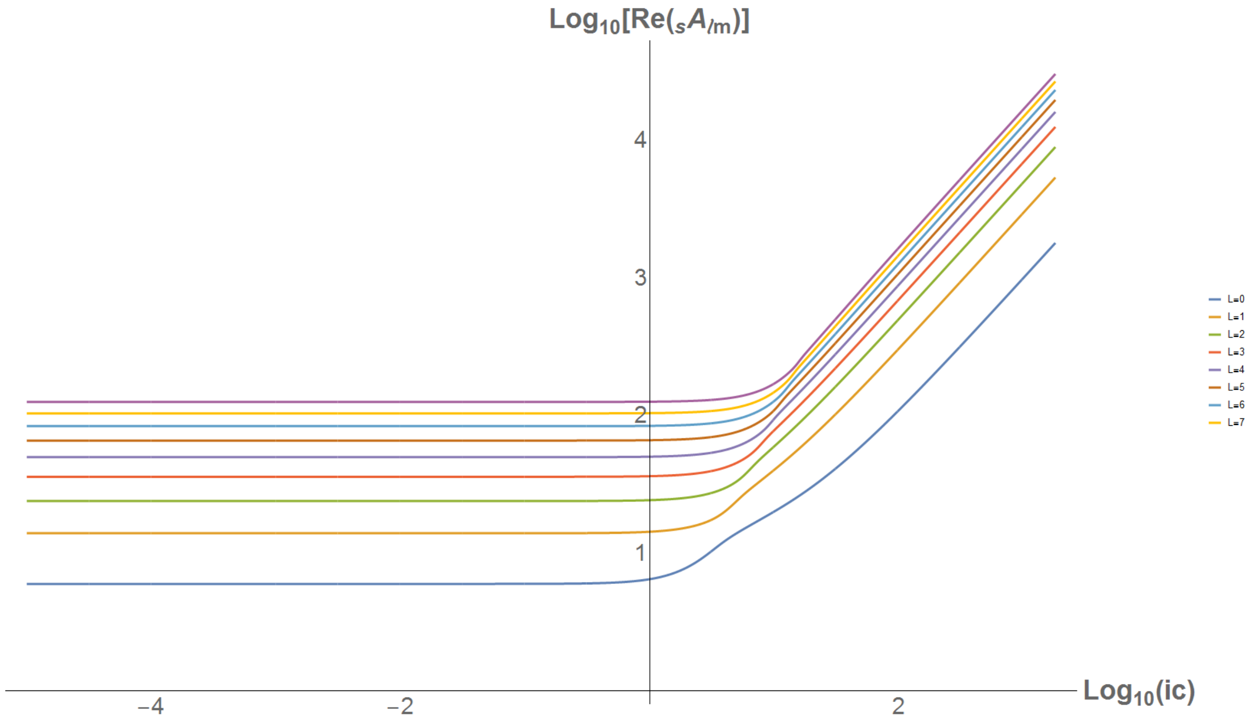


*Appendix 44: Log-log plot of Re($_sA_{lm}$) for SWSHs with m=3, s=2 from ic=0 to 20, and for L=0,...,6.*

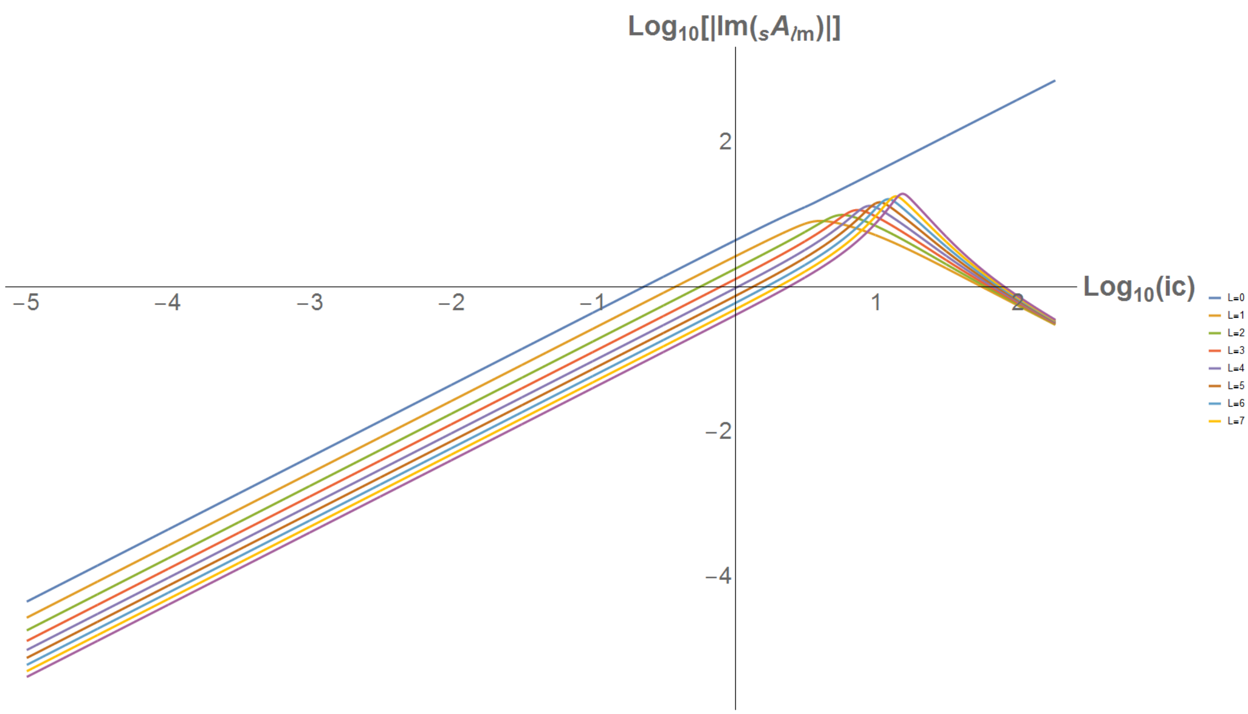


*Appendix 45: Log-log plot of Im($_sA_{lm}$) for SWSHs with m=3, s=3 from ic=0 to 20, and for L=0,...,6.*

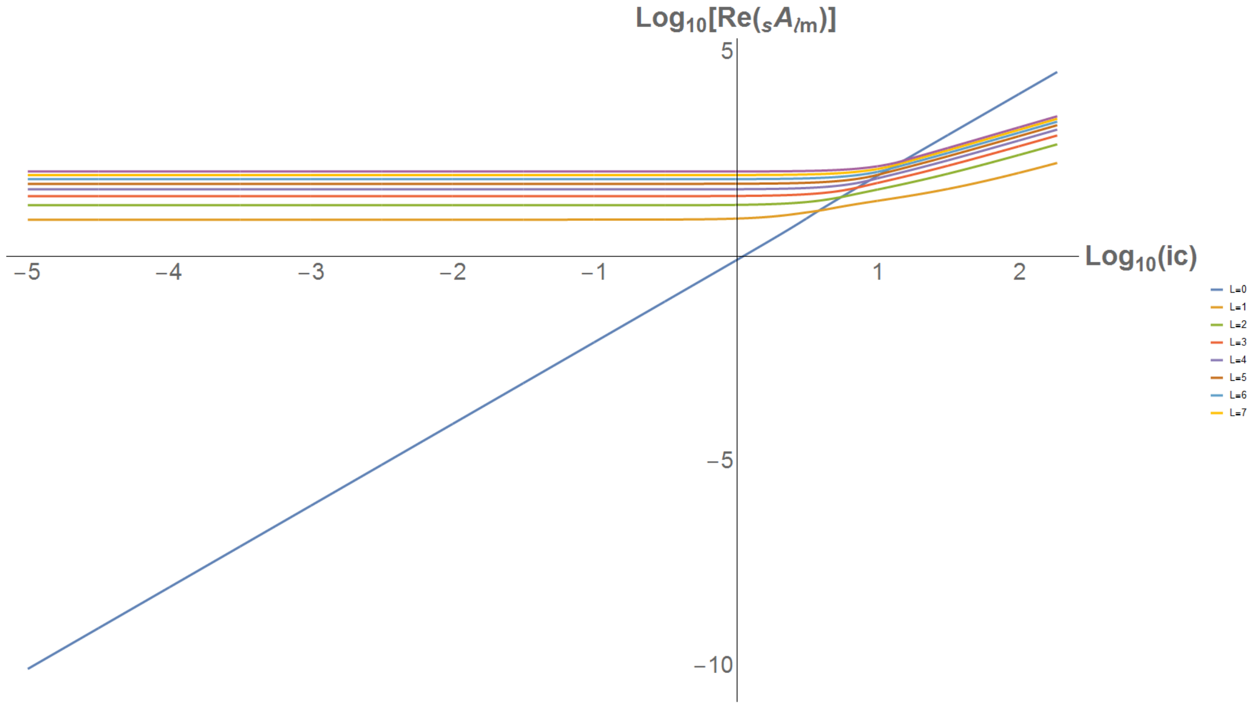


*Appendix 46: Log-log plot of Re($_sA_{lm}$) for SWSHs with m=3, s=3 from ic=0 to 20, and for L=0,...,6.*

$m = 4$

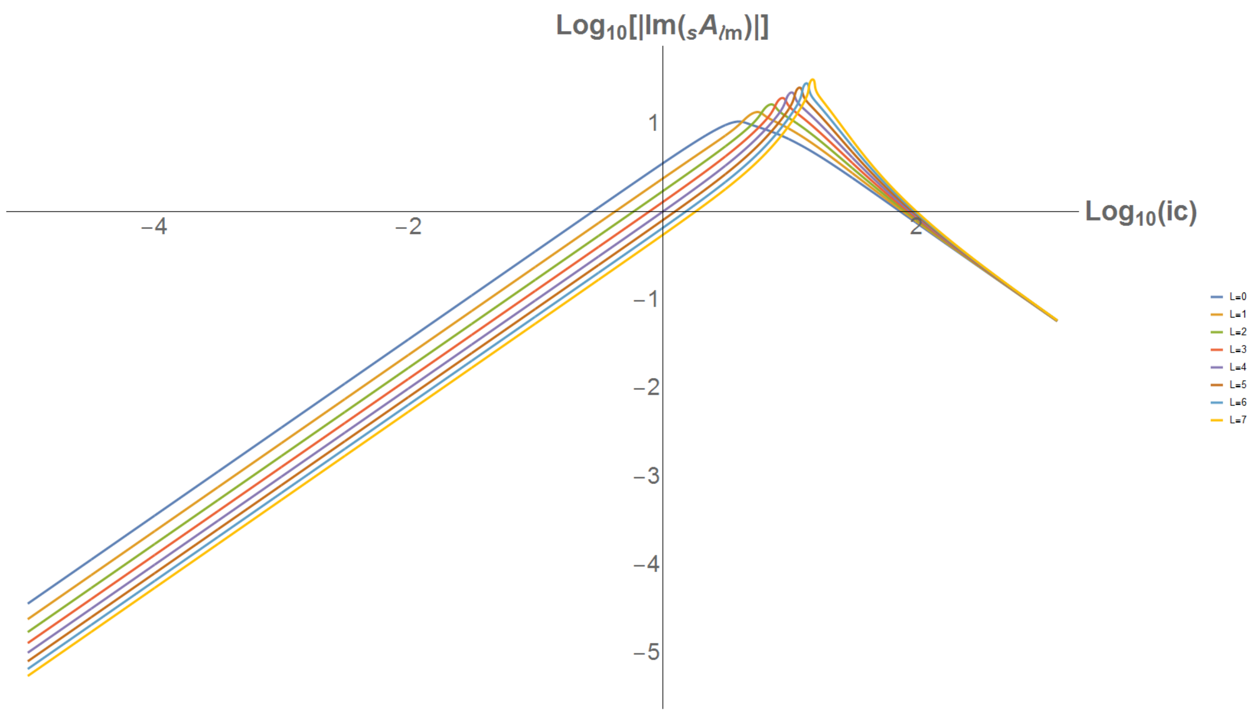


*Appendix 47: Log-log plot of Im($_sA_{lm}$) for SWSHs with m=4, s=-3 from ic=0 to 20, and for L=0,...,6.*

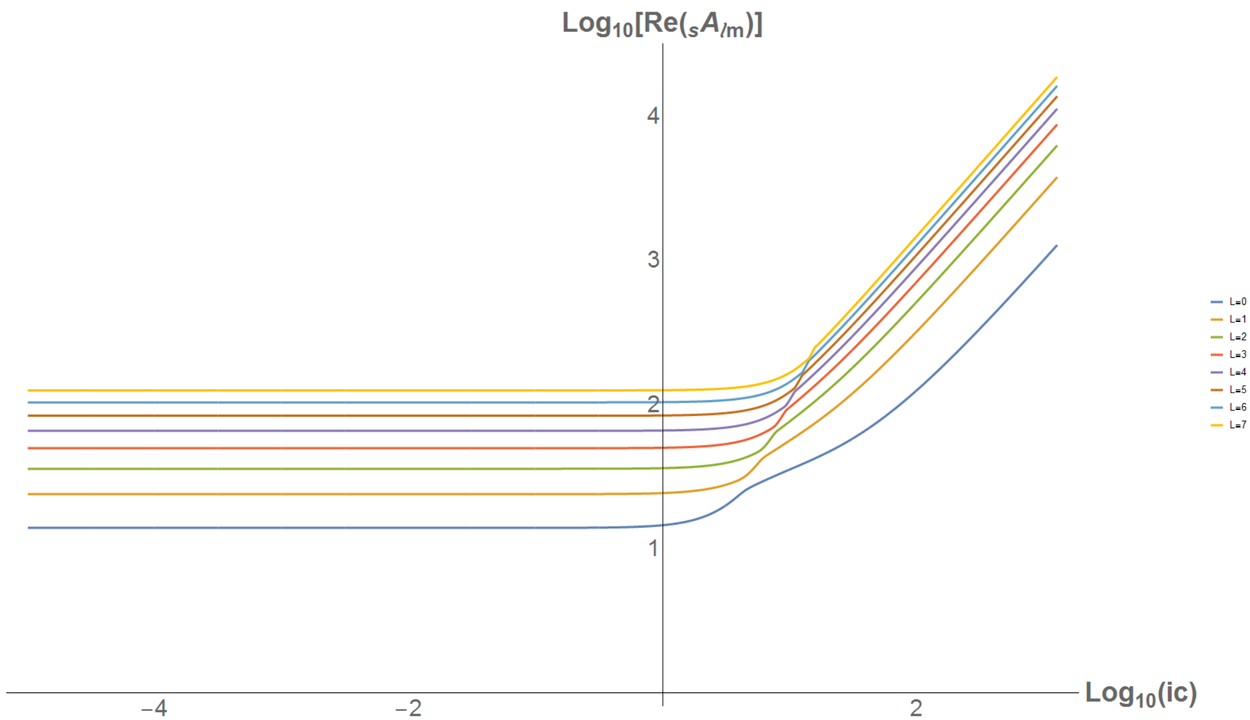


*Appendix 48: Log-log plot of Re($_sA_{lm}$) for SWSHs with m=4, s=-3 from ic=0 to 20, and for L=0,...,6.*

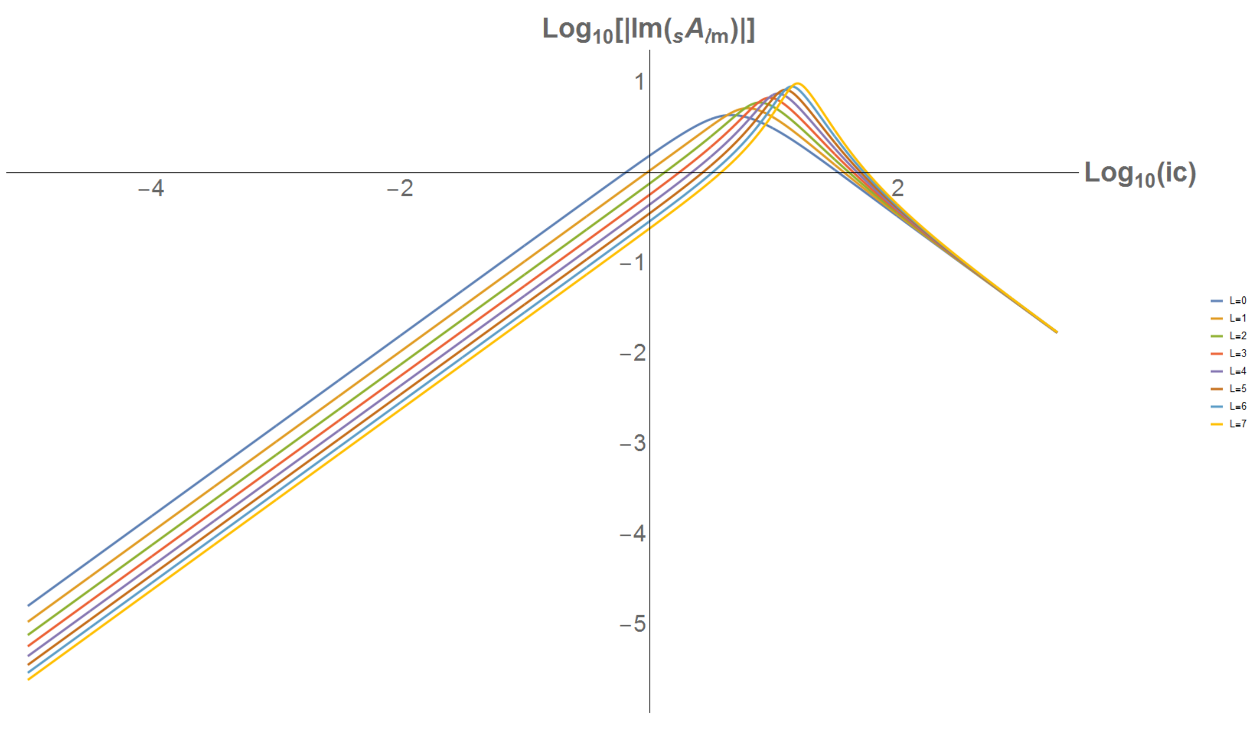


*Appendix 49: Log-log plot of Im($_sA_{lm}$) for SWSHs with m=4, s=-2 from ic=0 to 20, and for L=0,...,6.*

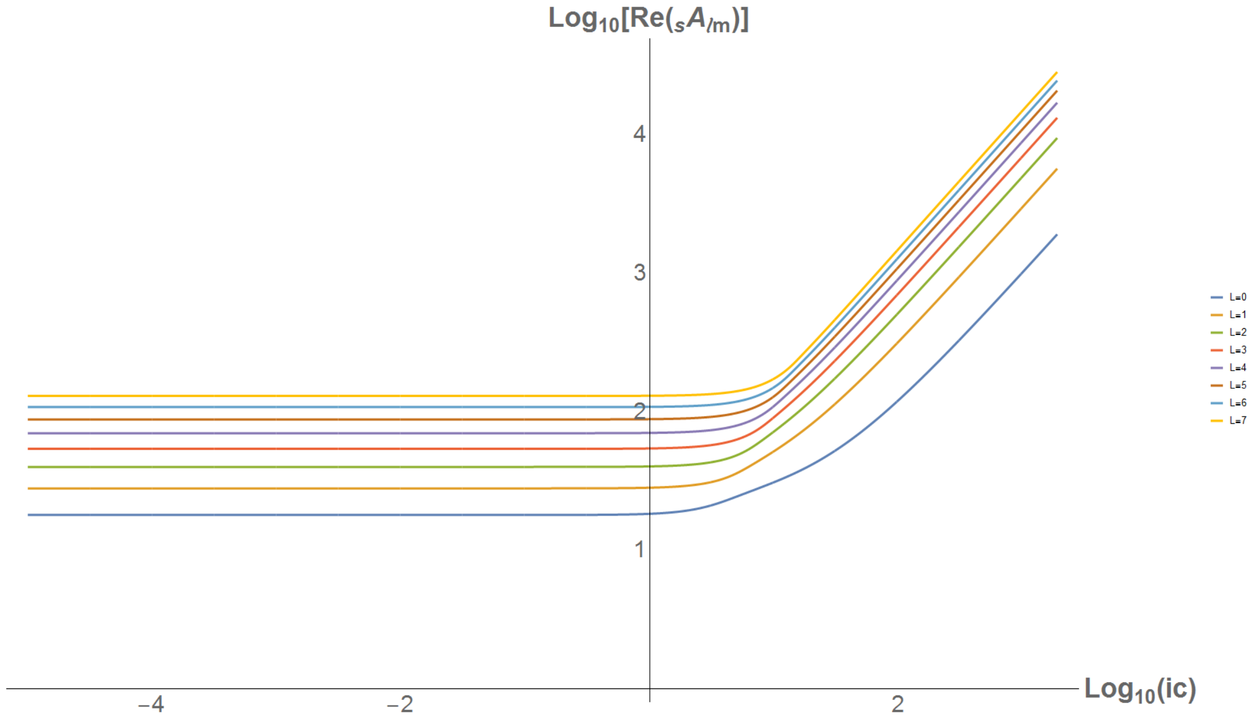


*Appendix 50: Log-log plot of Re(${}_sA_{lm}$) for SWSHs with m=4, s=-2 from ic=0 to 20, and for L=0,...,6.*

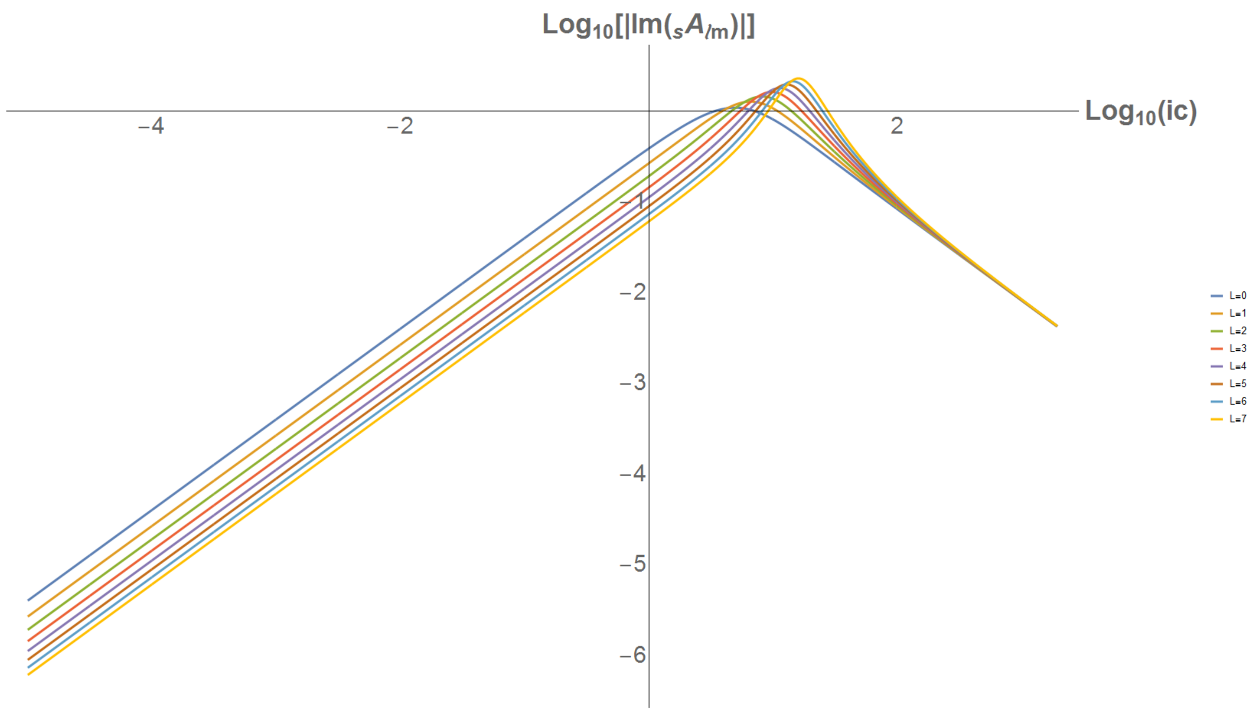


*Appendix 51: Log-log plot of Im(${}_sA_{lm}$) for SWSHs with m=4, s=-1 from ic=0 to 20, and for L=0,...,6.*

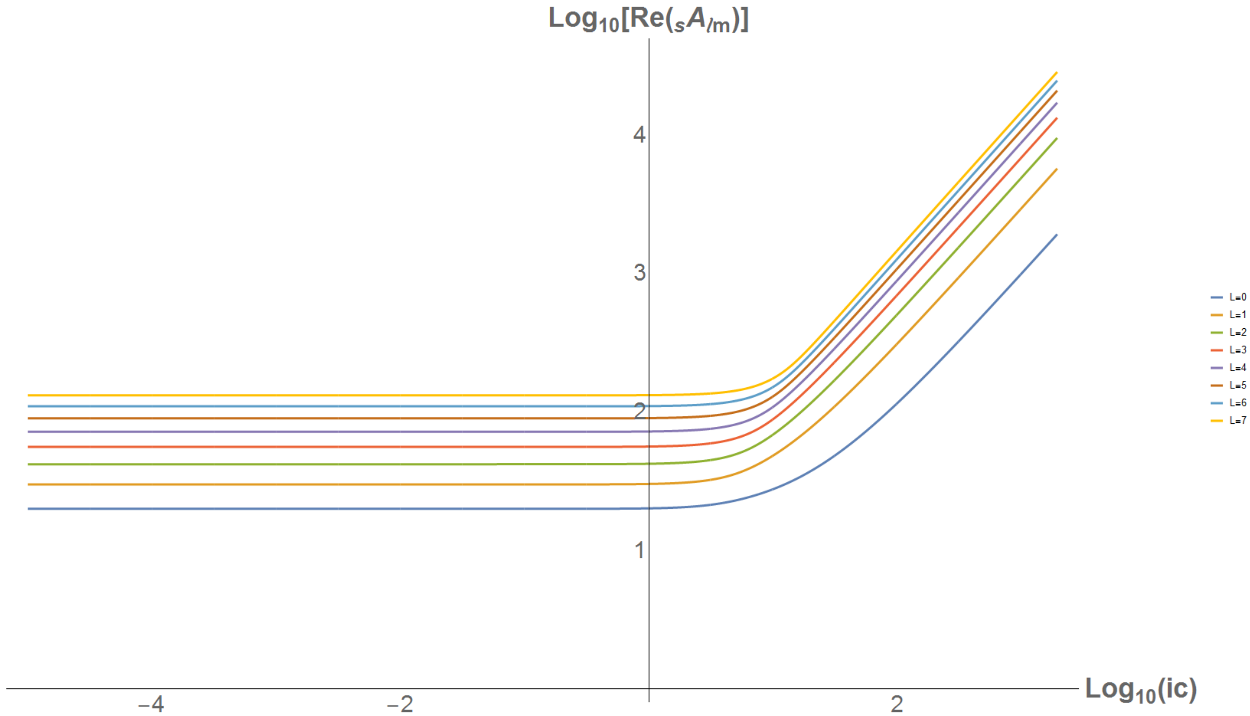


*Appendix 52: Log-log plot of Re($_sA_{lm}$) for SWSHs with m=4, s=-1 from ic=0 to 20, and for L=0,...,6.*

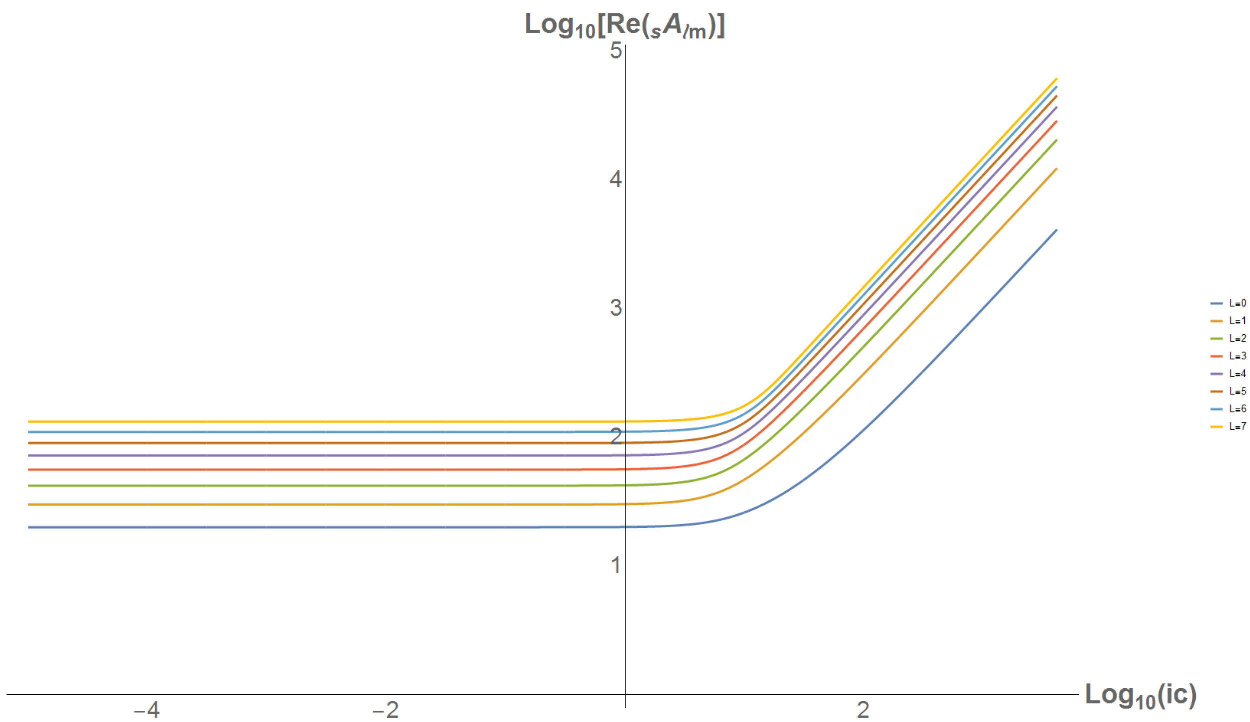


*Appendix 53: Log-log plot of Re($_sA_{lm}$) for SWSHs with m=4, s=0 from ic=0 to 20, and for L=0,...,6.*

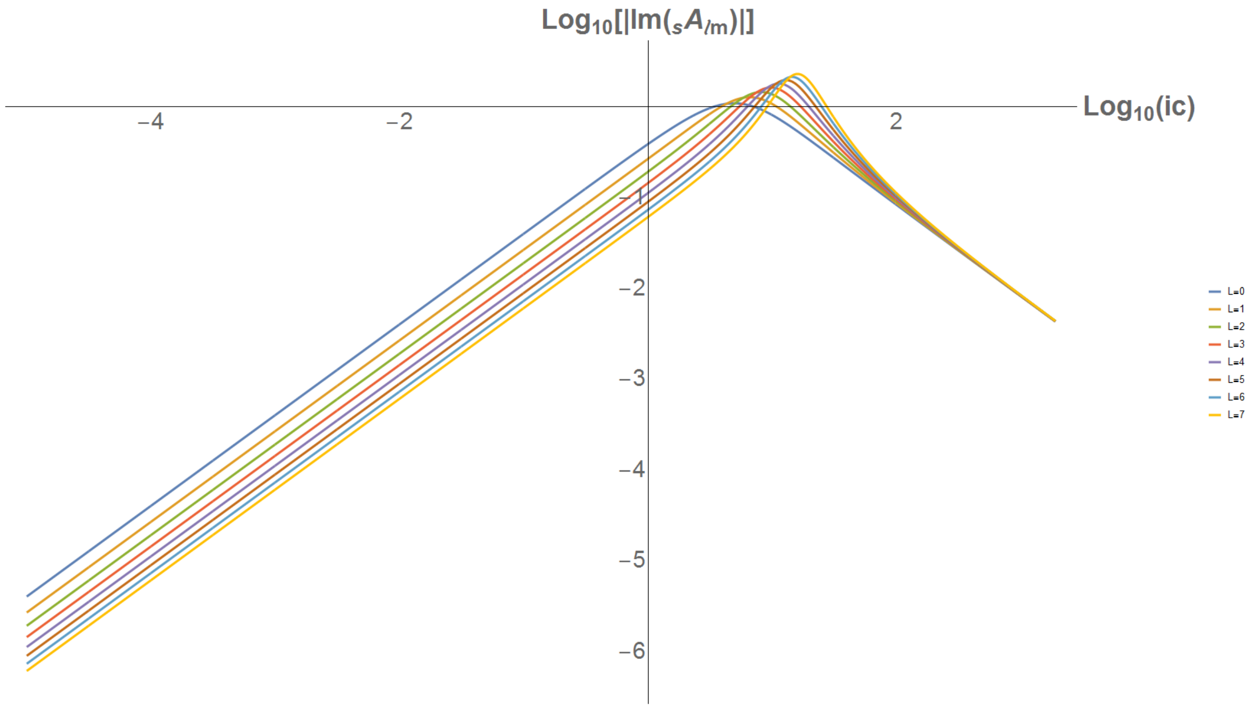


*Appendix 54: Log-log plot of $Im({}_sA_{lm})$ for SWSHs with m=4, s=1 from ic=0 to 20, and for L=0,...,6.*

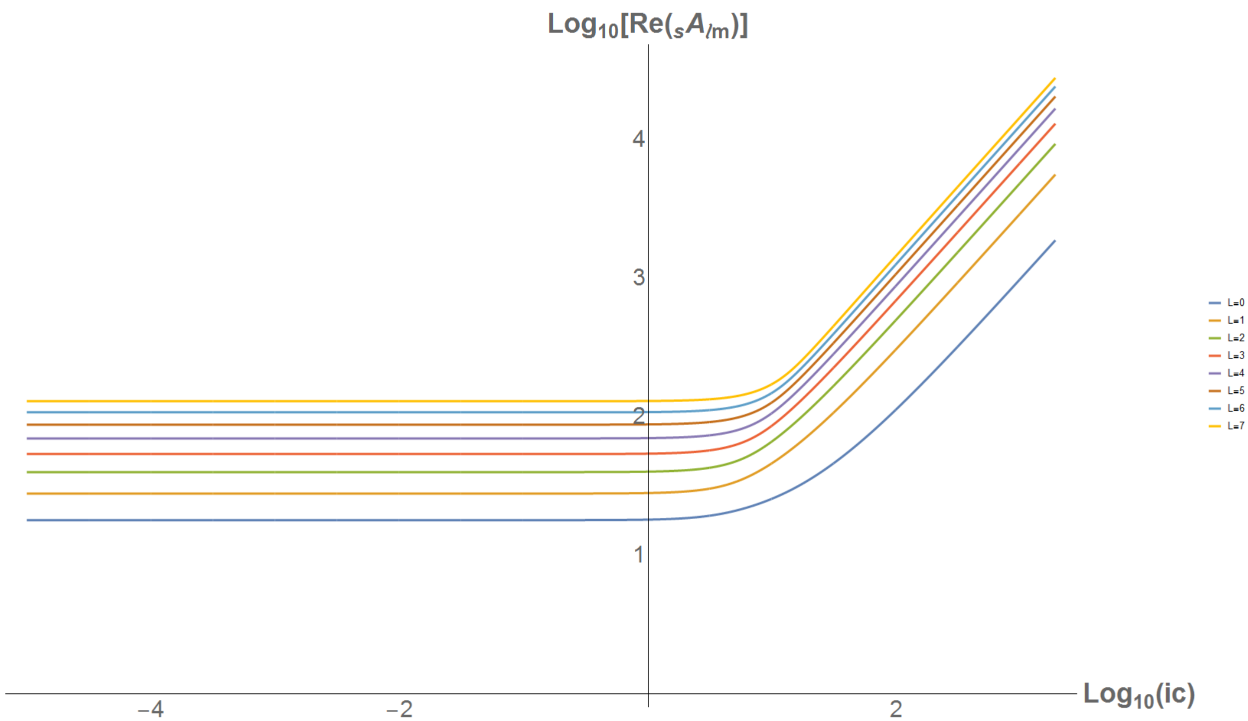


*Appendix 55: Log-log plot of $Re({}_sA_{lm})$ for SWSHs with m=4, s=1 from ic=0 to 20, and for L=0,...,6.*

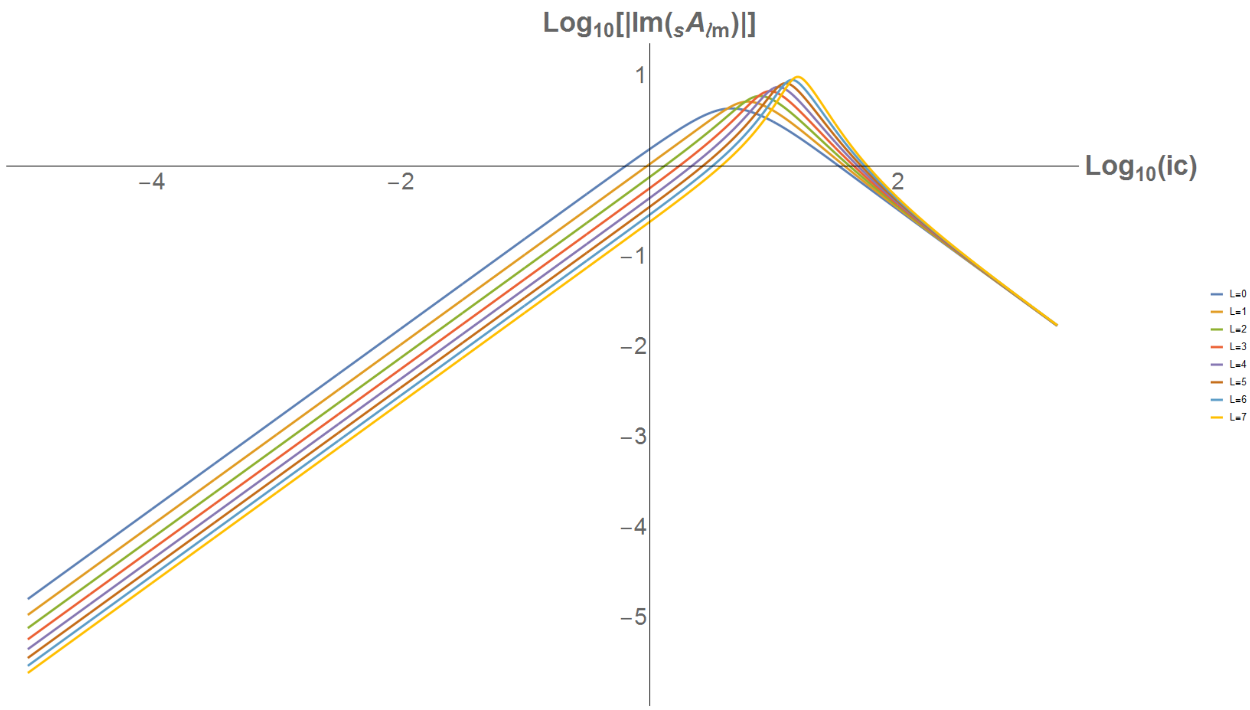


*Appendix 56: Log-log plot of Im($_sA_{lm}$) for SWSHs with m=4, s=2 from ic=0 to 20, and for L=0,...,6.*

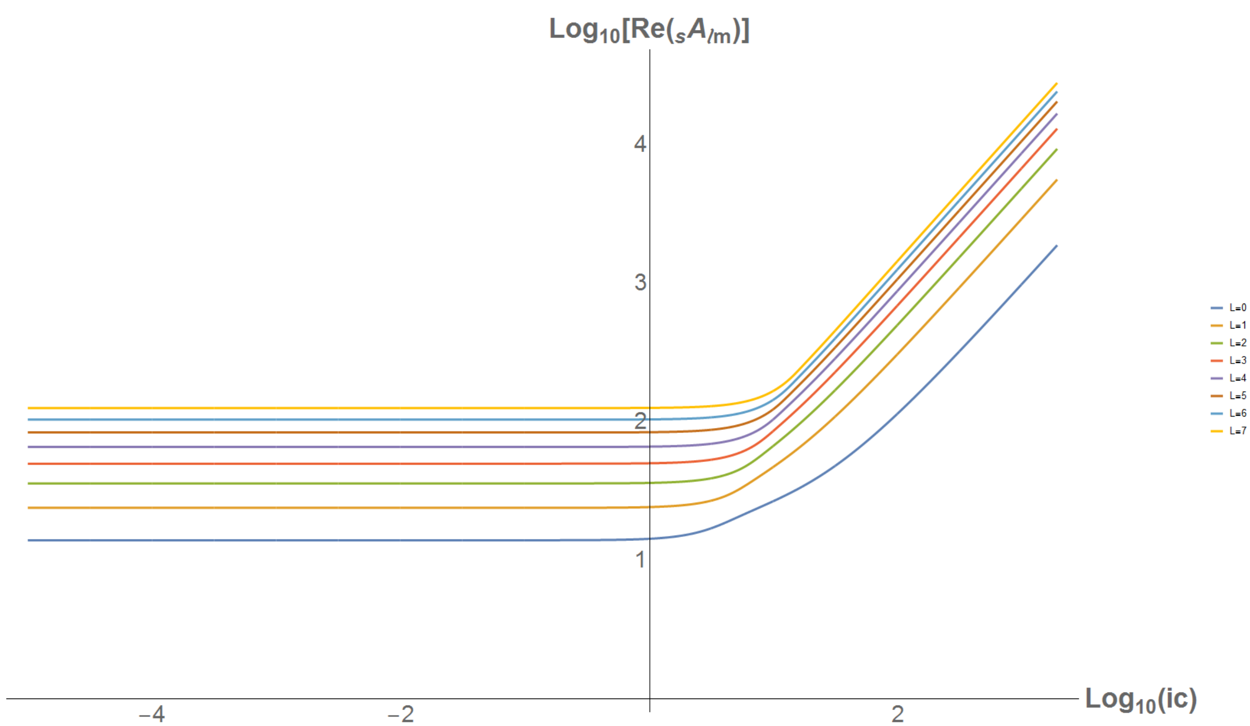


*Appendix 57: Log-log plot of Re($_sA_{lm}$) for SWSHs with m=4, s=2 from ic=0 to 20, and for L=0,...,6.*

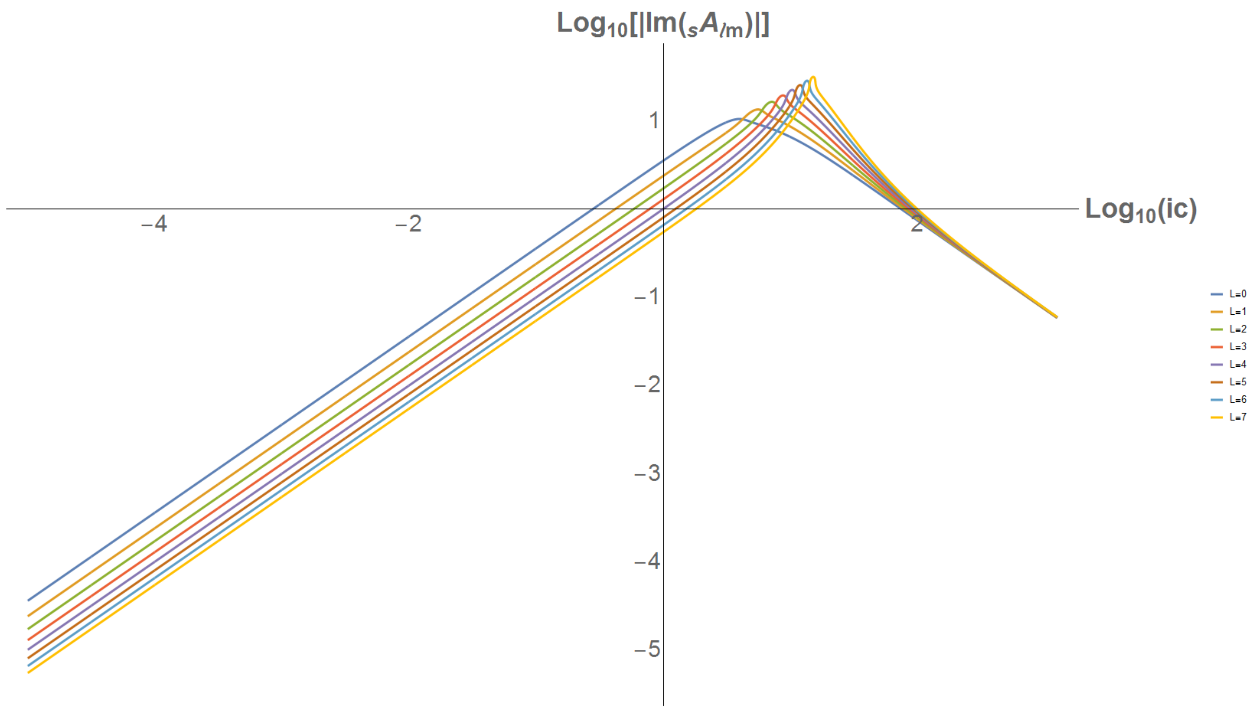


*Appendix 58: Log-log plot of $Im(_sA_{lm})$ for SWSHs with m=4, s=3 from ic=0 to 20, and for L=0,...,6.*

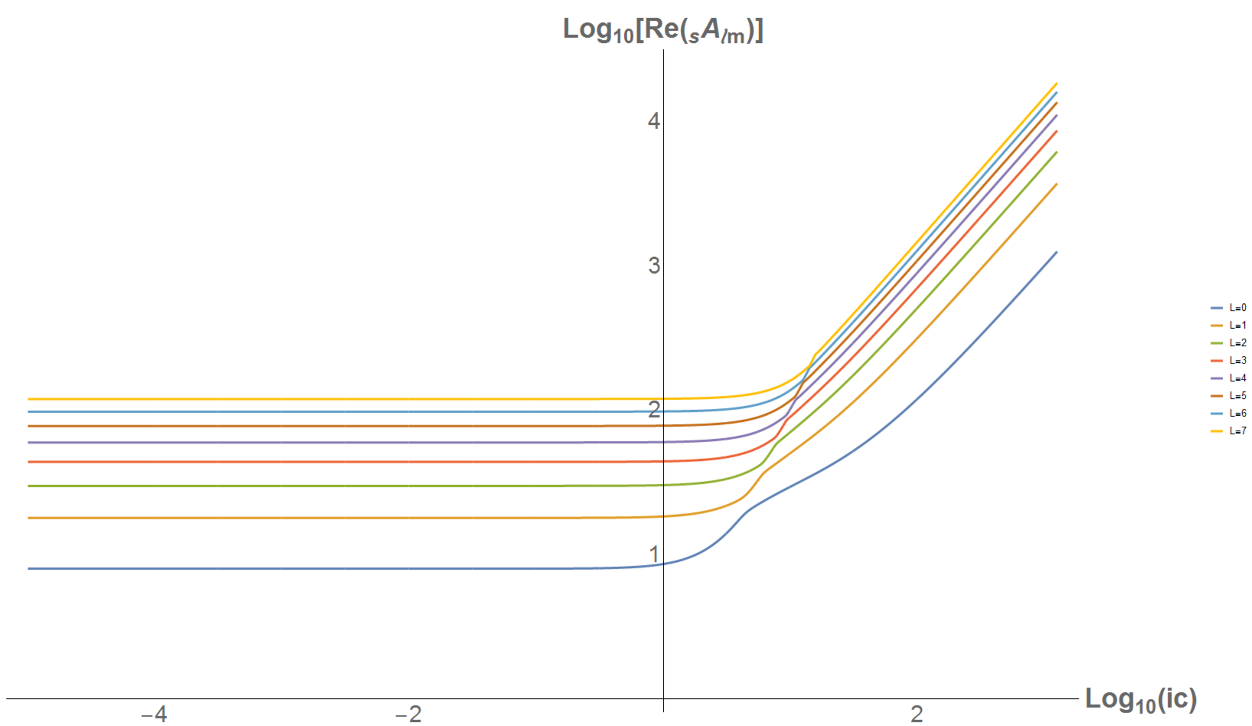


*Appendix 59: Log-log plot of $Re(_sA_{lm})$ for SWSHs with m=4, s=3 from ic=0 to 20, and for L=0,...,6.*

$m = 5$

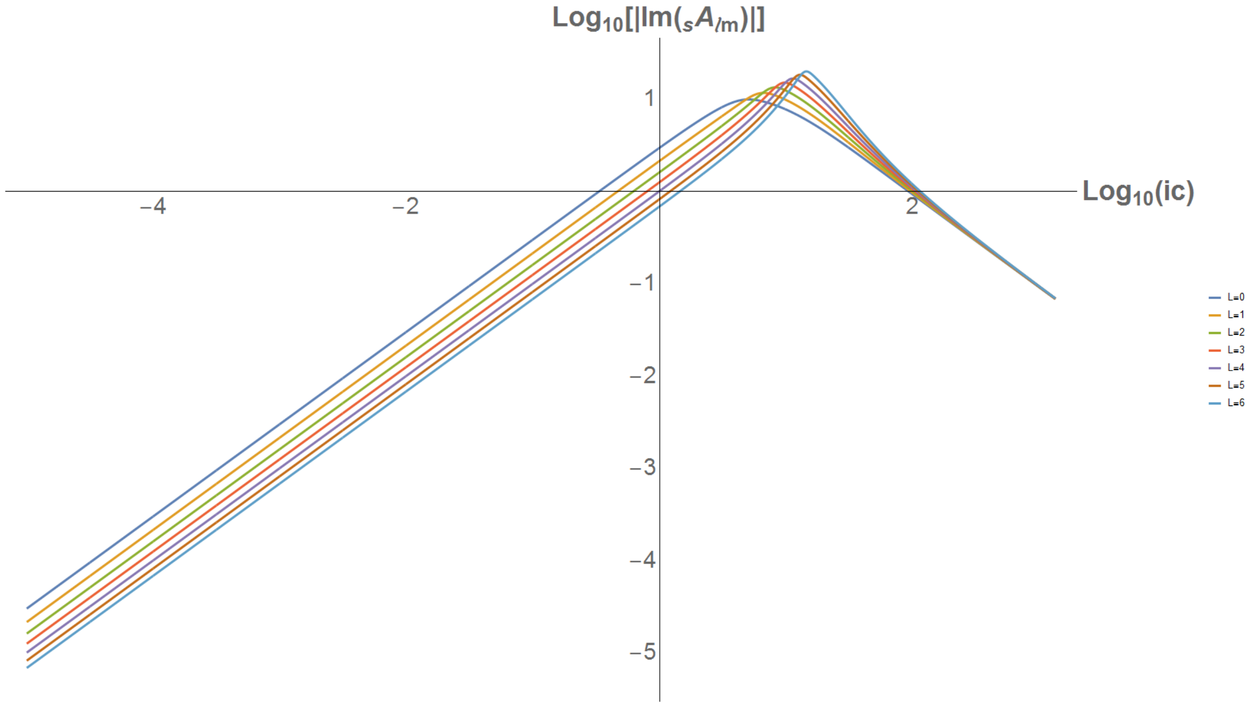


*Appendix 60: Log-log plot of Im($_sA_{lm}$) for SWSHs with m=5, s=-3 from ic=0 to 20, and for L=0,...,6.*

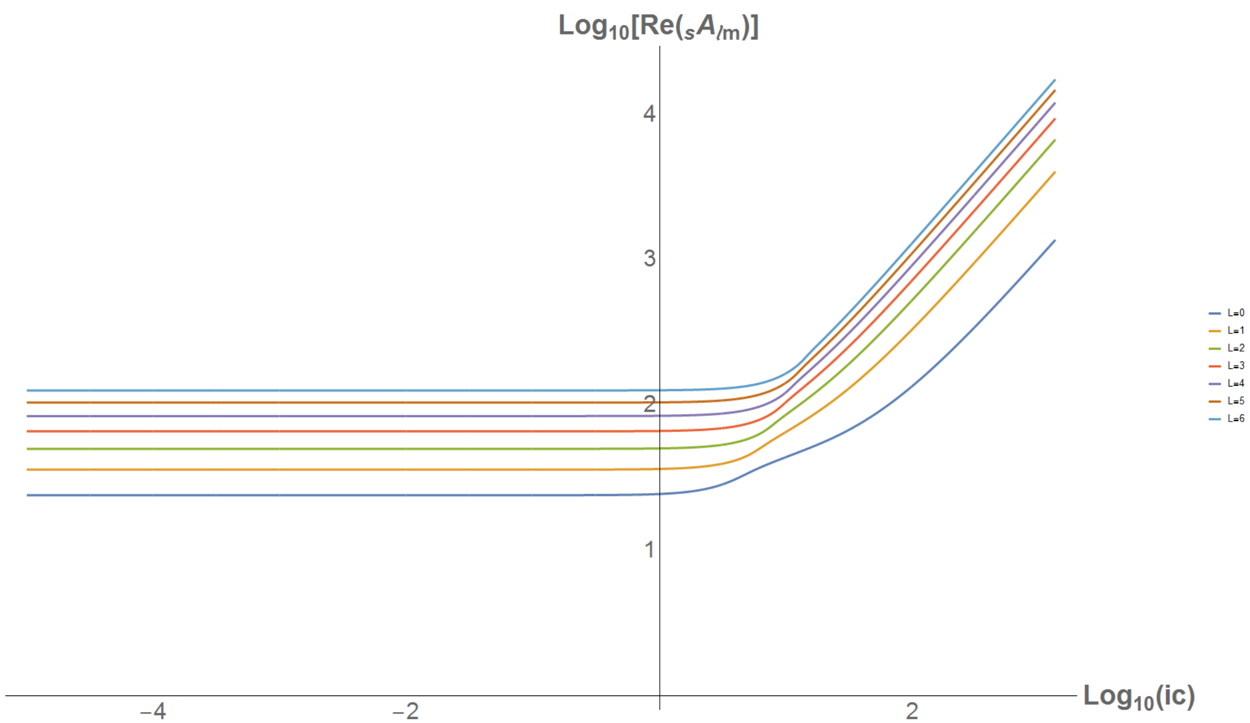


*Appendix 61: Log-log plot of Re($_sA_{lm}$) for SWSHs with m=5, s=-3 from ic=0 to 20, and for L=0,...,6.*

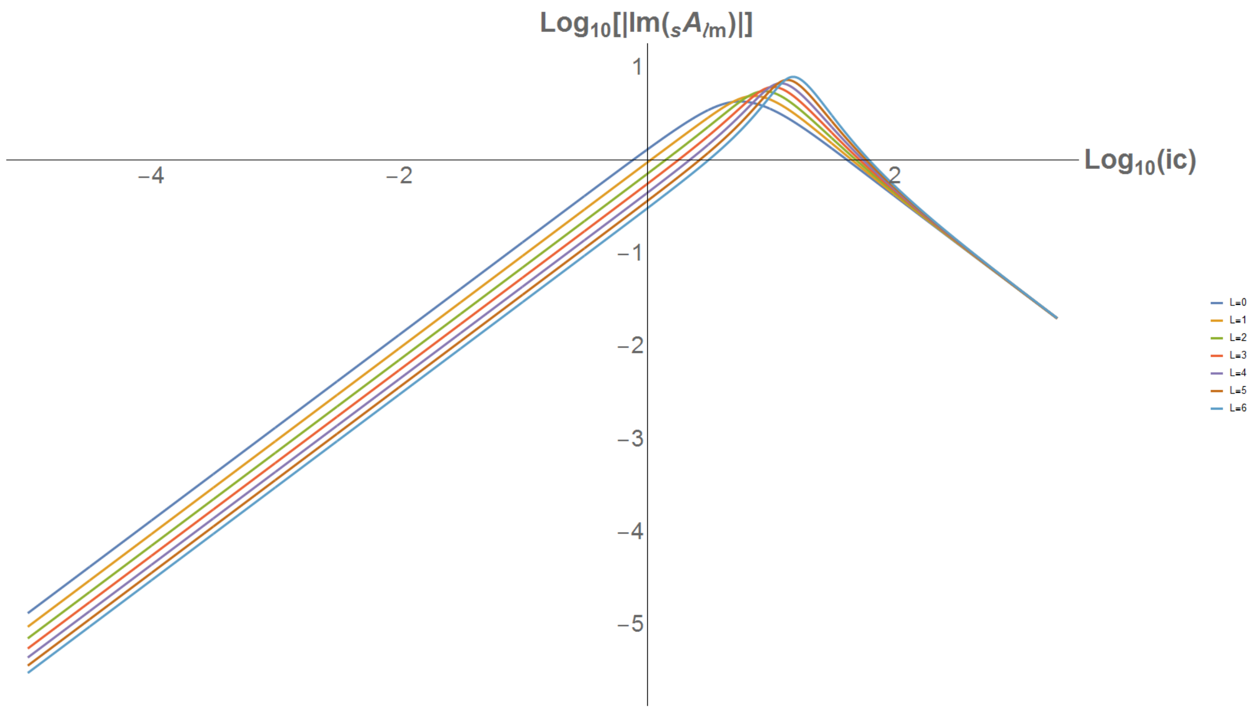


*Appendix 62: Log-log plot of $Im({}_sA_{lm})$ for SWSHs with m=5, s=-2 from ic=0 to 20, and for L=0,...,6.*

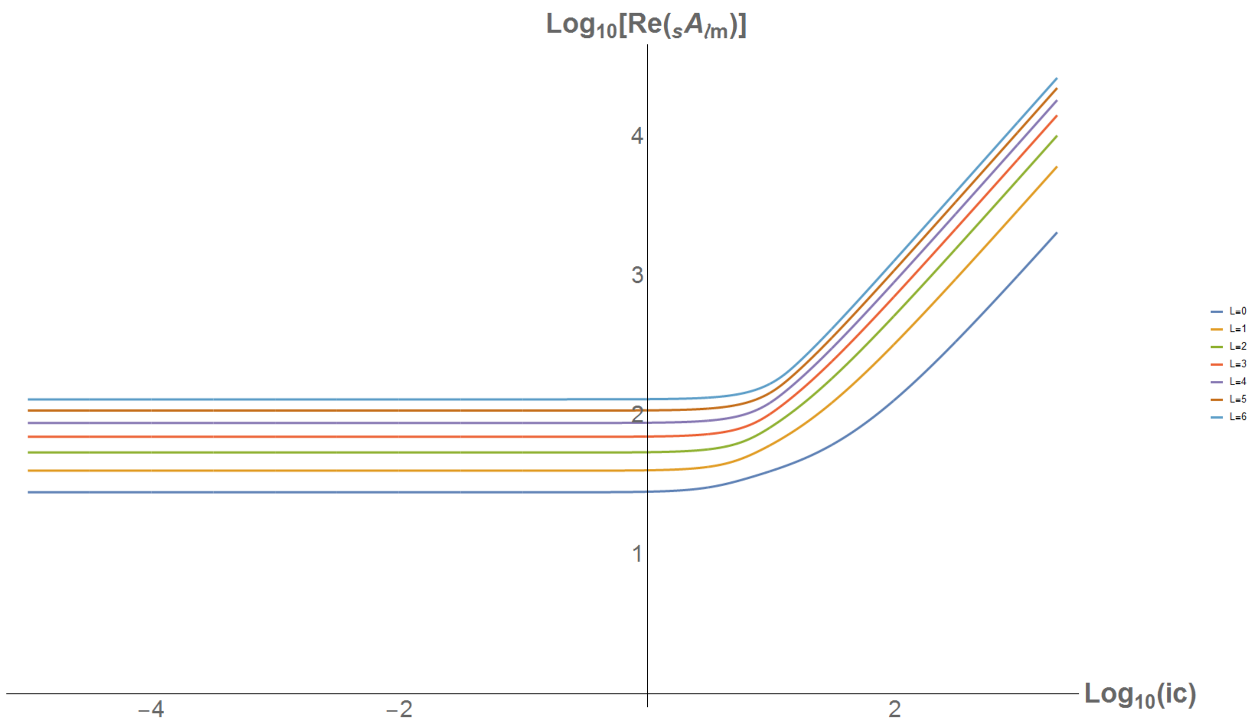


*Appendix 63: Log-log plot of $Re({}_sA_{lm})$ for SWSHs with m=5, s=-2 from ic=0 to 20, and for L=0,...,6.*

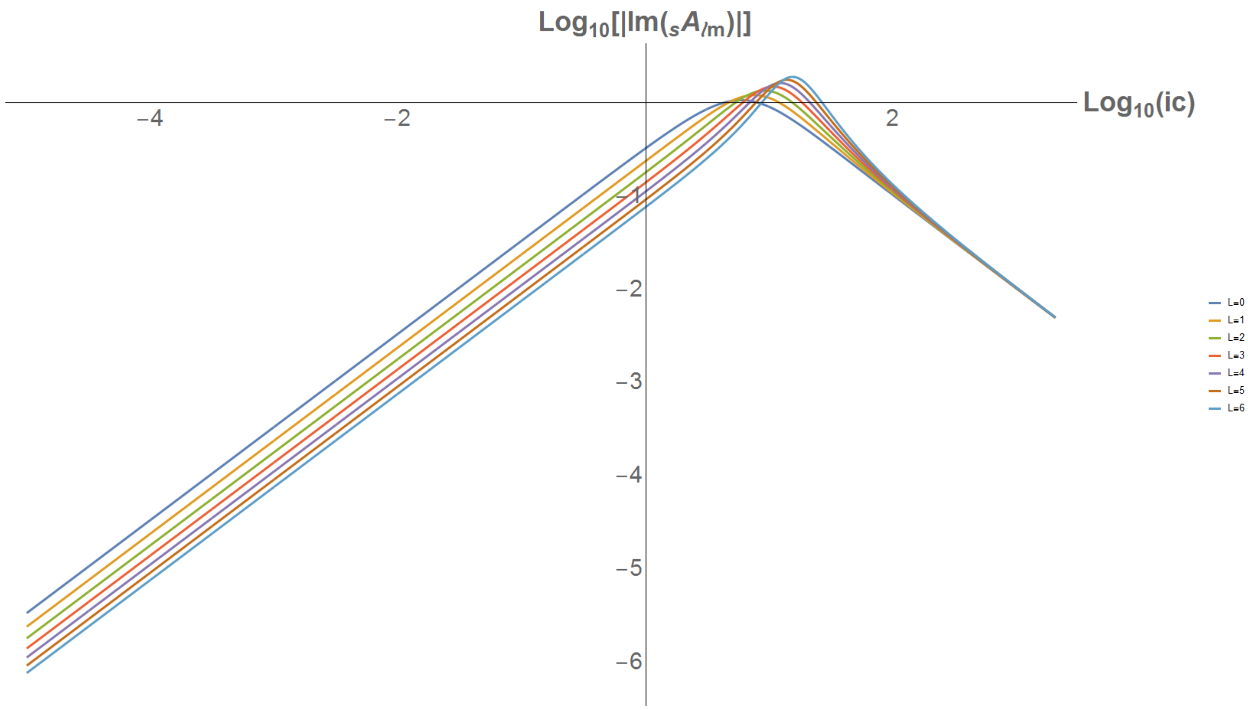


*Appendix 64: Log-log plot of $Im({}_sA_{lm})$ for SWSHs with m=5, s=-1 from ic=0 to 20, and for L=0,...,6.*

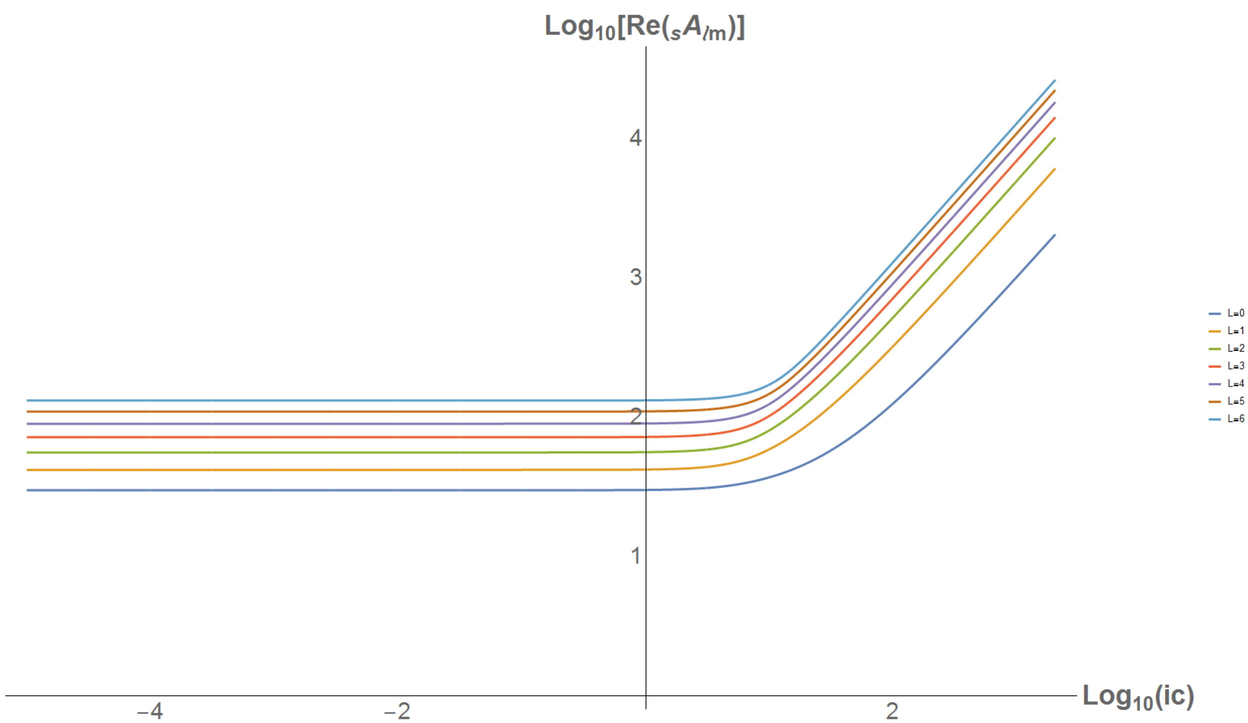


*Appendix 65: Log-log plot of $Re({}_sA_{lm})$ for SWSHs with m=5, s=-1 from ic=0 to 20, and for L=0,...,6.*

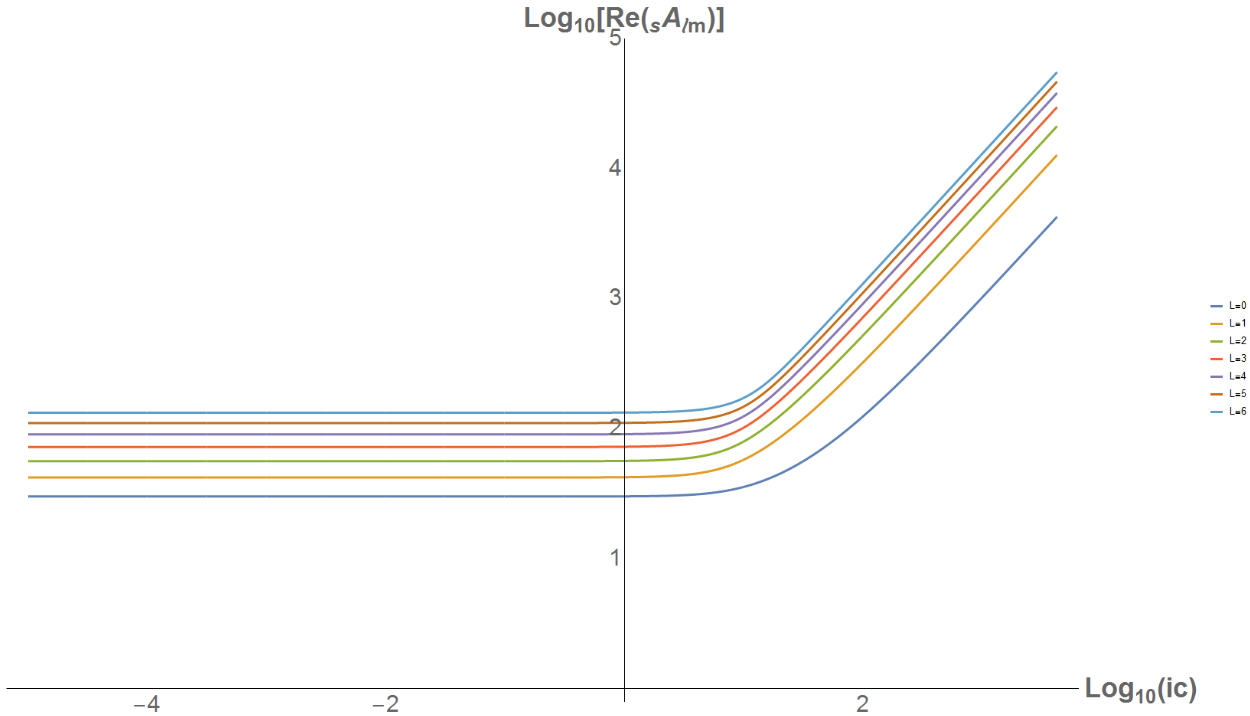


*Appendix 66: Log-log plot of Re($_sA_{lm}$) for SWSHs with m=5, s=0 from ic=0 to 20, and for L=0,...,6.*

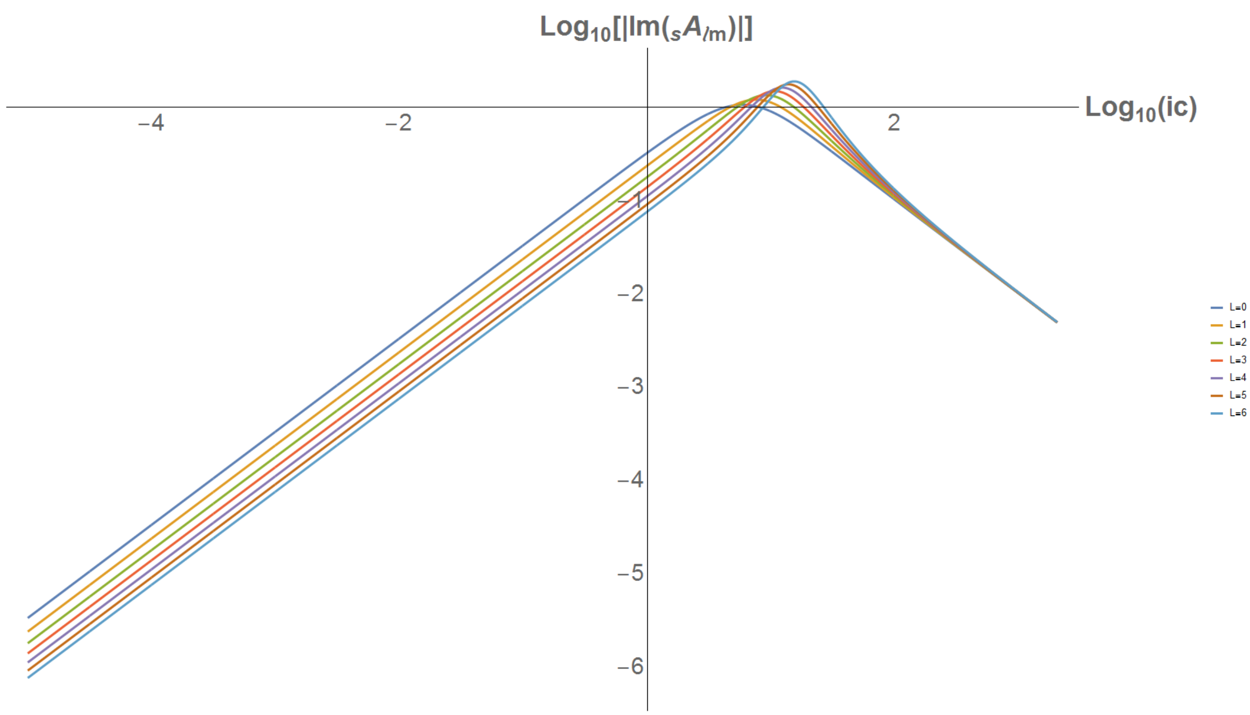


*Appendix 67: Log-log plot of Im($_sA_{lm}$) for SWSHs with m=5, s=1 from ic=0 to 20, and for L=0,...,6.*

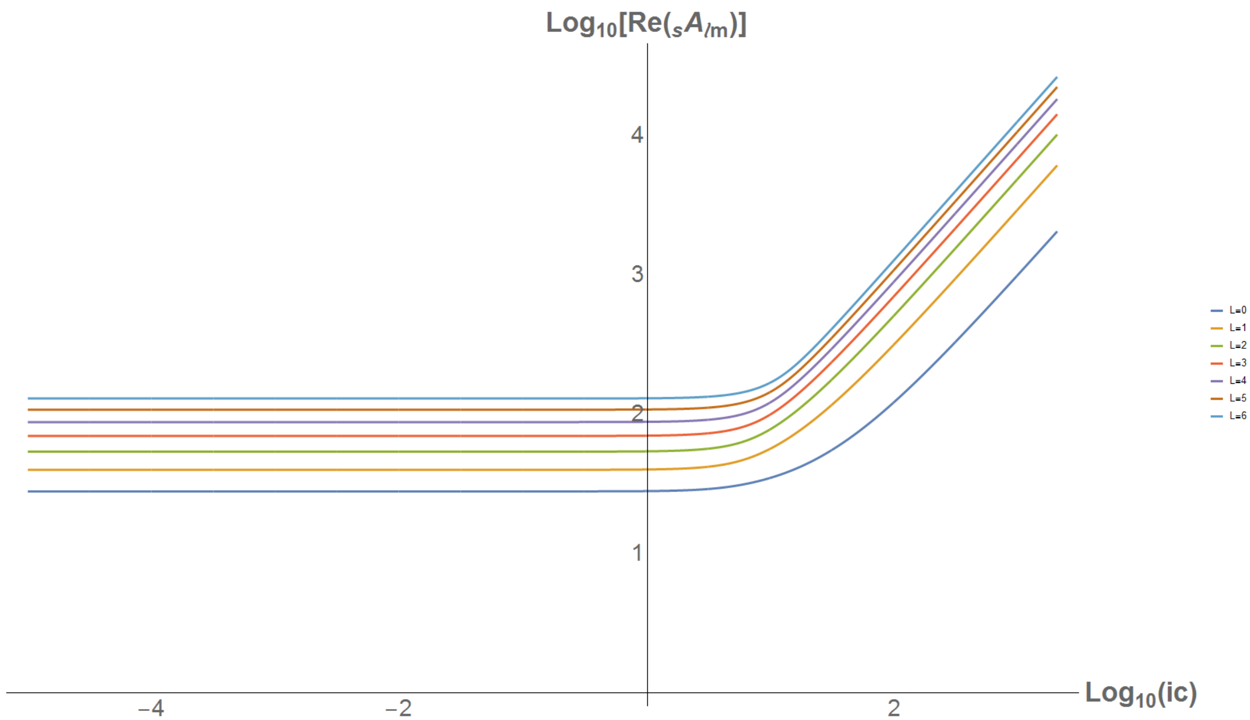


*Appendix 68: Log-log plot of Re($_sA_{lm}$) for SWSHs with m=5, s=1 from ic=0 to 20, and for L=0,...,6.*

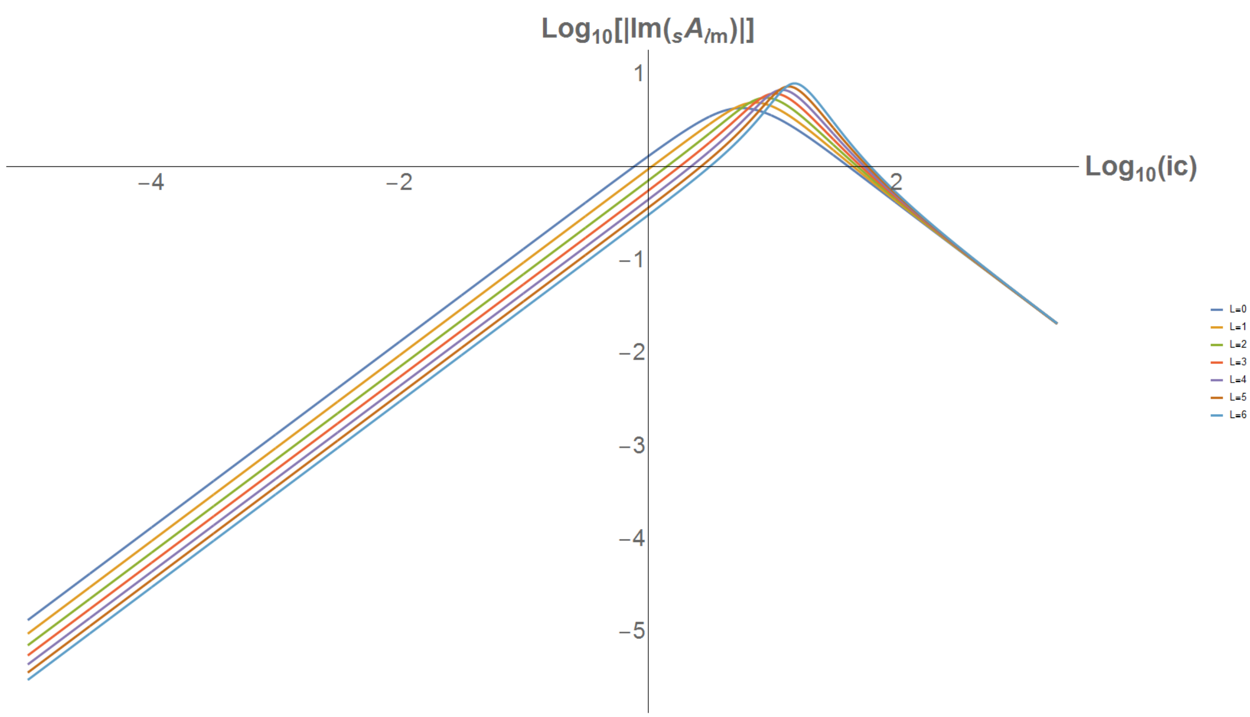


*Appendix 69: Log-log plot of Im($_sA_{lm}$) for SWSHs with m=5, s=2 from ic=0 to 20, and for L=0,...,6.*

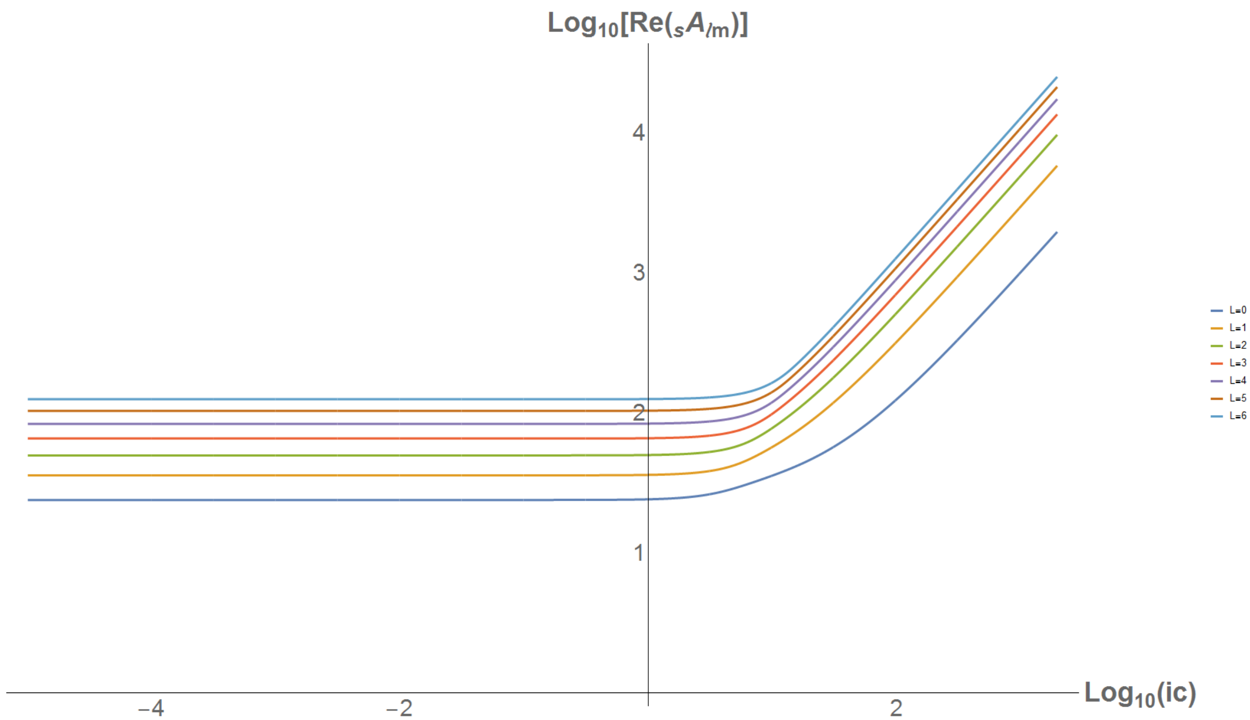


*Appendix 70: Log-log plot of Re($_sA_{lm}$) for SWSHs with m=5, s=2 from ic=0 to 20, and for L=0,...,6.*

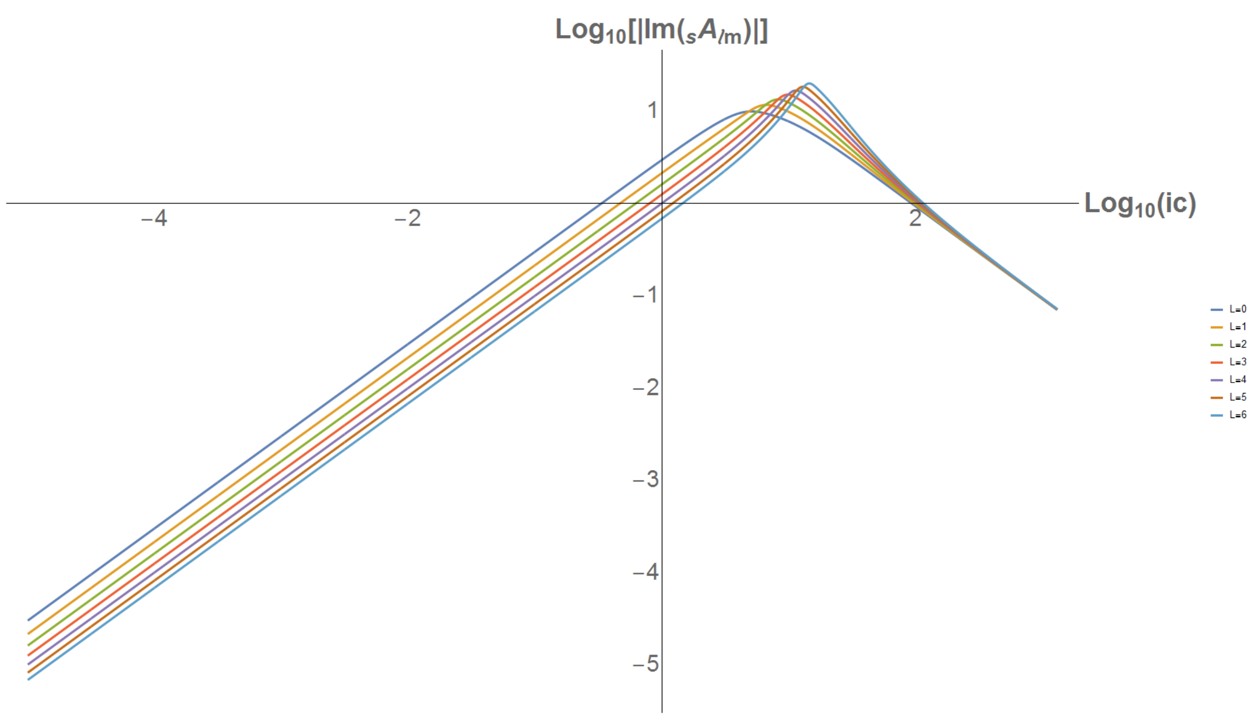


*Appendix 71: Log-log plot of Im($_sA_{lm}$) for SWSHs with m=5, s=3 from ic=0 to 20, and for L=0,...,6.*

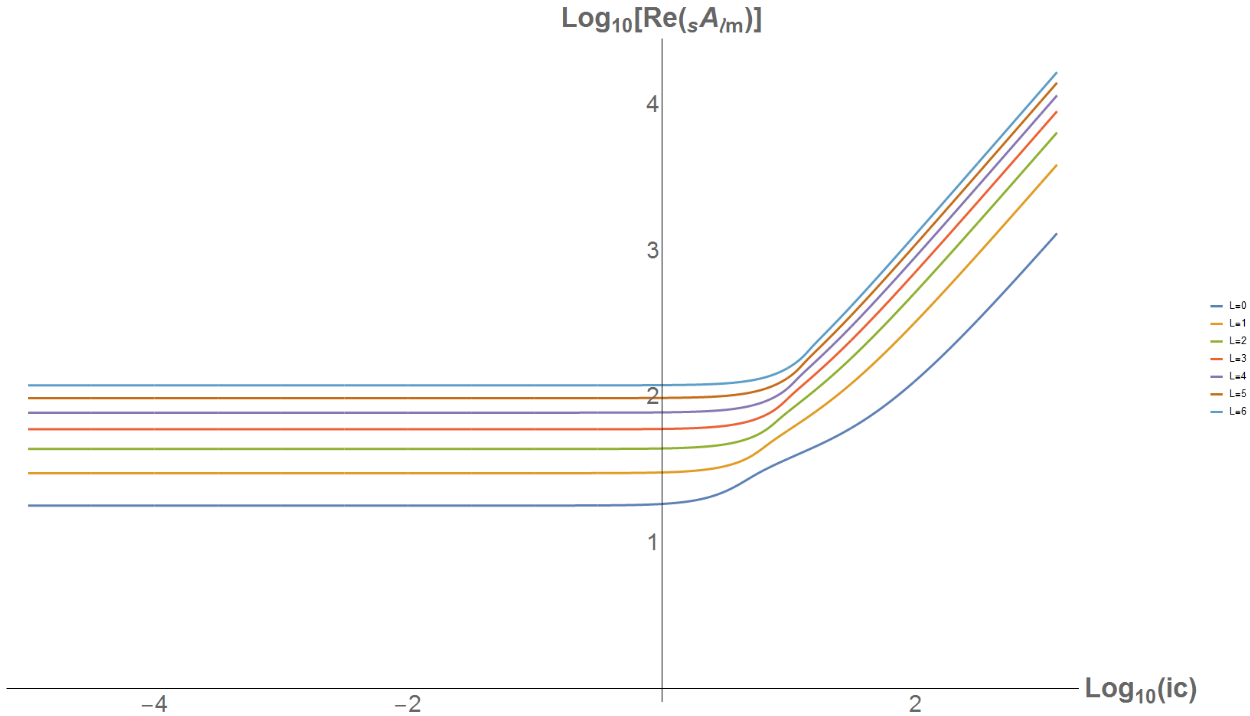


*Appendix 72: Log-log plot of Re(${}_sA_{lm}$) for SWSHs with m=5, s=3 from ic=0 to 20, and for L=0,...,6.*